The Hong Kong Polytechnic University

Department of Building Services Engineering

Novel-structure Dye-sensitized Solar Cells Based on Highly Ordered Titania Nanotube Arrays

Wang Yuanhao

A thesis submitted in partial fulfillment of the requirements for the Degree of Doctor of Philosophy

March 2011

CERTIFICATE OF ORIGINALITY

I hereby declare that this thesis is my own work and that, to the best of my knowledge and belief, it reproduces no material previously published or written, nor material that has been accepted for the award of any other degree or diploma, except where due acknowledgement has been made in the text.

I also declare that the intellectual content of this thesis is the product of my own work, even though I may have received assistance from others on style, presentation and language expression.

_____ _____ (Signed)

_____Wang Yuanhao_____ (Name of student)

ABSTRACT

The nanocrystalline dye-sensitized solar cell (DSSC), initially developed by Grätzel and his research group in 1991, has drawn much attention due to its low cost, facile fabrication procedures and relatively high conversion efficiency. In general, a classically configured DSSC is built up as a flat sandwich structure which uses two pieces of transparent conductive oxide (TCO) glasses as the substrates. One of the TCO glass is coated with a thin layer mesoporous nanocrystalline titania film attached with dye molecules as the photoanode. Another TCO glass is platinized as the counter electrode. An liquid electrolyte layer is between the two substrates, which contains a redox couple such as iodide/triiodide to transfer electrons between the electrodes.

Although the record power conversion efficiency of over 11% has been achieved so far, there are still several problems preventing this kind of solar cell towards industrialization: (i) the highest conversion efficiency of 11.5% is obtained only on a very tiny scale DSSC (0.158 cm^2). For large-scale DSSCs, as they employ TCO glass as the substrates, the energy conversion efficiency is low in virtue of the high sheet resistance of TCO glass. (ii) Currently the titania nanoparticle film is coated onto the surface of the TCO glass through the screen printing method. Due to the affinity of interface between the TCO glass and titania film is not firm enough, sometimes the oxide coating would peel off after a period of time. (iii) As the most extensively studied DSSCs adopt nanoparticle film as the active layer of photoanode and due to the multiple trapping/detrapping events occurring within the grain boundaries between the 3D networks of interconnected nanoparticles, the electron transportation rate in the nanoparticle film is very low, which will lead to high interface recombination reactions

and finally lower the efficiency. Recently the highly ordered, self-organized titania nanotube arrays obtained through electrochemical anodization of an Ti foil have been shown to offer direct electrical pathways for rapid collection of electrons. However, due to the opacity of the Ti foil, the highly ordered titania nanotube arrays can be only applied on backside illuminated DSSCs. In the backside illumination configuration, the incident light will be attenuated by the platinized counter electrode and the electrolyte, which lowers the sunlight utilization and restricts the efficiency. Therefore, it is necessary to develop new structures and components to overcome the shortages and strive for a breakthrough to get better achievements in the development and commercialization of the inexpensive and high efficiency DSSCs.

The objective of this thesis is to improve the photovoltaic performance of the DSSCs by introducing new-structure, all-Ti-substrates based DSSCs combined with highly ordered titania nanotube arrays. According to the bionic idea, a series of DSSCs with novel structures are developed and systematically studied. By using the principle of the capillary network in a lung, a mesh-like DSSC is designed, which contains no TCO glass. The photoanode is prepared by using a Ti mesh as the substrate and then through the anodization method to directly synthesize highly ordered titania nanotube arrays as the active layer, where the Ti metal mesh serves as both the substrate and the source material. As a result, the affinity of the titania layer with the Ti mesh is better than its structure with a piece of TCO glass. The counter electrode is prepared by using a Ti sheet as the substrate and electrodeposited with Pt thin film as the catalyst layer. In the mesh-like configuration, the electrolyte could diffuse through the holes on the mesh freely to transfer the redox couple. With the increase of mesh number, the surface area

of the substrate is also increased, which means more titania nanotube arrays could be synthesized to enhance the dye loading capacity. Different lengths of titania nanotube arrays are also investigated to find their influence on the photovoltaic performances. The results indicate that a proper length of the nanotube array layer is a key factor to achieve high conversion efficiency. Compared with the backside illuminated DSSC, the mesh-like DSSC could allow sunlight irradiating through the photoanode side to avoid light loss. Besides, due to the low sheet resistance of Ti substrate, the size of the cell has only a little impact on the conversion efficiency. Through optimization, for a single unit cell with 4 cm^2 area, the energy conversion efficiency could achieve 5.0% under standard *AM 1.5* sunlight, which makes it possible to produce this type of DSSC in large scale with relatively high efficiency. The flexible mesh-like DSSCs are also fabricated by using transparent thermoplastic film as the sealing materials. The bendability is investigated and shows good mechanical and photovoltaic stability.

A DNA-like DSSC is developed by using an anodized Ti wire as photoanode and platinized Ti wire as counter electrode. These two wire-like electrodes are twisted together to make a double-helix structure just like a DNA molecule. The DNA-like DSSC is based on a 3-dimentional (3D) structure which shows superiority of tracking sunlight due to its symmetrical double-helix structure. Different thickness of the nanotube arrays are investigated to find their influence on the photovoltaic parameters and the cell with a 15.3 micron layer exhibited the highest conversion power, about 0.49 mW. To further increase the photovoltaic performance, a two-step formation of the titania nanowire-covered nanotube bilayer film technique is developed and applied in DNA-like DSSCs. The bilayer film is prepared by the electrochemical anodization first

to grow the lower nanotube layer and then through the hydrothermal method to grow the upper nanowire layer. From the reflectivity spectrum and scanning electron microscopy it is observed that the nanowire layer on the top could not only decrease the reflectivity of the film, but also play a role to modify the film cracks. Compared with the DSSC based on a single layer electrode, the cell with bilayer film showed higher photovoltaic parameters and lower dark current, which is due to its higher light harvesting efficiency and lower charge recombination process between the electrolyte and the substrates. The series–parallel connection characteristics of the DNA-like DSSCs reveal that the total voltage and the total short current equalled the sum of each cell's in series and in parallel, respectively. It is anticipated that the DNA-like structured DSSCs have great potential for the application in larger modules using integrated circuit techniques.

By combining the merits of the mesh-like DSSCs and DNA-like DSSCs, a new type of 3D double deck mesh-like DSSCs is further developed. One of the Ti mesh is anodized to in-situ synthesize highly ordered titania nanotue arrays. Another Ti mesh is platinized through electrodeposition as the counter electrode. The effect of mesh number on the 3D DSSCs is investigated through dye loading measurement, cyclic voltammetry and electrochemical impedance analysis. The results show that with the increase of mesh number, the dye loadings on the photoanode and the active surface area of Pt on the counter electrode are increased, while the diffusion of the electrolyte becomes more difficult due to the reduced diameter of the openings in the mesh. It has also been demonstrated that the performance of this 3D DSSC is capable of tracking sunlight just like the DNA-like DSSC due to its axial symmetrical structure. In the *I-V* measurement,

the 3D DSSC based on the 90-mesh photoanode and the 120-mesh counter electrode shows the highest conversion efficiency of 5.5% under standard *AM 1.5* sunlight.

***Keywords*:** dye-sensitized solar cells (DSSCs), titania, photovoltaic, nanotube, metal substrate, anodization, one-dimensional nanomaterials.

PUBLICATIONS DURING PHD STUDY

Journal papers during PhD study:

1. **Yuanhao Wang**, Hongxing Yang, Yong Liu et al., The use of Ti meshes with self-organized TiO_2 nanotubes as photoanodes of all-Ti dye-sensitized solar cells. *Prog Photovoltaics*, 2010. **18**: 285-90.
2. **Yuanhao Wang**, Hongxing Yang, Lin Lu, Three-dimensional double deck meshlike dye-sensitized solar cells. *J Appl Phys*, 2010.**108**: 064510-13.
3. **Yuanhao Wang**, Hongxing Yang, Hongmei Xu, DNA-like dye-sensitized solar cells based on TiO_2 nanowire-covered nanotubebilayer film electrodes. *Mater Lett*, 2010. **64**:164-66.
4. **Yuanhao Wang**, Yong Liu, Hongxing Yan et al., An investigation of DNA-like structured dye-sensitized solar cells. *Curr Appl Phys*, 2010. **10**: 119-23.
5. **Yuanhao Wang**, Hongxing Yang, Lin Lu, Electrochemical detachment of TiO_2 nanotube arrays layer by two step anodization process and its application in front-side illuminated dye-sensitized solar cells, submitted to Electrochemistry Communication.
6. **Yuanhao Wang**, Hongxing Yang, Lin Lu, Flexible dye-sensitized solar cells based on graphite mesh. Under preparation.

Conference papers during PhD study:

1. **Yuanhao Wang**, Hongxing Yang, Yong Liu, Hai Wang, Hui Shen. Dye sensitized solar cells based on different types of counter electrodes. *The 1st International Symposium on Solar Cells and Solar Fuels*, Dalian, China, P115 2008.12.10-12.12.

2. **Yuanhao Wang**, Hongxing Yang, Lin Lu. Bionic dye sensitized solar cells. *The 4th international conference on the industrialisation of dye solar cells*, 2010.11.01-11.04

Patents:

1. **Yuanhao Wang**, Hongxing Yang, The detachment of TiO_2 nanotube film from the Ti sheet and its application in dye-sensitized solar cells. China Patent, Patent Application Number: 201010233899.3
2. **Yuanhao Wang**, Hongxing Yang, A spherical dye-sensitized solar cell. China Patent, Patent Application Number: 201010005219.2
3. **Yuanhao Wang**, Hongxing Yang, Lin Lu, A new method to prepare the screen-printing paste for dye-sensitized solar cells. China Patent, Application Number: 201010564588.5

ACKNOWLEDGEMENTS

This thesis would not be finished without the help and support of those who are gratefully acknowledged here.

First and foremost, I would like to express my gratitude most sincerely to my chief supervisor, Prof. Yang Hongxing, for his invaluable support, patient guidance, and overly enthusiasm throughout my research work.

I would also like to acknowledge my co-supervisor Dr. Lu Lin who helped me a lot and kept an eye on the progress of my research work.

My sincere gratitude is devoted to Dr. Liu Yong who gave me great assistance and useful suggestions throughout my PhD study. His diligence and preciseness gave me a profound influence for my research work. I am also grateful to Prof.Hui Shen for his support to complete my experiments.

Furthermore, I would like to express my gratitude to all the members in the Renewable Energy Research Group for their support and advice throughout my research work.

I would like to express my heartfelt thanks to my family for their endless love, support, encouragement. This thesis is dedicated to all of them.

Finally, I want to thank everyone who directly or indirectly gave help and support to this thesis.

TABLE OF CONTENTS

LIST OF FIGURES

LIST OF TABLES

LIST OF ABBREVIATIONS AND NOTATION

AM: air mass

APCE: absorbed photon-to-current efficiency

CB: conduction band

CV: cyclic voltammetry

DSSCs: dye-sensitized solar cells

EG: ethylene glycol

EIS: electrochemical impedance spectra

FESEM: field-emission scanning electron microscopy

FTO: fluorine doped tin oxide glass

HOMO: highest occupied molecular orbital

HRTEM: high-resolution transmission electron microscopy

IPCE: incident photon-to-current conversion efficiency

LHE: light harvesting efficiency

LUMO: lowest unoccupied molecular orbital

SCE: saturated calomel electrode

SHE: standard hydrogen electrode

VB: valance band

XRD: X-ray diffraction

TBP: 4-*tert*-butylpyridine

TCO: transparent conducting oxide

TEM: transmission electron microscopy

E_g: band gap energy

D_n: diffusion coefficient

E_{BD} (V): breakdown potential

λ(nm): wavelength

I_{corr}: corrosion current density

V_{oc}: open-circuit voltage

J_{sc}: short-circuit current

ff: fill factor

η: conversion efficiency

CHAPTER 1 INTRODUCTION

1.1 Photovoltaics

Nowadays, about 80% of the energy consumption all over the world is based on fossil fuels, including oil, gas, coal and so on. Especially in recent years, the demand for fossil energy increases dramatically mainly due to the population explosion, higher living standard and economic growth. It is predicted that the consumption demand may exceed the annual production within the next two decades. As shown in **Figure 1.1**, the proved reserves of oil, gas and uranium will be exhausted within this century at the current rates of consumption. The situation of coal reserves is a little better, as they would be adequate at least for the next 250 years. However, the use of fossil fuels, especially coals, causes serious environmental and social problems.

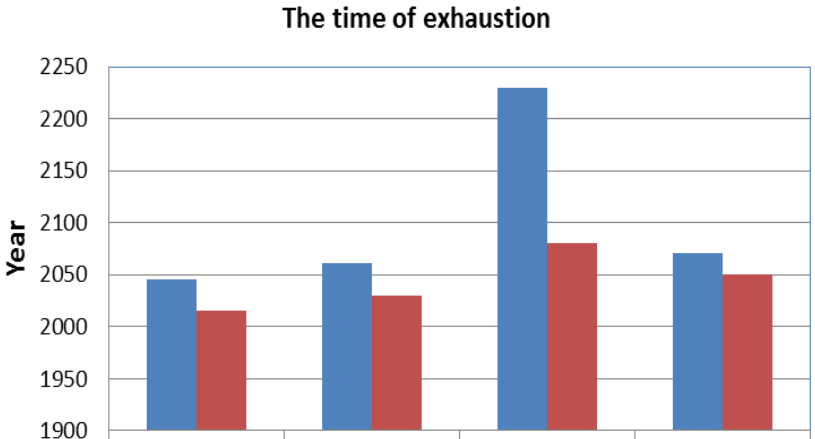

	Oil	Nature gas	Coal	Uranium
Global	2045	2061	2230	2071
China	2015	2030	2081	2050

Figure 1.1 Estimation of conventional non-renewable energy resources **[1]**

The unprecedented increase in energy consumption, along with the pressure that fossil energy resources might be exhausted soon encouraged the search for alternative energy resources. Solar radiation is the most abundant energy source in our planet. For thousands of years, human beings relied solely on solar energy: making use of direct forms like light or heat, and indirect forms like wind or biomass. However, nowadays the relatively high cost of the renewable energy prohibits its widespread application. Fortunately, more and more people in the world recently are paying attention to the climatic change of the worldwide CO_2 emissions, impending energy crisis and other environmental problems. These concerns raised great interest in renewable energy sources, politically and economically. Now people in the world realize that it is actually a curse to depend on fossil fuels sources, which causes environmental problems, geopolitical tensions, and puts our climate at stake tragically. It is urgent for us to build a more sustainable energy economy.

1.1.1 Solar energy

Solar energy, includes radiant light and heat from the sun, has been applied by humanity for thousands of years by using a wide range of technologies. Solar radiation, along with wind and wave power which are the secondary solar-powered resources, account for the most of the available renewable energy on our planet. However, only a small fraction of the available renewable energy is utilized. Outer planet receives about 174 petawatts (PW) of the incoming solar radiation at the upper atmosphere **[2]**. About 30% is reflected to space, and the rest is absorbed by clouds, oceans and land, as shown

in **Figure 1.2**. At the surface of earth, the solar spectrum is spread mostly across the visible and near-infrared area, and only a small fraction is in near-ultraviolet **[3]**.

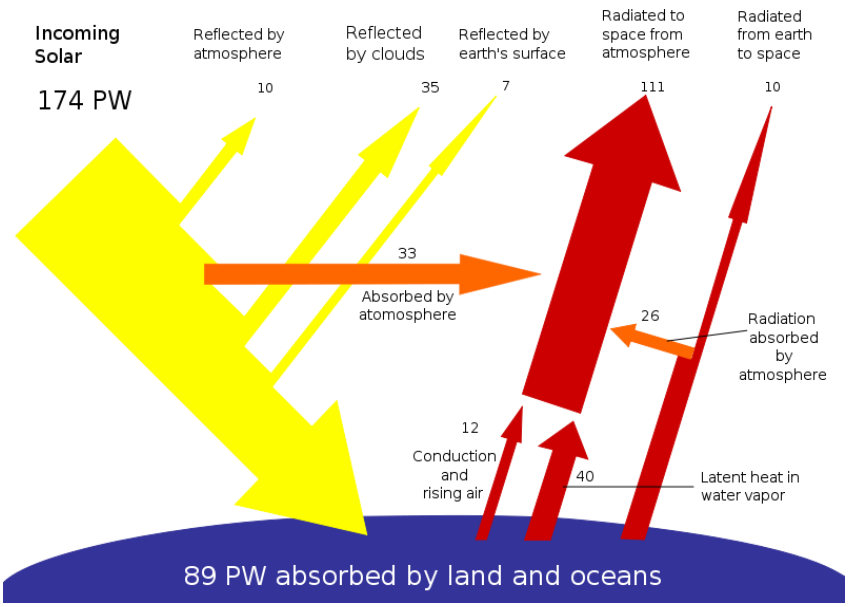

Figure 1.2 The absorptions and reflections of the incoming solar radiation at the surface of earth **[4]**

The total solar energy absorbed by our planet, including the earth's atmosphere, oceans and land, is about 3,850,000 EJ per year **[2]**. In 2002, the solar energy absorbed by earth in one hour was more than the world energy consumption in that year **[3, 5]**. Photosynthesis accumulates about 3,000 EJ per year in the form of biomass **[6]**. Consequently the total solar energy reaching our planet surface is so substantial that it is about twice as much as the amount of energy generated from all of the non-renewable resources on our planet, including oil, coal, natural gas and so on **[7]**.

From the table of yearly solar fluxes and human energy consumption, it can be seen that renewable energy, including solar, wind and biomass energy, would be sufficient to

our energy needs. However the widely use of biomass has a negative effect on global warming and would increase food prices dramatically [8]. As intermittent energy resources, solar and wind energy cannot be used to produce electricity constantly. Solar energy can be applied in various levels worldwide. It varies with the geographical locations and the most abundant solar energy is near the equator [9].

Table 1.1 Yearly solar fluxes and human energy consumption [4]

Wind	2,250 EJ [10]
Solar	3,850,000 EJ [2]
Biomass	3,000 EJ [6]
Primary energy use (2005)	487 EJ [11]
Electricity (2005)	56.7 EJ [12]

1.1.2 Solar cells

Solar cell is a kind of solid state device which is designed to directly convert sunlight into electricity based on photovoltaic effect. The development of solar cell originated from the French physicist Antoine-César Becquerel in 1839. Becquerel discovered photovoltaic effect while doing experiments with a solid electrode in an electrolyte solution. He noticed that the voltage increased when light fell on the electrode. Almost half a century later, Charles Fritts installed the first solar cell using junctions, by coating the semiconductor selenium with an ultrathin, almost transparent gold layer. However this kind of solar cell was very inefficient, with only less than 1 % of the absorption of light into electricity. The photovoltaic effect could be finally explained with the outstanding theoretical work of Albert Einstein in 1905 (for which he received the Nobel Prize). He suggested that electrons were emitted from a solid due to

the absorption of “light quanta” - now called photons. At present, the photovoltaic effect, by which the sunlight converts into electricity in classical semiconductor devices, crystalline or polycrystalline silicon junctions, is well understood. Nowadays, crystalline silicon solar cells dominate the PV market, holding nearly 80% of the share. Semiconductor thin film technologies, such as amorphous silicon thin film, CdTe, and CIGS (Cu, In, Ga, Se) account for the rest of market share.

1.1.3 Working principle of solar cells based on p-n junctions

When photons hit the solar cells, they will be absorbed by semiconductor materials such as silicon. The energy will be transferred from photons to electrons when photons are absorbed in the silicon crystal lattice. Generally, these electrons are in the valence band, which are bound tightly in the covalent bonds, forming with neighboring atoms, and hence not easy to lose. After receiving the energy from photons, electrons were excited from the valence band into the conduction band, where it is able for them to move easily around within semiconductor. After losing an electron, a hole formed in the covalent bond where the electron occupied previously. The electrons bonded in neighboring atoms are able to move into the hole due to the missing covalent bond, forming another hole correspondingly. By this way, a hole can move easily through the crystal lattice. In short, mobile electron-hole pairs were formed in the semiconductor when photons were absorbed. However, it will happen only when the energy transferred from a photon to an electron is greater than that of the band gap. If so, the electron would be excited from the valence band into conduction band.

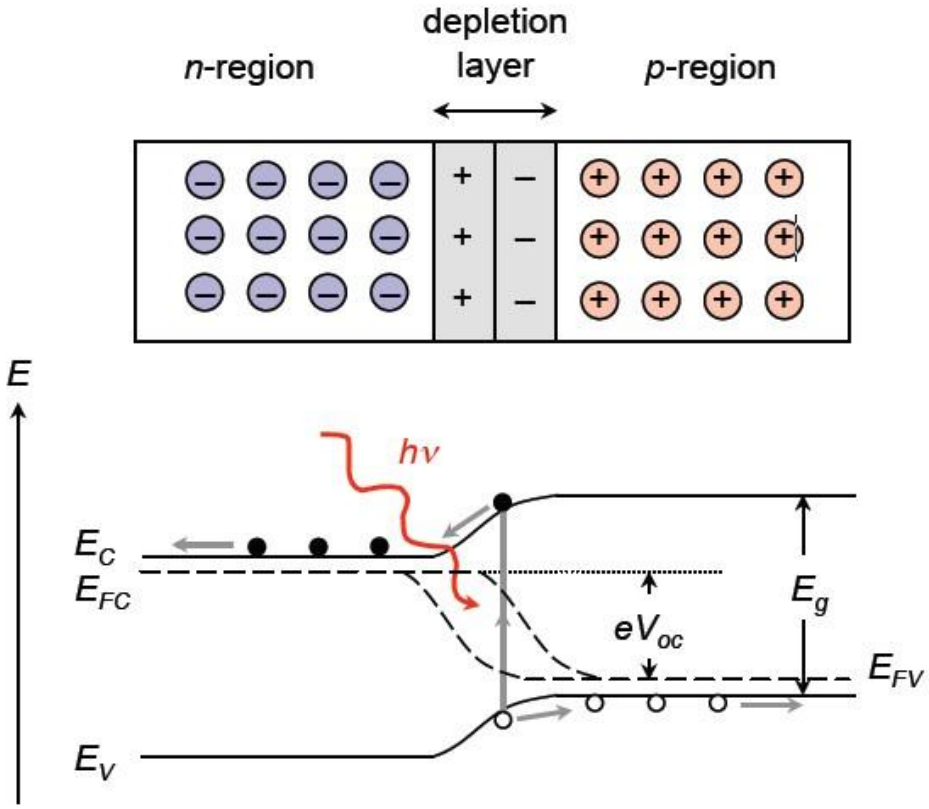

Figure 1.3 Energy band diagram of silicon solar cell **[13]**

Commonly the solar cell is well known as a large p-n junction made of silicon, as shown in **Figure 1.3**. In silicon by diffusing an n-type dopant, like phosphorus into one side of p-type wafer, p-n junctions of solar cells can be made. Then the electrons excited from covalent band to conduction band when the solar cell absorbed the photons, would diffuse from the region of high electron concentration, namely the n-type side of the junction, into the region where the electron concentration is low, namely the p-type side of the junction. On each side of the p-n junction, there is an electric field which makes the electrons diffuse across the p-n junction, without being recombined with holes on the p-type side. Also this electric field forms a diode which promotes charge flow, named

drift current. Because the region where electrons and holes diffuse across has no longer any mobile charge carriers, it is called the depletion region, also known as space charge region.

1.1.4 Solar cell materials

Semiconductors are usually used for the construction of photovoltaic cells **[14-15]**. The most commonly used semiconductor material for solar cells is silicon. Several forms of silicon are used for the construction, such as single-crystalline, multi-crystalline and amorphous. Besides, apart from silicon, other materials including III-V materials can also be used to build solar cells, such as CdTe, CIGS and GaAs solar cells.

1.1.5 Solar cell markets

Solar energy markets show significant annual growth in the last decade, as shown in **Figure 1.4**. Renewable energies oriented business seems to have reached a certain degree of maturity, i.e. moving from governmentally subsidized activity towards a truly market steered industry. Photovoltaic markets clearly have two mainstreams. One is to produce electricity as cheaply as possible and the other is to maximize the performance of the solar energy system at the moderate level of costs.

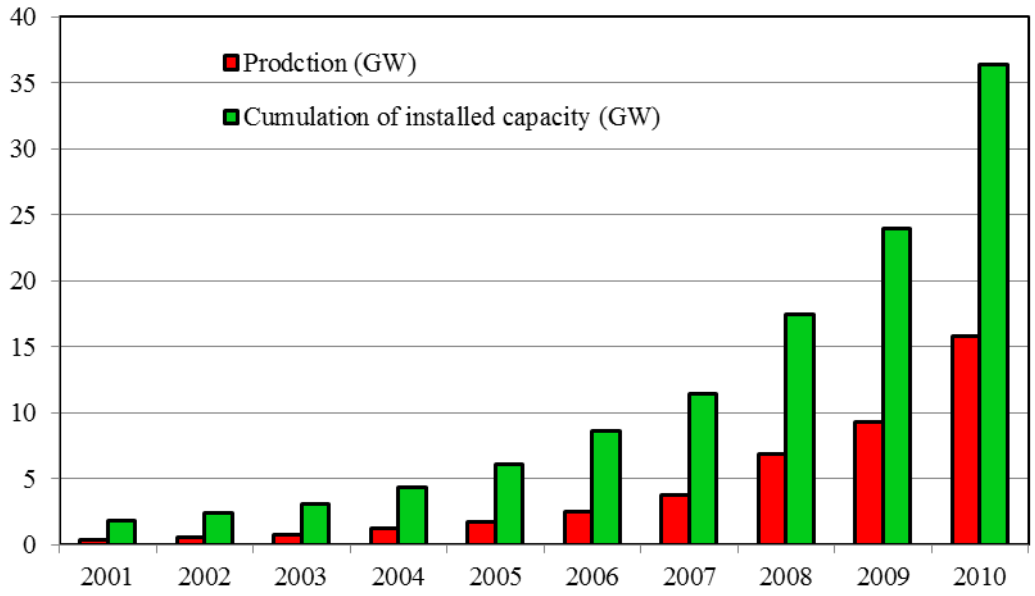

Figure 1.4 Annual production and cumulation of installed PV capacity **[16]**

1.2 Dye-sensitized solar cells (DSSCs)

1.2.1 The history and background of DSSCs

The history of DSSCs can be traced back to the late 1960s **[17-18]**. At that moment, a compact single crystal zinc oxide layer was coated onto the transparent conductive oxide (TCO) glass as the photoanode and then it was sensitized by natural dyes such as chlorophyll to fabricate the first generation of DSSC. Here the word "sensitize" means the dye molecules were chemisorbed onto the surface of zinc oxide. When the dye molecule was excited by sunlight, it would inject its charge into the conduction band of zinc oxide. Therefore, DSSC is also called as excitonic solar cell. For the next couple of years lots of efforts were put into the basic research of photoanodes based on zinc oxide single crystals, however, the photo-electric conversion efficiency was poor, no more

than 1%. This is mainly due to the compact single crystal zinc oxide layer can only absorb a monolayer of dye molecules, which restricts the amount of sunlight absorption. After many years of silence, the research and development of DSSCs became active again when Grätzel et al. drastically increased the conversion efficiency up to 7.1%-7.9% **[19]**. The key factor of this breakthrough was that they adopted the nanoporous crystalline titania film as the active layer of photoanode and absorbed Ruthenium-based dyes as the sensitizer. Due to the higher roughness factor (the ratio of actual surface area / geometric surface area) of nanoporous titania electrode, the amount of dye loading was largely increased, which finally improved the light harvesting efficiency. Besides, the Ruthenium-complex dye (N3) was more capable to capture photons in the range of solar spectra. After two years, the research group of Grätzel further increased the conversion efficiency up to 10.0% **[20]**. Since then, the DSSC had attracted considerable attention as it offered the prospect of low cost and relatively high conversion efficiency **[21-33]**. Compared with silicon based solar cells, they do not need "the free of dust" environment, which dramatically reduce the fabrication cost. In 2009, the inventor of DSSC, Prof. Grätzel have been honored the Balzan Prize and in 2010 he received the Millennium Technology Prize, the largest technology prize in the world. Until now the state-of-art record conversion efficiency was 11.5% achieved by a research group in Taiwan **[34]**.

1.2.2 Structures and operation principles

The basic structure of a typical DSSC is shown in **Figure 1.5**, which is composed of three main components: photoanode, electrolyte and counter electrode. Sometimes, people nicknamed DSSCs as sandwich cells.

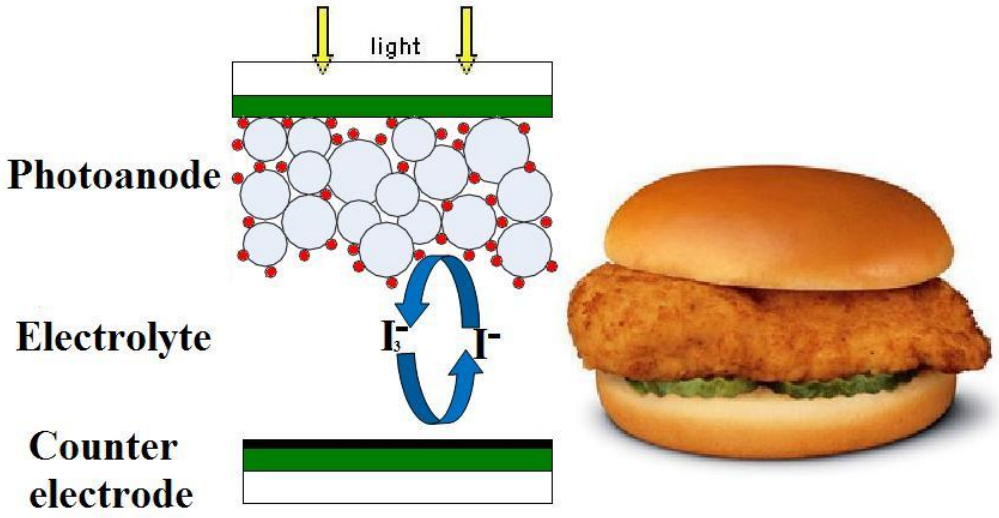

Figure 1.5 The typical sandwich-like structure of DSSC

Photoanode: Photoanode plays the role to capture the photons, inject the light-generated electrons into the conduction band of semiconductor and transport them to the substrate. Usually the photoanode utilizes conductive glass as the substrate covered with a thin layer of nanoporous semiconductor such as titania. The conductive glass consists of a glass sheet deposited with a transparent conductive oxide (TCO) layer such as fluorine-doped tin oxide (FTO) or tin-doped indium oxide (ITO). For solar cell application, the conductive glass is required to have relatively low sheet resistance (no more than 15 Ω/□) and high transparency (better than 85 % visible wavelengths). The porous nanocrystalline titania film is formed by coating a titania paste onto the conductive glass and calcined at 450-550 ℃. Then the photoanode dips into the dye solution to get dye molecules chemisorbed on the semiconductor surface, which is called as sensitization. **Figure 1.6** is the schematic diagram of fabrication process of photoanode.

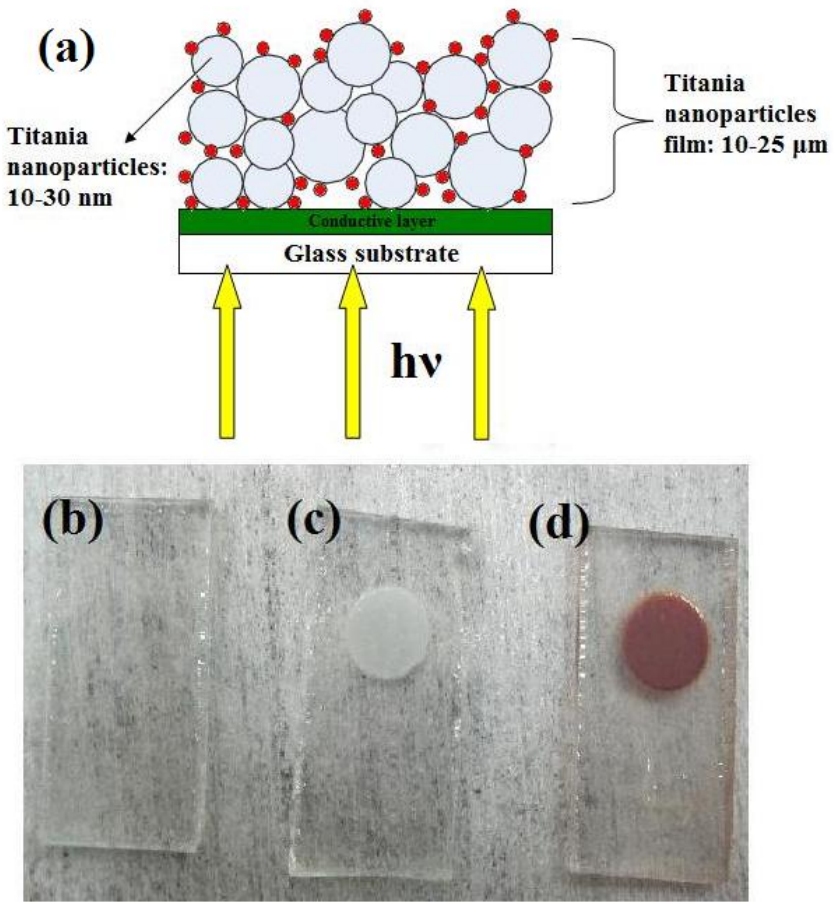

Figure 1.6 The basic structure of photoanode. (a) the schematic diagram of photoanode (b) the transparent conductive glass (FTO) (c) a thin layer of titania nanoparticles film covered on the transparent conductive glass (d) the sensitized titania nanoparticles film

Electrolyte: In terms of viscosity the electrolyte is divided into three types: liquid, quasi-solid state and solid state. The liquid electrolyte is widely used and extensively studied in virtue of its low viscosity, fast ion diffusion, high suffusion into the nanoporous film. Until now, the record conversion efficiency of DSSC is still based on liquid electrolyte due to its supervisor features. Generally the electrolyte is composed of redox couple, solvent and additives. The redox couple typically contains iodide/tri-

iodide ions as redox shuttle to transfer between the dye molecular and the catalyst layer. The solvents usually include nitrile e.g. acetonitrile and esters e.g. ethylene carbonate. The additives such as 4-tert-butylpyridine (TBP) are commonly used to renovate the dye-uncovered surface, which inhibits the dark current, resulting in the enhancement of open circuit voltage **[35]**. **Table 1.2** shows the most commonly used 3 types of liquid electrolyte in DSSCs **[36]**.

Table 1.2 The most commonly used 3 types of liquid electrolytes.

Chemicals	Type 1	Type 2	Type 3
LiI	0.1	_	_
I_2	0.05	0.1	0.03
1,2-dimethyl-3 Propylimidazolium iodide (DMPII)	0.6	0.8	_
Butylmethylimidazolium iodide (BMII)	_	_	0.6
N-methylbenzimidazole (NMBI)	_	0.1	_
4-TBP	0.5	_	0.5
Guanidinium thiocyanate	_	_	0.1
Solvent	Acetonitrile	3-Methoxypropionitrile	Acetonitrile and Valeronitrile (volume ratio: 85:15)

Counter electrode: As well as the photoanode, typically the counter electrode also adopts conductive glass as the substrate coated with a thin film of catalyst layer, as

illustrated in **Figure 1.7**. The catalyst layer plays a part in reducing the tri-iodide ions to iodide ions. Currently, the most commonly used catalyst for DSSC research is platinum mainly due to its excellent catalytic properties. Although the required amount of platinum to catalyze the reaction is very little, no more than 5-10 μg/cm^2 **[20]**, since platinum is also a precious metal, it is not suitable for large scale application. Grätzel et al. **[37]** found that carbon was also a good candidate to catalyze the reaction although it was not as efficient as platinum. It is worthy of being mentioned that recently the conversion efficiency of DSSC using carbon as the catalyst achieved 9% which is a promising result **[38]**.

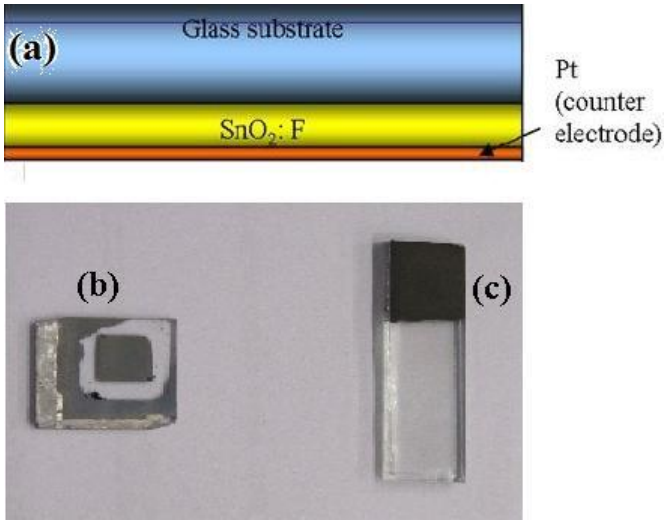

Figure 1.7 The basic structure of counter electrode. (a) the schematic diagram of counter electrode. (b) a Pt layer covered on the FTO glass. (c) a carbon layer covered on the FTO glass

The operating principle of the DSSC is depicted in **Figure 1.8**. The detailed steps of photons to electrons are as follows:

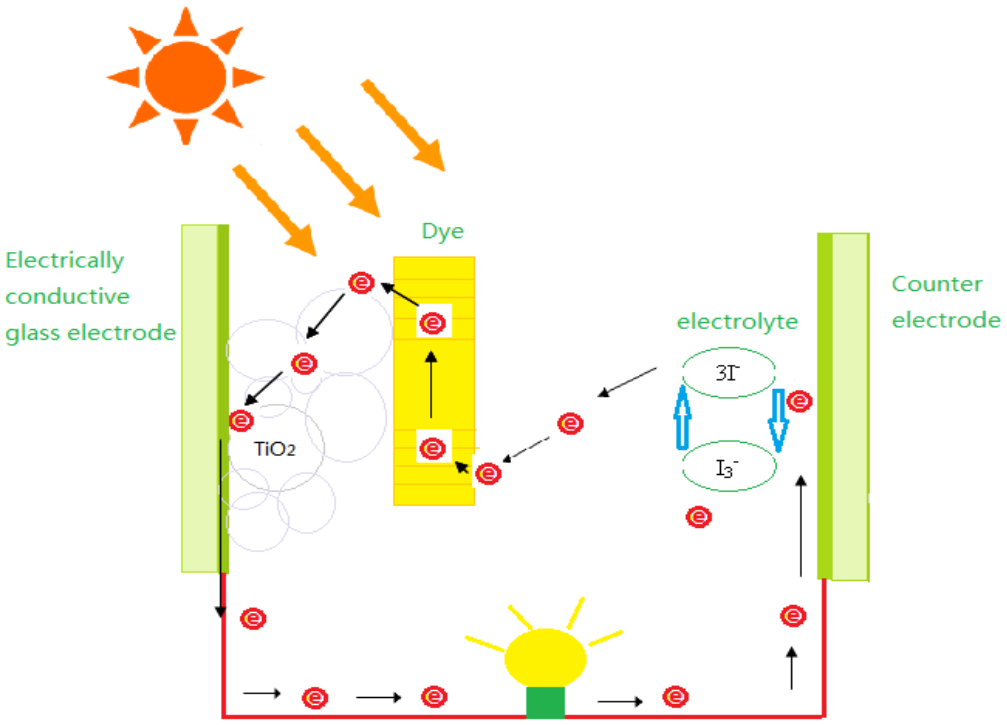

Figure 1.8 The operating principle of DSSCs

1. Excitation: Firstly the surface anchored dye molecule in the ground state (*S*) is sensitized by absorbing the incident photon ($h\nu$) to the excited state (*S**).

$$S + h\nu \rightarrow S^* \tag{1.1}$$

2. Injection: As the dye molecule in the excited state (*S**) is not stable, it injects one electron into the conduction band (E_c) of semiconductor, which is occurred in the ultrafast timescale (femtosecond to picosecond). This step is more rapid than the time for the excited dye molecule (*S**) relaxes back to its ground state (*S*).

$$S^* \rightarrow S^+ + e^- \text{ (conduction band of semiconductor)} \tag{1.2}$$

$$S^* \rightarrow S \tag{1.3}$$

3. Percolation: The injected electrons in the conduction band of semiconductor are finally percolated into the substrate of photoanode such as the conductive glass and collected to the external circuit. Finally through the external circuit, the electrons are gathered on the counter electrode.

$$e^-\text{ (conduction band of semiconductor)} \rightarrow e^-\text{ (substrate)} \tag{1.4}$$

4. Dye Regeneration

The positive dye cation (S^+) is regenerated by iodide ions (I^-) in the electrolyte in a few microseconds. On the contrary, the back reaction for the dye cation reduced by injected electrons in the conduction band of semiconductor occurs in the millisecond and is consequently several orders of magnitude slower than the previous one. This big difference caused the efficient charge separation in the DSSCs.

$$S^+ + 3I^- \rightarrow S + I_3^- \tag{1.5}$$

$$S^+ + e^-\text{ (conduction band of semiconductor)} \rightarrow S \tag{1.6}$$

5. Electrolyte regeneration: The tri-iodide ions (I_3^-) diffuse to the counter electrode and then are reduced by the electrons gathered on the counter electrode into iodide ions (I^-). This step is the predominant process while there are two other back reactions. One is the reduction by the injected electrons in the conduction band of semiconductor. The other is the reduction by the substrate of photoanode due to the uncompleted coverage of semiconductor.

$$I_3^- + 2e^-\text{ (counter electrode)} \rightarrow 3I^- \tag{1.7}$$

$I_3^- + 2e^-$ (conduction band of the semiconductor) $\rightarrow 3I^-$ (1.8)

$I_3^- + 2e^-$ (the substrate of photoanode) $\rightarrow 3I^-$ (1.9)

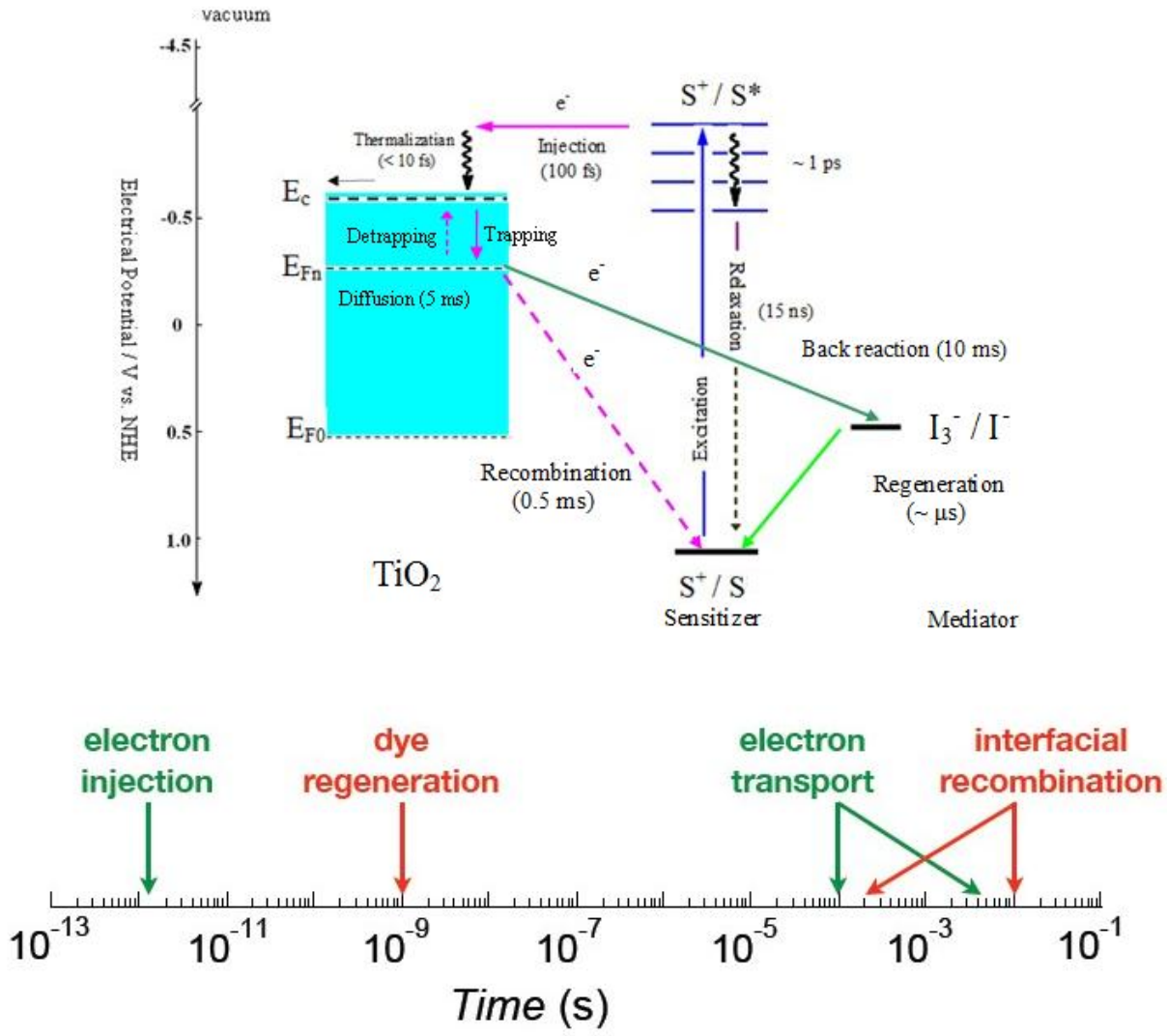

Figure 1.9 Energy diagram of the DSSC showing the dynamics of different electron transfer processes **[39-42]**

Overall, the DSSC converts light energy into electrical energy without any permanent change of chemicals in the system. As illustrated in **Figure 1.9**, the

photovoltaic conversion in DSSCs is operating on the basis of balanced interplay of different kinetics, which distinguishes DSSCs from conventional p-n junction solar cells that utilize the built-in electric field to separate the carriers and holes. The difference between DSSCs and p-n junction solar cells are summarized in **Table 1.3**. At dark, the Fermi level of electrons in the semiconductor is in equilibrium with the energy level of the electrolyte redox couple (E_{redox}). When the semiconductor is illuminated under open-circuit condition, the Fermi level of the electrolyte redox couple remains unchanged, whereas the Fermi level of the semiconductor changes. It is due to additional injected electrons from the excited dye molecules defining a quasi-Fermi level, E_{Fn}, which is mainly influenced by the charge generation rate in the semiconductor, the transport rate and the recombination rate. The open circuit voltage (V_{oc}) generated under solar illumination is determined by the gap between E_{Fn} and E_{redox}. For DSSC using titania as the semiconductor, the V_{oc} is usually around from 0.6 V to 0.9V.

Table 1.3 The difference between DSSC and p-n junction solar cell **[43-44]**

DSSC	p-n junction solar cell
No significant space charge region	Charge separation in space charge field
Grain surface maximization necessary up to 10^3 times increased contact area	Grain boundaries, high recombination probability at junction should be avoided or minimized
Existence (and importance) of an electric field not established	Photovoltage from neutralization of internal built-in field
Carriers of only one type are present in the semiconductor	Both minority and majority carriers are present in the semiconductor

1.2.3 Advantage and weakness

Compared with traditional silicon based solar cells, the DSSCs have the following advantages:

Facile fabrication process and low manufacture cost: Compared with silicon solar cells, the fabrication process of DSSCs is simple which does not need the free of dust environment. Besides, most of the raw materials of the device are cheap and abundant, such as titania. In spite of the usage of expensive metals such as Pt and Ru, the total amount is very little. The industrial chain is relatively short and easy to realize low cost commercialization. It is estimated that the total cost of DSSC is only 10%-20% of that of the silicon cells **[36]**.

Environmental friendly: During the production of crystalline silicon solar cells, the raw material silicon tetrachloride is extremely poisonous and easy to leak. In addition, the whole process requires high temperature and vacuum processing and would consume large amount of energy. By comparison, the titania utilized as the photoanode material is nontoxic and stable, which has already been widely used as the white pigment in toothpaste, paint and food additives. Consequently DSSCs have no negative effect on the environment and there is no recovery problems existed.

Better relative performance at higher temperatures: Compared to monocrystalline silicon or polycrystalline silicon solar cells, the peak output power of DSSCs depends much less on panel temperature and drops much less with the increase of temperature **[45]**.

Less sensitive to angle of incidence: It is reported **[46]** that DSSC modules yearly generated 10–20% more electricity than conventional crystalline silicon modules of the same rated output power. DSSCs are less sensitive to the angle of incident light and have better performance in diffuse light especially in the time of morning and evening.

Multiple colors and adjustable transparency: As the dye molecules can be designed to different colors, the colorful DSSC panels could be utilized on the building integrated photovoltaic (BIPV) to enhance the architectural appeal. Furthermore, by controlling the thickness of semiconductor materials, the DSSCs can be designed to transparent, semitransparent or opaque devices.

Until now only a few companies have realized the commercialization of the DSSCs, such as Dyesol in Australia, Solaronix in Switzerland and G24i in Britain. The main reasons hampered the progress of DSSCs is summarized briefly as follows:

The large-scale of device size: Currently most of the DSSCs including the commercialized ones employ TCO glass such as FTO glass as the substrates. As the sheet resistance of FTO glass is usually around 8 Ω/□ to 15 Ω/□, in order to maintain relatively low resistive losses, the active area of one single cell should be no more than 1 cm^2 **[47]**. To collect the current, one approach is to utilize metal figures to connect all the single cells together. However, due to the corrosivity of iodide based electrolyte, it is essential to protect these silver gridlines by some kind of polymer materials. As the size of the protection section is nearly the same as the size of a single cell, the total active area of the DSSC module is largely reduced **[48]**. On the other hand, the protection of silver grid lines would also increase the fabrication cost. Although some research group

tried to replace one side of the FTO glass with metal substrate and achieved better photovoltaic performance **[49-54]**, however, due to the opacity of the metal substrate, it was hard to realize all metal substrates based DSSCs.

The collection efficiency of photo generated electrons: Since Prof. Grätzel largely increased the conversion efficiency of DSSCs in 1991, for most of the study, the nanocrystalline titania nanoparticles film has been used as the active layer of photoanode. Although the 3D networks of interconnected nanoparticles could provide sufficient specific area to anchor the light-harvesting dye molecules, the trap sites in the surface defects and grain boundaries can lower the electron transportation speed and increase the recombination process. Consequently, one photo generated electron has to encounters millions of trapping/detrapping events at the trap sites in the titania nanoparticles film before it could reach the FTO glass **[55-56]**. Recently the highly ordered, self-organized titania nanotube arrays obtained through electrochemical anodization of Ti foil have been shown to offer direct electrical pathways for rapid collection of electrons **[57-59]**. However due to the opacity of Ti foil, the highly ordered titania nanotube arrays can be only applied on backside illuminated DSSCs **[60]**. In the backside illumination configuration, the incident light will be attenuated by the platinized counter electrode and the electrolyte, which lowers the sunlight utilization and restricts the efficiency.

The sealing of liquid electrolyte: Nearly all the high efficient DSSCs are based on liquid electrolyte. Due to the volatility of solvents, for long term application, it is a critical challenge to prevent the leakage of electrolyte. Some research attempts to

replace the liquid electrolyte into solid electrolyte, however the conversion efficiencies were much lower and the attenuating effect is significant.

The wide band absorption: Until now, the main absorption region of the as developed dye molecules is limited in visible light. To increase the light harvesting efficiency, it is essential to board the light spectrum functionality of DSSCs by design new dye molecules.

1.2.4 Objectives

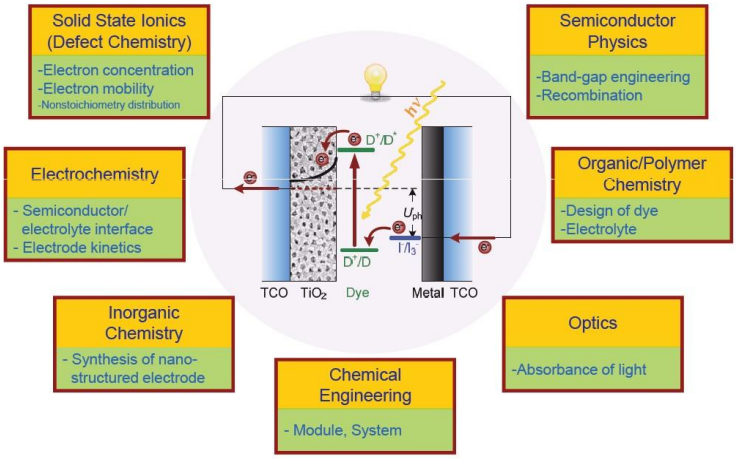

Figure 1.10 The relationship between DSSC and other subjects

As illustrated in **Figure 1.10**, the DSSC is the combination of multidisciplinary science. It is hard for a research group to investigate all the remaining problems of the device. Based on the existing conditions of our laboratory, new structures of the DSSCs were proposed in this thesis based on all metal Ti substrates to solve the high sheet resistance of conventional TCO substrates. Besides, combined with in situ anodization technique, the titania nanoparticles film is replaced by highly ordered titania nanotube

arrays to increase the charge collection efficiency. The objectives of this thesis are summarized as follows:

(i) Develop new-structure DSSCs for advanced solar cell development.

(ii) Realize the front-side illuminated DSSCs based on all metal substrates to exhibit both higher light harvesting efficiency and lower sheet resistance.

(iii) Develop the front-side illuminated DSSCs based on highly ordered titania nanotube arrays to increase the electron collection efficiency without light absorption loss.

(iv) Increase the affinity between the substrate and titania film by employing in situ synthesis technique.

(v) Scale up the size of DSSC without decreasing the photovoltaic conversion efficiencies.

(vi) Absorb more diffuse sunlight by utilizing the 3 dimensional (3D) spaces to increase photo-generated current.

1.2.5 Methodology

First, before any further development of new structures of DSSCs, it is essential to repeat and familiarize the fabrication process of conventional structure DSSCs to master the key points which would influence the photovoltaic performance of the device. Only when the relevant photovoltaic parameters reach the same level of data from international publications, it makes sense to investigate the possibility of new structures of DSSCs. Otherwise, it is hard to determine the effectiveness of the new structure devices.

Next, based on the experience from the investigation of conventional structure DSSCs, new structure DSSCs would be developed and investigated. For the purpose of reducing the sheet resistance of substrates, all the developed structures should be based on metal substrate. Besides, to overcome the deficiencies of titania nanoparticles film, highly ordered titania nanotubes film was used as the active layer of photoanode. As the titania nanotubes can only be in situ synthesized through the electrochemical anodization of Ti metal, in this study, Ti metal is choosed as the substrates.

The development of new structure DSSCs should include the following points:

(i) Front-side illumination with all metal substrates. This is the primary point as there are already back-side illuminated DSSCs with the photoanode based on metal substrate.

(ii) The operational principles should be reasonable. Before the fabrication of new structure DSSCs, it is necessary to rehearsal the operation steps.

(iii) The output photovoltaic parameters should be at least comparable with that of the conventional DSSCs. This is the evaluation criterion for the significance of the proposed DSSCs.

Finally, the new structure DSSCs would be measured through physical and chemical characterization to investigate their internal properties and to further optimize the photovoltaic parameters.

References

1. US Department of Energy - Energy Information Administration, World Proved Reserves of Oil and Natural Gas, Most Recent Estimates, 2009. http://www.eia.doe.gov/emeu/international/reserves.html
2. V. Smil, 2006. Energy: A Beginner's Guide. *Oxford: Oneworld Publications*, pp. 12.
3. O. Morton, Solar energy: A new day dawning? : Silicon Valley sunrise. *Nature*, 2006. **443:** 19-22.
4. Wikipedia. http://en.wikipedia.org/wiki/Solar_energy
5. N. S. Lewis, and D. G. Nocera, Powering the planet: chemical challenges in solar energy utilization. *Proc Natl Acad Sci U.S.A*, 2006. **103**: 15729-35.
6. Energy conversion by photosynthetic organisms. http://www.fao.org/docrep/w7241e/w7241e06.htm#TopOfPage
7. Exergy Flow Charts，http://gcep.stanford.edu/research/exergycharts.html
8. M. Grunwald, The Clean Energy Scam. http://www.time.com/time/magazine/article/0,9171,1725975,00.html
9. Solarenergybyzip. http://www.solarenergybyzip.com/
10. C. L. Archer, and M. Z. Jacobson, Evaluation of global wind power. *J Geophys Res*, 2005. **110**: D12110.
11. Energy Information Administration, International Energy Annual. *2006.* http://www.eia.gov/pub/international/iealf/table18.xls
12. World Total Net Electricity Consumption (Billion Kilowatthours), 2006. http://www.eia.gov/pub/international/iealf/table62.xls.
13. S. M. Sze. Semiconductor devices, physics and technology. John Wiley & Sons, New York, 2nd edition, 2002.

14. H. Shen, and Z. Q. Zeng, 2009. Solar photovoltaic technology. Chemical Industry Press.
15. K. L. Chopra, P. D. Paulson, and V. Dutta, Thin-film solar cells: An overview. *Prog Photovoltaics*, 2004. **12**: 69-92.
16. K. Analytics, Solar Photovoltaic Cell Market Report. 2010 Edition, pp.115.
17. H. Gerischier, H. Tributsch, and B. Bunsen-ges, Photocell using covalently-bound dyes on semiconductor surfaces. *Phys Chem*, 1968, **72**: 437-45.
18. H. Tributsch, H. Gerischer, and B. Bunsen-ges, The use of semiconductor electrodes in the study of photochemical reactions. *Phys Chem*, 1969. **73**: 251-60.
19. B. Oregan, and M. Gratzel, A low-cost, high-efficiency solar cell based on dye-sensitized colloidal TiO_2 films. *Nature*, 1991. **353**: 737-40.
20. M. K. Nazeeruddin, A. Kay, I. Rodicio, R. Humphry-Baker, E. Mueller, P. Liska, N. Vlachopoulos, and M. Graetzel, Conversion of light to electricity by cis-X2bis (2, 2'-bipyridyl-4, 4'-dicarboxylate) ruthenium(II) charge-transfer sensitizers (X = Cl-, Br-, I-, CN-, and SCN-) on nanocrystalline titanium dioxide electrodes. *J Am Chem Soc*, 1993. **115**: 6382-90.
21. K. Sayama, H. Sugihara, and H. arakawa, Photoelectrochemical properties of a porous Nb_2O_5 electrode sensitized by a ruthenium dye. Chem Mater, 12998. **10**: 3825-32.
22. K. Equchik, H. Koga, K. Sekizawa, and K. Sasaki, Nb_2O_5-Based Composite Electrodes for Dye-Sensitized Solar Cells. *J Ceram Soc of Jap*, 2000. **108**: 1067-71.

23. K. Hara, T. Korguchi, T. Kinoshita, S. Kazuhiro, S. Hideki, and A. Hironori, Highly efficient photon-to-electron conversion with mercurochrome-sensitized nanoporous oxide semiconductor solar cells. *Sol Energ Mat Sol C*, 2000. **64**: 115-34.

24. K. Hara, T. Korguchi, T. Kinoshita, S. Kazuhiro, S. Hideki, and A. Hironori, Highly Efficient Photon-to-Electron Conversion of Mercurochrome-sensitized Nanoporous ZnO Solar Cells. *Chem Lett*, 2000. **29** : 316-17.

25. K. Keis, J. Lindgren, S. Lindquist, and A. Hagfeldt, Studies of the adsorption process of Ru complexes in nanoporous ZnO electrodes. *Langmuir*, 2000. **16**: 4688-94.

26. T. N. Rao, and L. Bahadur, Photoelectrochemical Studies on Dye-Sensitized Particulate ZnO Thin-Film Photoelectrodes in Nonaqueous Media. *J Electrochem Soc*, 1997. **144**: 179-85.

27. G. Redmond, D. Fitzmaurice, and M. Graetzel, Visible light sensitization by cis-bis(thiocyanato) bis(2,2'-bipyridyl-4,4'-dicarboxylato)ruthenium(II) of a transparent nanocrystalline ZnO film prepared by sol-gel techniques. *Chem Mate*r, 1994. **6**: 686-91.

28. H. Rensmo, K. Keis, H. Lindstrom, S. Södergren, A. Solbrand, A. Hagfeldt, and S.-E. Lindquist, High light-to-energy conversion efficiencies for solar cells based on nanostructured ZnO electrodes. *J Phys Chem B*, 1997. **101**: 2598-2601.

29. C. Nasr, S. Hotchandani, and P. V. Kamat, Role of Iodide in Photoelectrochemical Solar Cells. Electron Transfer between Iodide Ions and Ruthenium Polypyridyl Complex Anchored on anocrystalline SiO_2 and SnO_2 Films. *J Phys Chem B*, 1998. **102**: 4944-51.

30. S. Nasr, P. V. Kamat, and S. Hotchandani, Photoelectrochemistry of composite semiconductor thin films. II. Photosensitization of SnO_2/TiO_2 coupled system with a ruthenium polypyridyl complex. *J Phys Chem B*, **102**: 10047-56.
31. J. E. Moser, and M. Gratzel, Excitation wavelength dependence of photoinduced charge injection at the semiconductor-dye interface: Evidence for electron transfer from vibrationally hot excited states. *Chimia*, 1998. **52**: 160-62.
32. S. Burnside, J. E. Moser, K. Brooks, and M. Gratzel, Nanocrystalline mesoporous strontium titanate as photoelectrode material for photosensitized solar devices: Increasing photovoltage through flatband potential engineering. *J Phys Chem B*, 1998. **103**: 9328-9332.
33. J. He, H. lindstrom, A. Hagfeldt and S. E. Lindquist, Dye-sensitized nanostructured p-type nickel oxide film as a photocathode for a solar cell. *J Phys Chem B*, 1998. **103**: 8940-43.
34. C.Y. Chen, M. Wang, J. Y. Li, N. Pootrakulchote, L. Alibabaei, C. H. Ngoc-le, J. D. Decoppet, J. H. Tsai, C. Gratzel, C. G. Wu, S. M. Zakeeruddin, and M. Gratzel, Highly Efficient Light-Harvesting Ruthenium Sensitizer for Thin-Film Dye-Sensitized Solar Cells. *ACS Nano*, 2009. **3**: 3103-09.
35. G. Boschloo, L. Ha¨ggman, and A. Hagfeldt, Quantification of the effect of 4-tert-butylpyridine addition to I^-/I_3^- redox electrolytes in dye-sensitized nanostructured TiO_2 solar cells. *J Phys Chem B*, 2006. **110**: 13144-50.
36. A. Hagfeldt, G. Boschloo, L. Sun, L. Kloo, and H. Pettersson, Dye-Sensitized Solar Cells. *Chem Rev*, 2010. **110**: 6595-63.

37. A. Kay, and M. Gra¨tzel, Low cost photovoltaic modules based on dye sensitized nanocrystalline titanium dioxide and carbon powder. *Sol Energ Mater Sol C*, 1996. **44** : 99-117.
38. S. Ahmad, J. H. Yum, H. J. Butt, M. K. Nzaeeruddin, and M. Gra¨tzel, Efficient Platinum-Free Counter Electrodes for Dye-Sensitized Solar Cell Applications. *Chem Phys Chem*, 2010. **11**: 2814 – 19.
39. S. A. Haque, E. Palomares, B. M. Cho, A. N. M. Green, N. Hirata, D. R. Klug, and J. R. Durrant, Charge separation versus recombination in dye-sensitized nanocrystalline solar cells: the minimization of kinetic redundancy. *J Am Chem Soc*, 2005. **127**: 3456-62.
40. J. E. Kroeze, N. Hirata, S. Koops, M. K. Nazeeruddin, L. Schmidt-Mende, M. Gratzel, and J. R. Durrant, Alkyl Chain Barriers for Kinetic Optimization in Dye-Sensitized Solar Cells. *J Am Chem Soc*, 2006. **128**: 16376-83.
41. J. N. Clifford, E. Palomares, M. K. Nazeeruddin, M. Gratzel, and J. R. Durrant, Dye dependent regeneration dynamics in dye sensitized nanocrystalline solar cells: Evidence for the formation of a ruthenium bipyridyl cation/iodide intermediate. *J Phys Chem C*, 2007. **111**: 6561-17.
42. E. Palomares, J. N. Clifford, S. A. Haque, T. Lutz, and J. R. Durrant, Control of charge recombination dynamics in dye sensitized solar cells by the use of conformally deposited metal oxide blocking layers. *J Am Chem Soc*, 2003. **125**: 475-82.
43. C.J. Huang, Anodic titanium dioxide layers: synthesis,properties and applications. The Hong Kong Polytechnic University, 2010. P58

44. D. Cahen, G. Hodes, M. Gratzel, J. F. Guillemoles, and I. Riess, Nature of Photovoltaic Action in Dye-Sensitized Solar Cells. *J Phys Chem B*, 2000. **104**: 2053-39.

45. Organic Solar Cells Now Produced in Volume. 2008, Nikkei Electronics Asia. http://techon.nikkeibp.co.jp/article/HONSHI/20080625/153868/

46. T. Toyoda, T. Sano, J. Nakajima, S. Doi, S. Fukumoto, A. Ito, T. Tohyama, M. Yoshida, T. Kanagawa, T. Motohiro, T. Shiga, K. Higuchi, H. Tanaka, Y. Takeda, T. Fukano, N. Katoh, A. Takeichi, K.Takechi, and M. Shiozawa, Low cost photovoltaic modules based on dye sensitized nanocrystalline titanium dioxide and carbon powder. *J Photoch Photobio A*, 2004. **164**: 203-07.

47. A. KAY, and Gratzel, Low cost photovoltaic modules based on dye sensitized nanocrystalline titanium dioxide and carbon powder. *Sol Energ Mater Sol C*, 1996. 44: 99-117.

48. M. Spath, J. van Roosmalen, P. Sommeling, N. van der Burg, H. Smit, D. Mahieu, N. Bakker, and J. Kroon, Reproducible manufacturing of dye-sensitized solar cells on a semi-automated baseline. *Prog Photovolt: Res App*, 2003. **11**: 207-20.

49. Y. Jun, J. Kim, and MG. Kang, A study of stainless steel-based dye-sensitized solar cells and modules. *Sol Energ Mater Sol C*, 2007. **91**: 779-84.

50. M. G. Kang, N. G. Park, K. S Ryu, S. H. Chang, and K. J. Kim, 4.2% efficient flexible dye-sensitized TiO_2 solar cells using stainless steel substrate. *Sol Energ Mater Sol C*, 2006. **90**: 574-81.

51. K. Onoda, S. Ngamsinlapasa, T. Fujieda, and S. Yoshikawa, The superiority of Ti plate as the substrate of dye-sensitized solar cells. *Sol Energ Mater Sol C*, 2007. **91**: 1176-81.

52. S. Kayama, Y. Wakizaka, and K. Kondo, Metal Oxide Dispersion, Metal Oxide Electrode Film, and Dye Sensitized Solar Cell, photoactive electrode. US Patent No 7, 157, 788, 2002.

53. H. Sugihara, K. Hara and K Sayama, et al. Platinum complex for use as sensitizer for semiconductor electrode of solar cell. US Patent No 6, 274, 806, 2000.

54. K. Okada, H. Matsui, T. Kawashima, T. Ezure, and N. Tanabe, 100mm×100 mm large-sized dye sensitized solar cells. *J Photochem Photobiol A: Chem*, 2004. **164**: 193-98.

55. N. Kopidakis, E. A. N. G. Park, J. van de Lagemaat, and A. J. Frank, Ambipolar diffusion of photocarriers in electrolyte-filled, nanoporous TiO2. *J Phys Chem B*, 2000. **104**: 3930-36.

56. G. Kron, T. Egerter, J. H. Werner, and U. Rau, Electronic transport in dye-sensitized nanoporous TiO_2 solar cells-comparison of electrolyte and solid-state devices. *J Phys Chem B*, 2003. **107**: 3556-64.

57. J. R. Jennings, A. Ghicov, L. M. Peter, P. Schmuki, and A. B. Walker, Dye-Sensitized Solar Cells Based on Oriented TiO_2 Nanotube Arrays: Transport, Trapping, and Transfer of Electrons. *J Am Chem Soc*, 2008. **130**:13364-72.

58. D. Kim, A. Ghicov, S. P. Albu, and P. Schimuki, Bamboo-Type TiO_2 Nanotubes: Improved Conversion Efficiency in Dye-Sensitized Solar Cells. *J Am Chem Soc*, 2008. **130**:16454-55.

59. J. M. Macak, H. Tsuchiya, and P. Schmuki, High-aspect-ratio TiO_2 nanotubes by anodization of titanium, *Angew Chem Int Edit*, 2005. **44**: 2100-02.

60. M. Paulose, K. Shankar, O. K. Varghese, G. K. Mor, B. Hardin, and C. A. Grimes, Backside illuminated dye-sensitized solar cells based on titania nanotube array electrodes. *Nanotechnology*, 2006. **17**: 1446-48.

CHAPTER 2 Experimental methods

2.1 Characterization tools

2.1.1 Scanning electron microscopy (SEM)

Scanning electron microscopy (SEM) images were recorded with the JEOL Model JSM-6490 as shown in **Figure 2.1**. It can image up to 300,000X with high resolution of 3nm at an electron energy of 12 keV. The instrument is also equipped with an energy dispersive X-ray spectroscopy (EDX) detector to make the X-ray analysis of elements down to boron.

Figure 2.1 The Scanning electron microscopy (JEOL Model JSM-6490)

In this study, some of the morphology information including the diameters of titania nanotubes, the film thickness of anode is directly obtained by SEM observation. To

increase the resolution of SEM images, a thin layer of gold is coated onto the surface of the sample to increase the conductivity. Besides, the sample is also bridged with the specimen disk.

2.1.2 X-ray diffraction (XRD)

The crystal forms of the titania film is analyzed based on the Bruker D8 Advance X-ray diffraction (XRD) as shown in **Figure 2.2** to detect the diffraction peaks by using Cu-Kα (λ=0.1540 nm) radiation with Ni filter. The rest parameters are set as: current: 40 mA; scan mode: step scan; step size: 0.02 deg; scattering slit: 2mm; receiving slit: 1mm; voltage: 40 kV

Figure 2.2 X-ray Diffractometer (Bruker D8 Advance)

2.1.3 Spectrophotometer

Spectrophotometer is an instrument which can measure the absorbance of a sample at the certain range of wavelength. All the dye loading measurements in this thesis are

based on the ultraviolet-visible spectroscopy spectrophotometer (HITACHI, U-4100) as shown in **Figure 2.3**. The range of scanning wavelength is between 200nm to 1200nm with the scan rate of 120 nm / min. The detailed processes to measure the dye loadings are as follows:

Figure 2.3 Ultraviolet-visible spectroscopy spectrophotometer (HITACHI, U-4100)

(i) Dissolve 3mg dye molecules in a 100 ml 0.1 M NaOH solution and then measure its absorbance spectrum from 200nm to 800nm. For N719 dye, the maximum absorbance wavelength is at 499.5 nm.

(ii) Dilute the as prepared dye solution into five different concentration and then measure their absorbance at the maximum absorbance wavelength such as 499.5nm.

(iii) Establish calibration plot of dye solution according to the data of process ii.

(iv) Desorb the dye molecules from the unknown sample and measure its absorbance at the maximum absorbance wavelength.

(v) Calculate the concentration of dye solution according to the calibration plot.

2.1.4 *I-V* measurement

For photovoltaic conversion efficiency measurement, a solar simulator (Newport Oriel 91192) is served as the light source. The light intensity was adjusted with a reference standard Si cell to 1 sun light intensity of 100 mW cm^{-2}. The *I-V* curves were measured with a Keithley 2400 source meter. The system is shown in **Figure 2.4** and the main equipments is shown in **Figures 2.5** and **2.6**, respectively.

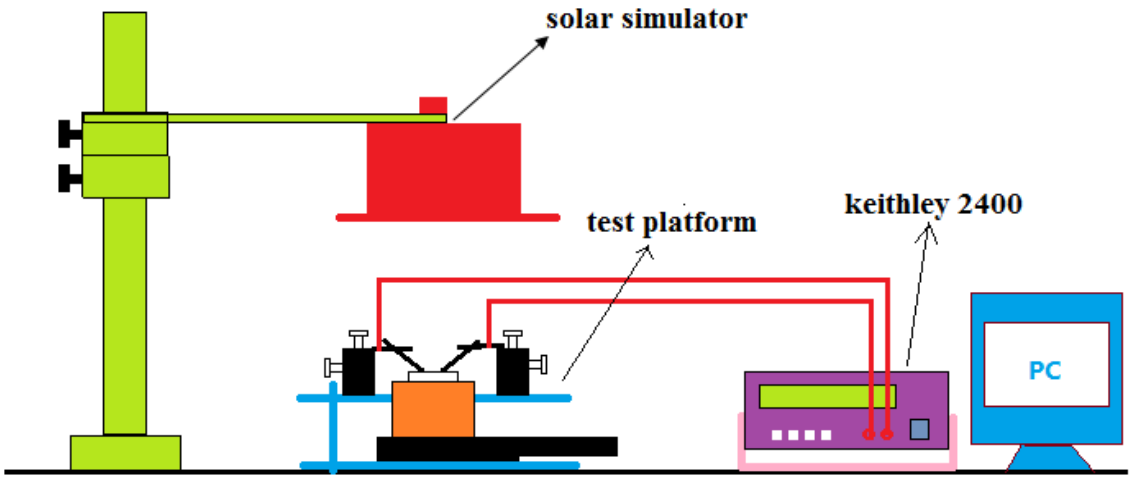

Figure 2.4 Photovoltaic measurement system

Figure 2.5 Solar simulator (Newport Oriel 91192)

Figure 2.6 *I-V* tracer (Keithley 2400)

The scanning range is from -1 V to +1 V with the scan rate of 0.05 V/s. The useful data is in the range of fourth quadrant. A typical *I-V* curve of a DSSC is shown in **Figure 2.7**. From the *I-V* characteristic curve, open circuit voltage (V_{oc}), short circuit

current (I_{sc}) and the maximum output power could be achieved, which determine the fill factor (*ff*) and power conversion efficiency (η) of a solar cell. By comparing these parameters, the photovoltaic properties of a DSSC can be evaluated.

Short circuit current (I_{sc}): the current of the solar cell if no potential is applied.

Open circuit voltage (V_{oc}): open circuit voltage corresponds to the potential when there is no current in the DSSC.

Fill factor (ff): the ratio between the maximum power and the product of the short circuit current and the open circuit potential.

$$FF = \frac{I_{\max} V_{\max}}{I_{sc} V_{oc}} \tag{2.1}$$

Photo to electric energy conversion efficiency (η): the ratio between the maximum output power of a DSSC and the incident solar radiation (P_I) on it.

$$\eta = \frac{P_{\max}}{P_I} = \frac{I_{\max} V_{\max}}{P_I} = \frac{FFI_{sc} V_{oc}}{P_I} \tag{2.2}$$

From Equation 2.2 it could be seen that η is the function of I_{sc}, V_{oc} and *ff*. Consequently to increase the conversion efficiency η, it is essential to optimize these parameters.

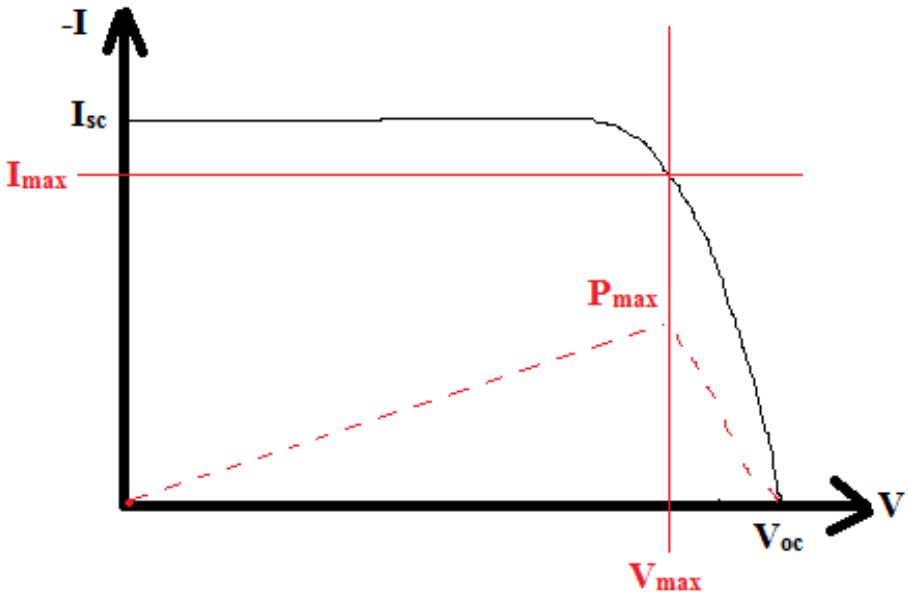

Figure 2.7 *I-V* curves of a typical DSSC under illumination

2.2 Fabrication tools

2.2.1 Film coating

The screen printing machine is used for the coating of titania film onto the TCO glass. The patterns are made of 42 circles which can be seen in **Figure 2.8**. The diameter of each hole is 6mm. The chassis under the screen can be connected with a vacuum air pump to absorb the TCO glass. The vernier adjustment knobs are used to fix position of the screen for the purpose of repeating print.

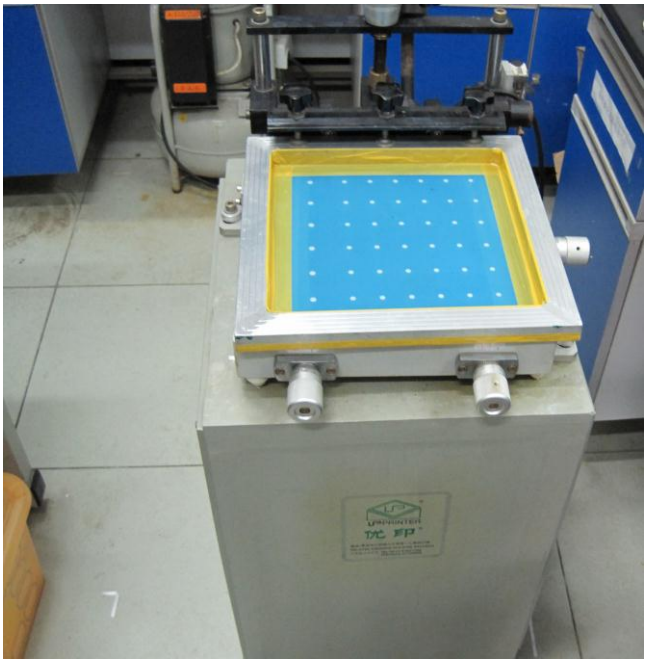

Figure 2.8 The screen printing machine (UP-S7090M)

2.2.2 Device sealing

As shown in **Figure 2.9 (a)**, the main part of a hot press (JCH-C602H) is its upper and lower pressure plate. By connecting the hot press with a vacuum air pump, which is shown in **Figure 2.9 (b)**, both of the plates could provide positive pressure up to 6.0 MPa. Besides, the temperature of each plate could be adjusted from room temperature to 300 ℃. In this study, for the fabrication of TCO based DSSCs, usually the positive pressure is set as 1.5 MPa and the temperature of upper and lower plate is set as 90 ℃ and 110 ℃, respectively.

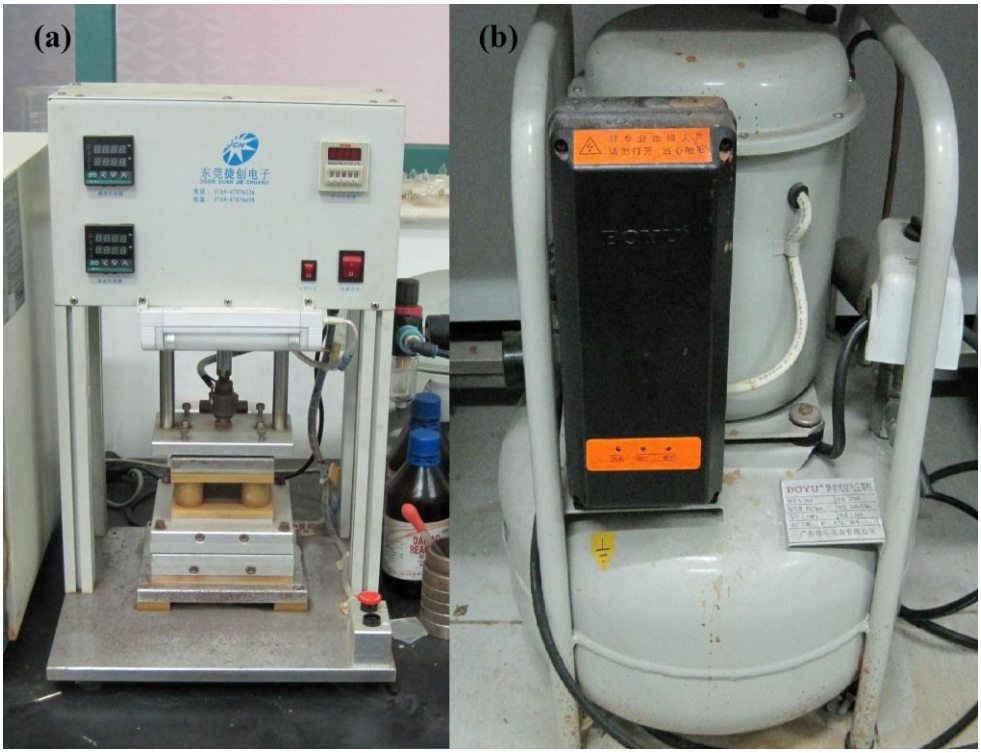

Figure 2.9 The sealing system for the fabrication of DSSCs

2.2.3 Drilling system

To inject electrolytes into the inside of DSSCs, in most of the case it is needed to drill a hole from the substrate of counter electrode (FTO glass). However, for the traditional electric drill it is impossible to achieve a hole with the diameter less than 1mm. Besides, it is hard to control the drill bit during the drilling process and sometimes it is easy to break the FTO glass. Ultrasonic single-needle punch machine is usually used in the jewellery industry to drill a hole on the pearl. By converting ultrasonic wave into mechanical energy, the needle on the machine could give the emery impulse and lead emery to a fixed point of the glass. By many times of sandblasting, a small hole with diameter of 0.8mm could be formed. During the whole process, it is very important

to ensure the movement of water as the sandblasting process would release a large amount of heat.

Figure 2.10 Ultrasonic single-needle punch machine

2.2.4 Glass cutting

As the FTO glass used in this study is based on toughened glass, we adopt the manual glass cutting machine to break them up into specified size. The conductive side should be faced down on a soft substrate during the cutting process to avoid the damage of FTO layer.

Figure 2.11 The manual glass cutting machine (HSRL-400)

CHAPTER 3 Optimization of conventional DSSCs based on TCO substrates

3.1 Introduction

The dye-sensitized solar cell (DSSC), since its energy conversion efficiency was significantly increased to 7% in 1991 **[1]**, has been extensively investigated all around the world. From the structure to materials, nearly every part of the DSSC has been explored in detail by more than dozens of papers. However, until now the limited numbers of record conversion efficiency are still related with Grätzel or his research group, including the latest champion conversion efficiency of 11.5% **[2]**. This is mainly because the DSSC is an intergraded chemical, physical and engineering system. Although some research groups have more advanced techniques on one part of DSSC, i.e. the synthesis of titania **[3-5]**, the development of new dye molecules **[6-8]**, due to their less experience of other parts of the DSSC or the whole fabrication process, they could not increase the conversion efficiency of the DSSC independently. One solution is to work with Grätzel's group **[9-10]**; however, it is impossible for all the DSSC related research groups such as our group to cooperate with him. Another alternative is to investigate and master the basic fabrication process by our own effort. Consequently before any other research, it is extremely necessary to familiarize with the conventional fabrication techniques of the DSSCs. This chapter is to report our effort to produce these conventional DSSCs for making new structure DSSCs.

3.2 Experimental materials and equipment

3.2.1 Experimental materials

All the materials used in the experiments are listed in Table 3.1.

Table 3.1 Experimental materials

Name	Remark	Manufactory
Ru complex dye	N719	Solaronix
Anhydrous LiI	AR. 98+%	Fluka
I_2	AR.	Fluka
4-tertbutylpyridine	AR. 99%	Aldrich
Conductive glass	15 Ω/sq thickness 2.2mm	Wuhan geao instrument company
Titania nano-powder	P25	Degussa
Acetonitrile	AR.	Tianjin damao chemical instrument supply station
Platinic chloride	AR.	Shenyang research institute of nonferrous metals
Anhydrous ethyl alcohol	AR.	Guangzhou chemical reagent factory
Acetylancetone	AR.	Tianjin fuchen chemical reagent factory
Ethyl cellulose	AR.	Guangzhou chemical reagent factory
Terpineol	AR.	Guangzhou chemical reagent factory
Acetic acid	AR.	Tianjin chemical reagent ltd.
Isopropyl alcohol	AR.	Tianjin chemical reagent ltd.
Titanium tetrachloride	AR.	Guangzhou chemical reagent factory
Surlyn 1702 film and resin	30μm-100 μm	Dupont
AB epoxy transparent glue	15s	Singapore miradur specialty chemicals ltd.

3.2.2 Equipment

All the equipment is listed in Table 3.2.

Table 3.2 Equipment list

Name of instrument	Instrument model	Manufactory
Rotary evaporator	ZFQ-85A	Shanghai medical apparatus and instruments specialized factory
Manual glass cutting machine	HSRL-400	Guangzhou meishun mechanical & electrical co., ltd
Manual screen printing machine	UP-S7090M	Dongguan dalang screen printing machine factory
Oil-free PTFE Chemical Diaphram Vario Pump	MZ2C	Beijing saimeisiyi instrument ltd.
Low-temperature resistance furnace	SX-2.5-10	Shanghai wuyangshan international trading co., ltd
Table-type electrothermal constant-temperature dry box	DHG-9023A	Guangzhou kerun electronics co., ltd
Hot press	JCH-C602H	Dongguan electronic equipmnet factory
Manual ultrasonic wave single-needle key punch machine	KL-350	Foshan kelin ultrasonic equipment co., ltd
Ultrasonic generator	JP-060	Guangzhou ultrasonic electronic equipmnet co., ltd
Electronic balance	ES120	Shenzhen zhicheng electronic balance co., ltd
Solar simulators	91192	Newport

3.3 Dye-sensitized solar cells based on titania nanoparticles film

3.3.1 Titania paste for screen printing

To realize the high efficient DSSC, it is important to get a porous nanocrystalline photoanode with a high surface area titania film as well as good adhesion with the FTO glass. The properties of the titania film such as roughness factor, pore size, surface area and modification between FTO and titania nanoparticles are mainly determined by the formation of titania paste and the film preparation technique. Currently the most commonly used film preparation method is the fast screen printing because it can control the position and film thickness accurately and make it possible to integrate any desired image on the DSSC module. However, as the reported research utilized different types of titania nanoparticles to prepare the screen printing paste, it was hard to compare their fabrication techniques. In 2007, Grätzel and his group members published a paper **[11]** investigating the fabrication of screen printing pastes made from P-25 type titania powders. The final result demonstrated that a conversion efficiency of 8.7% was obtained by using a single layer of titania film made of P-25 type titania nanoparticles. Besides, by covering one more layer of St-1 type titania layer as the light-scattering films, the conversion efficiency increased up to 9.2%. This work is significant as it is the first time to report the highest conversion efficiency so far based on commercially-available titania powders. Through comparison with this work, by employing the same materials such as the P-25 type titania nanoparticles, people could evaluate whether or not they have master the key points of fabrication techniques for DSSCs. Consequently the fabrication process reported in this paper could be treated as standard process. The detailed procedures to prepare the titania paste are as shown in **Figure 3.1**.

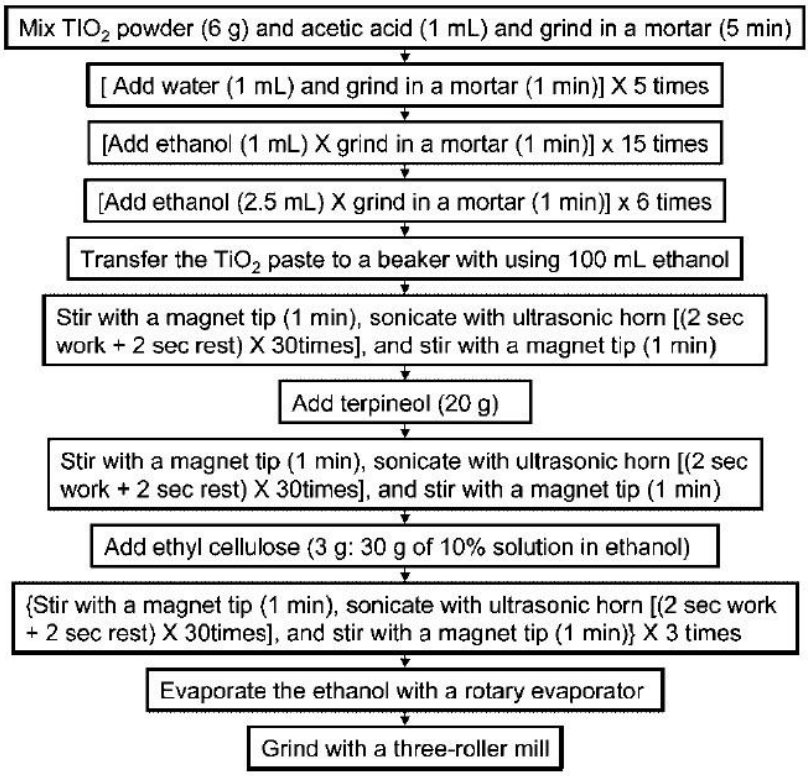

Figure 3.1 Fabrication scheme of screen-printing paste from a nanocrystalline-titania powder from Grätzel et al. **[11]**

The procedures above are complicated and time consuming, which is not suitable for volume production. Based on several times of preliminary experiments, in this chapter, the fabrication process of titania paste was improved by our group in order to simplify the designing process and reduce facility costs. Instead of using rotary evaporator to distill the paste under reduced pressure, in the new process, by adjusting the amount of terpineol and ethanol added, the viscosity of paste is controlled to match different types of mesh screen. Besides, to guarantee the unique thickness of nanoporous film, the titania paste needs to be well dispersed. Consequently, the acetic acid is also added to enhance the dispersion of titania nanoparticles. The improved fabrication process of titania paste is summarized as follows:

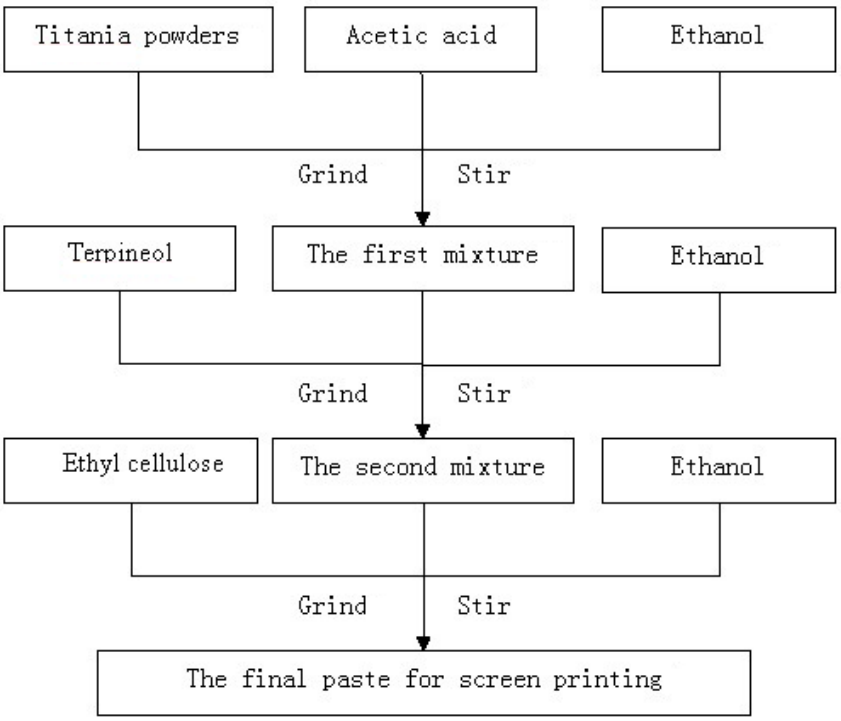

Figure 3.2 The improved fabrication process of screen printing paste for DSSCs

As there are several kinds of titania powders in the market, in order to compare the photovoltaic performance with other research groups in the same condition, a commercially-available titania powder named as P25 type from Degussa is adopted to fabricate the paste. First, 1g P25 titania nanopowder was mixed with 0.5g ethanol and 0.2g acetic acid (75%) in a PTFE mortar of planetary ball mill. Then, by adjusting the rotation speed to 500 rpm, the first mixture was stirred and grinded for 20 minutes in order to grind large titania aggregates. After that a mixture of 3g terpineol with 3g ethanol was then added to the mortar, followed by stirring and grinding for 60 minutes with 800 rpm. Finally 0.5g ethyl cellulose dissolved in 1.5g ethanol was added to the second mixture and continued to stir and grind for another 360 minutes with the rotation speed of 800 rpm. The final paste for screen printing was transferred from the mortar to

a small bottle for reservation. The bottle should be sealed to prevent the evaporation of terpineol and ethanol. Sometimes after long time reservation, the viscosity of the paste is a bit higher due to the volatilization of solvent， which would block the mesh holes during the screen printing. This problem could be resolved by adding a small amount of terpineol to adjust the viscosity.

Figure 3.3 The screen printing paste made by titania nanoparticles

It is very important to add acetic acid solution (75%) into the titania powder. The water in the acetic acid solution could provide hydroxides (–OH) to make good chemical bonding between the titania nanoparticles. The protons ionized from the acetic acid are absorbed on the surface of titania nanoparticles, which positively shift the Zeta potential to repel the particles from aggregation.

3.3.2 Preparation of nanocrystalline titania photoanodes

The FTO glass was cut into 1 cm × 2.5 cm rectangular pieces by the manual glass cutting machine as the substrates of electrodes. As the cleanness of FTO glass plays a key role to make good contact between the SnO_2 surface and the titania film, the FTO glass was first ultrasonically cleaned in a mixture of acetone and ethanol for 20 minutes, and then rinsed with deionized water and ethanol for 10 minutes, respectively, followed by drying in a nitrogen stream. In order to coat a compact titania layer onto the surface of substrate to decrease the back reaction, the FTO glass was immersed into a 50 mM $TiCl_4$ aqueous solution at 80 ℃ for 20 minutes, then washed with deionized water. Nest they were placed on the proper place of the ink pad and the mesh holes were filled with titania paste. Through the press of squeegee on the mesh screen, the paste was pressed through the mesh holes onto the FTO glass to coat one layer of titania. The appearance of the titania layer is a circle with the diameter of 6mm. Consequently the geometric surface area to calculate the photovoltaic parameters was 0.3cm × 0.3cm × 3.14=0.283 cm^2. Next the layer of titania film was putting into a low-temperature resistance furnace to dry the paste under 120 ℃ for 5 minutes. This step can evaporate volatile solvents in the paste. By repeating the coating and drying process, the film thickness of photoanode could be controlled. For each time of screen printing, the thickness of one layer titania is usually around 3 μm to 5 μm, depending on the press force of the operator and the viscosity of the paste.

After screen printing, the titania layers were sintered at 450 ℃ in air to remove the organic components of the paste and form the necking structures between the titania

nanoparticles. The heating and cooling rate should be very slow as the titania paste contains a lot of organic components which decompose in the temperature range from 200 ℃ to 350 ℃. If the heating rate is too high, then during the decomposition lots of CO_2 is produced which would rip the film and remain several cracks. Besides, if the cooling rate is too high, the titania layer is easy to peel off from the FTO glass due to the different coefficients of heat expansion. After sintering, the as prepared titania film was immersed into the 50 mM $TiCl_4$ aqueous solution again at 80 ℃ for 20 minutes, then rinsed with deionized water and finally sintered at 450 ℃ for 30 minutes. After the second calcination, when the temperature had cooled down to 80 ℃, the titania electrodes were immersed into the dye solution containing 0.5 mM N719 dye molecules dissolved in a mixture of acetonitrile and tert-butylalcohol (volume ratio 1:1) and conserved in a sealed bottle for 24 hours at room temperature.

3.3.3 Preparation of counter electrodes

Before the platinization, FTO glass sheets were firstly drilled by ultrasonic sand blasting to make a conical hole with diameter of 1mm, and then washed with deionized water and ethanol for 30 minutes in an ultrasonic bath. After drying in a nitrogen stream, the FTO glass was platinized by dripping 3-5 drops of H_2PtCl_6 solution (5×10^{-3} mol/L) on the conductive layer surface and spread the solution by shaking the glass slightly. After the solvents were evaporated, the FTO glass sheets were fired again at 380 ℃ for 30 minutes in air. When the sintering was finished, it could be seen that a thin layer of Pt black was coating on the FTO substrate. If more than 10 drops of H_2PtCl_6 solution was dripped on the FTO surface, after the heat treatment, a shiny Pt mirror would be formed.

However, compared with Pt mirror, Pt black which is composed of small Pt clusters has higher catalytic activity due to the superior dispersion of Pt.

3.3.4 DSSC assembling

To accurately measure the photovoltaic parameters of DSSCs, it is necessary to fabricate the device with good sealing quality. A piece of hot melt film (Surlyn 1702) with the thickness of 25 μm was utilized as the spacer and sealant to separate the electrodes and seal the electrolytes. The Surlyn film was cut into a square frame with the side length of 7mm which is 2mm larger than that of the titania layer. The hot melt film was sandwiched between the photoanode and counter electrode and pressed by the hot press for 100 seconds with positive press of 1.5 MPa. To avoid the damage of dye molecules, the temperature of photoanode side was set to 90 ℃ while that of the counter electrode side was 110 ℃. The two electrodes should overlap partly with each other to have enough room to connect with the lead wire. The electrolyte, consisting of 0.6 M BMII (butylmethylimidazolium iodide), 0.03 M I_2, 0.5 M 4-tert-butylpyridine and 0.1M GuSCN (guanidinium thiocyanate) in the mixture of valeronitrile and acetonitrile (volume ratio: 85/15), was introduced through the hole of counter electrode employing vacuum backfilling method. When the electrolyte was completely filled into the inside of the cell, the hole in the counter electrode side was firstly covered with a piece of glass and then sealed by the Surlyn 1702 film and resin. From **Figure 3.4** it is apparent to see that a liquid electrolyte column was sealed inside the FTO glass.

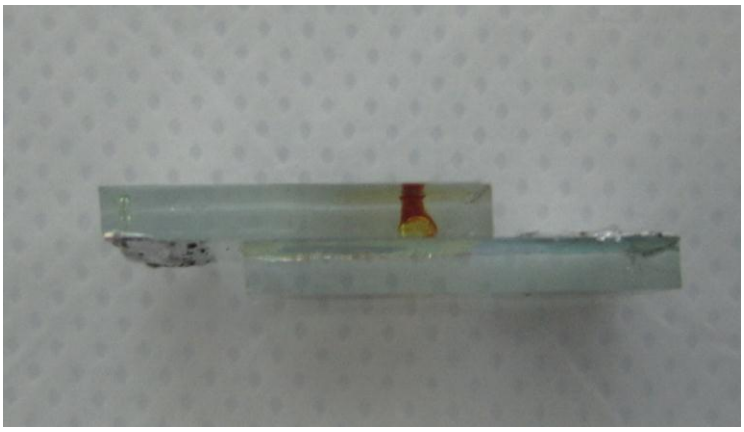

Figure 3.4 The side view of the fabricated DSSC

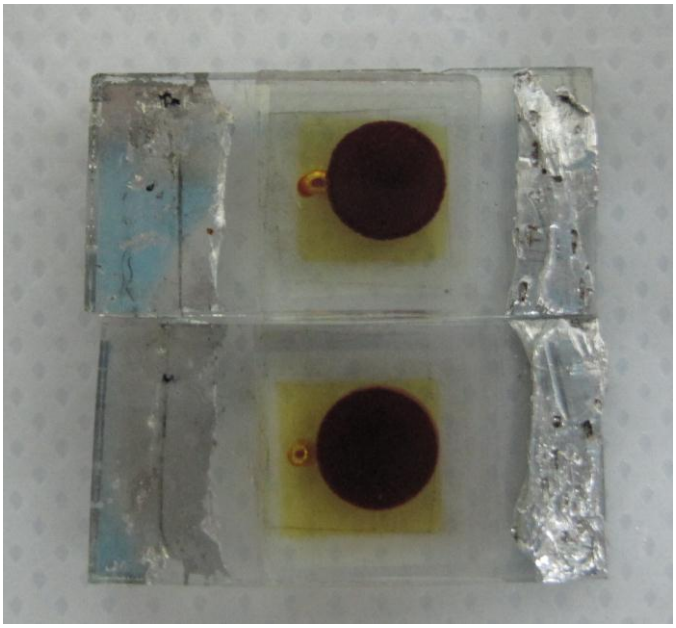

Figure 3.5 The top view of two pieces of fabricated DSSCs

As the affinity between the FTO layer and metal tin was poor, the lead wire cannot be connected with the FTO glass through conventional welding method by using tin. However, it was investigated that the indium had a good connection with the FTO layer. Consequently, by welding a thin layer of indium on the FTO surface, the lead wire was connected with the FTO glass.

3.3.5 Morphorlogy

Figure 3.6 is the SEM image of the as prepared nanocrystalline porous film made by P25 type titania nanoparticles. It can be estimated from the diagram that the diameters of the particles were between 20-30 nm, which was consistent to the data provided by Degussa. The porous structure favored the diffusion of redox couple in the electrolyte. After calcination some of the titania nanoparticles were connected together to form the necking structure, which was beneficial to the transport of photo generated electrons. However due to the incomplete formation of necking structure between particles and the random transportation roots of electrons, the electron transport rate in the nanocrystalline porous structure is relatively lower than that in the one dimensional nanomaterials.

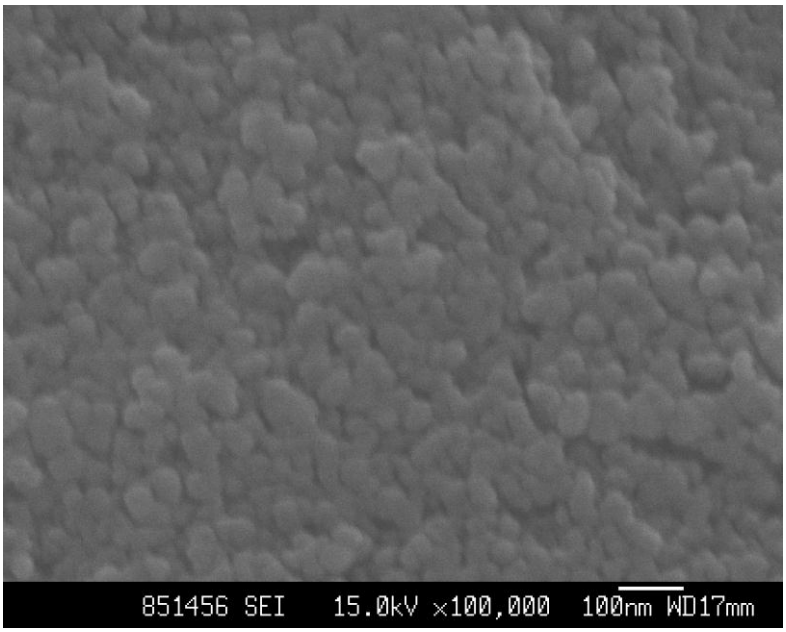

Figure 3.6 SEM image of the nanocrystalline porous film made by P25 type titania nanoparticles

Titania is usually composed of three main crystal forms **[12]**: anatase, rutile and brookite. Among them, the brookite form is not stable naturally. Generally, anatase is stable at low temperatures, while rutile is mainly generated in high temperature. It is reported that anatase is more suitable for DSSCs due to its larger band gap and higher conduction band edge energy, which would increase the open circuit voltage in the same conduction band electron concentration. **Figure 3.7** shows the XRD pattern of as prepared nanocrystalline porous film made by P25 type titania nanoparticles. Peaks at 2θ= 25.3 ° and 48.1 ° were corresponding to the (101) and (200) planes diffraction of anatase, while small diffraction peak at 2θ= 27.4 ° was related to rutile phase. It can be seen that the commercial P25 type titania is mixed crystals which is composed of anatase and rutile. As for the photoanode of dye-sensitized solar cells, some research reported that the anatase phase was more suitable than rutile. One reason is that the electrons transportation rate in anatase titania is faster than in rutile titania. Besides, the photo generated electrons in rutile titania are easy to be recombined by the holes.

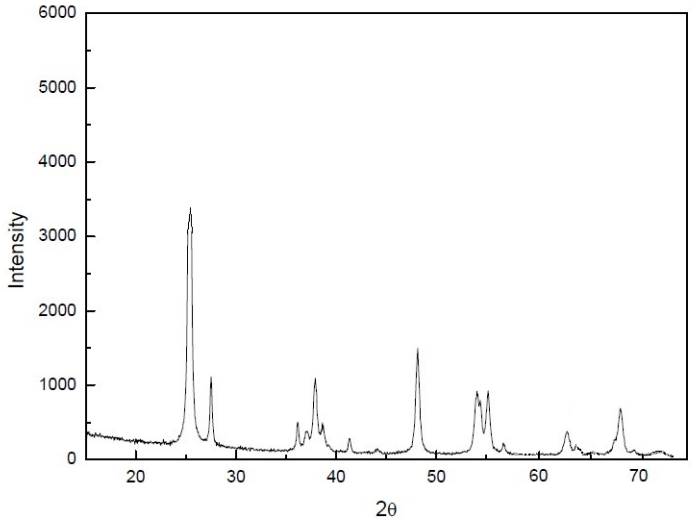

Figure 3.7 XRD pattern of nanocrystalline porous film made by P25 type titania nanoparticles

3.3.6 Influence of film thickness and device size

Table 3.3 The photovoltaic parameters of DSSCs based on different thickness of titania films.

Film thickness（μm）	V_{oc} (V)	J_{sc} (mA/cm^2)	*ff*	η (%)
10.5	0.79	9.78	0.70	5.41
12.8	0.79	11.75	0.68	6.31
14.6	0.78	13.80	0.67	7.21
16.8	0.77	13.40	0.66	6.80
18.7	0.73	14.53	0.62	6.58
21.9	0.71	13.58	0.59	5.69

The photovoltaic parameters of DSSCs based on different thickness of titania nanoparticles film are shown in **Table 3.3**. The best optimization thickness was between 14-17 μm. So far the highest conversion efficiency achieved by our lab was 7.79% in a 15.3μm thickness titania nanoparticles film, which is shown in **Figure 3.8**. However, when the device size increased from 0.283 cm^2 to 4 cm^2 while the film thickness remained constant, the conversion efficiency dropped considerably, as shown in **Figure 3.9**. The high sheet resistance of FTO glass is the reason behind which largely increased the internal resistance. Consequently it is necessary to report the efficiency of DSSC combined with the device size.

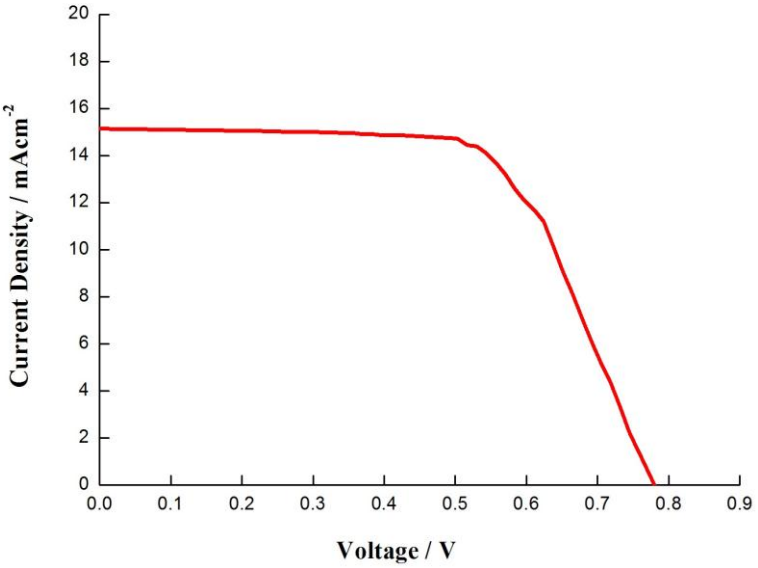

Figure 3.8 *I-V* curve of the best-efficiency DSSC using commercially available P25 titania nanoparticles. Device size: 0.283 cm^2, film thickness: 15.3 μm, *AM 1.5*, 100 mW/cm^2.

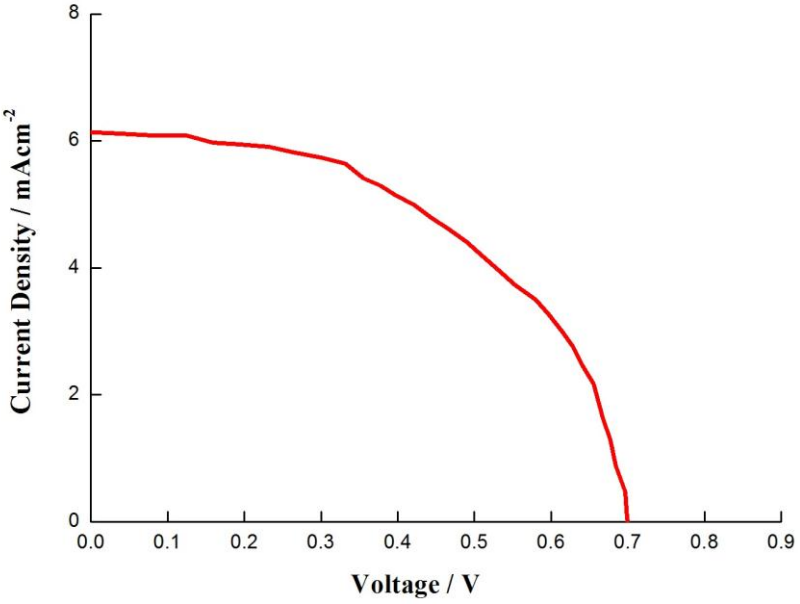

Figure 3.9 *I-V* curve of the DSSC with the device size of 4 cm^2.

3.4 Dye-sensitized solar cell with titania nanotubes film

Until now most of the DSSCs are based on three dimensional titania nanoparticulate films which has achieved the highest conversion efficiency over 11%. However, it is reported that there are abundant grain boundaries between titania nanoparticles which act as trap sites to lower the electron mobility and enhance the charge recombination process **[13-14]**. To develop highly ordered material architectures offering higher electron transportation rate and longer electron diffusion length, many 1-dimensional (1D) titania materials, such as nanowires **[15]**, nanotubes **[16]** and nanorods **[17]** have been successively synthesized and applied on the DSSCs to overcome the limitation of randomly oriented nanoparticles. Highly ordered titania nanotubes fabricated by anodization of Ti foil have attracted much attention for application in DSSCs due to their 1D structures providing direct pathways for electrons from the injection points to the substrate **[18-20]**. Zhu et al. have shown that the charge-collection efficiency of the titania nanotubes based DSSC is 25% higher than the corresponding nanoparticles based DSSC **[21]**. Besides, it is estimated that the titania nanotubes could increase the light-harvesting efficiency due to their enhanced light-scattering properties **[22]**.

Currently, most of the research for the application of titania nanotubes on DSSCs has been limited to the back-side illumination configuration because of the opacity of Ti foil. Although recently **[23]** Grimes' group has optimized the overall conversion efficiency up to 6.89% by using the 20-μm-long titania nanotubes in the back-side illuminated DSSCs, the efficiency is still much lower than that of the front-side illuminated DSSCs. The main reason is that when the sunlight irradiates from the counter electrode side, some of the light is reflected by the counter electrode substrate and the other is absorbed by the Pt on the counter electrode and the iodine in the

electrolyte. Consequently, the best choice to increase the upper limit of efficiency is to realize the front-side illumination by synthesis titania nanotubes from the transparent TCO glass. With this as motivation, Grime and his coworkers have fabricated a transparent titania nanotubes-based photoanode by anodizing a pre-sputtered Ti layer on TCO glass and the DSSC with 17.6-μm-long titania nanotubes yielded an overall conversion efficiency of 6.9% **[24]**. However, due to the high fabrication cost of RF sputtering technology, it is not applicable for large-scale production. Another approach is to detach the titania nanotubes layer from Ti foil and transfer it to TCO glass **[25-27]**. This process is usually divided into three steps: First the titania nanotubes layer is detached from the Ti foil by physical or chemical methods. Second, the closed bottom of the titania nanotubes layer is opened by using etching agents. This step is not essential but very important as the opened-ended titania nanotubes layer would have less resistance for the dye solution and electrolyte to fill in than the closed-bottom titania nanotubes layer. Finally the opened-ended titania nanotubes layer is fixed onto the transparent TCO glass by using titanium-bearing adhesive. For the first step, as the titania nanotubes layer is thin and brittle, how to detach the titania nanotubes layer without damage is a key factor. In addition, the time of detachment should not be too long, especially from the viewpoint of industrial application. For the second step, due to the complicated and time-consuming process, most of the relevant studies omitted this step. Until now only a little research group adopted oxalic acid solution or HF vapors as the etching agents, which were complicated and toxic. As a result, it is requested to find more suitable method to prepare transparent titania nanotubes-based photoanode.

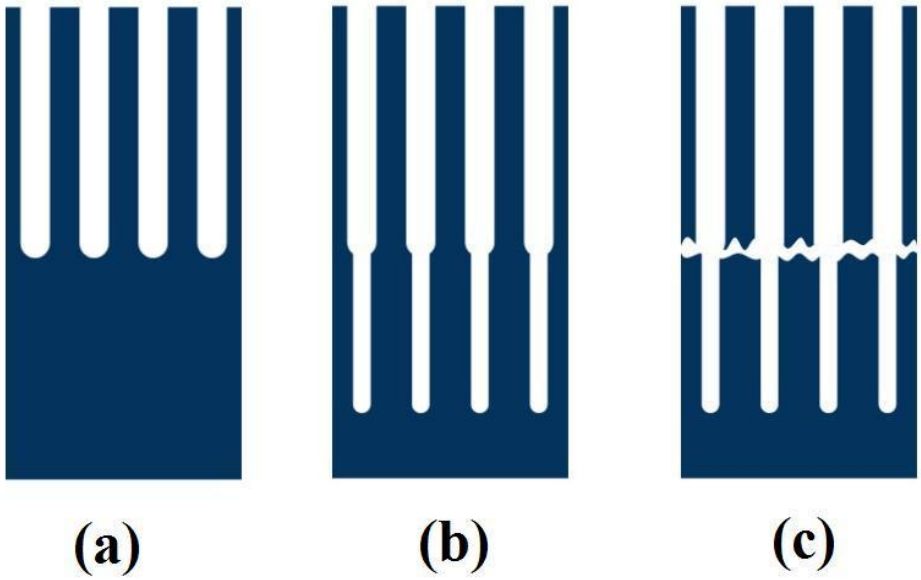

Figure 3.10 The schematic diagram of the titania nanotubes layer detachment process : (a) the upper layer of titania nanotubes film. (b) the lower layer of titania nanotubes film. (c) the detachment of upper layer.

In the present work we report a facile and cost-effective method to fabricate transparent open-ended titania nanotubes-based photoanode by combining the original three steps into one step. During the whole process, the titania nanotubes layer is protected safely. The toxic etching step is also replaced by the two step anodization under different voltages, which means it is environment friendly. The schematic diagram of this detachment process is summarized in **Figure 3.10**. A 500 μm thick Ti foil was first cleaned with ethanol and distilled water in ultrasonic bath to remove surface contaminants, then anodized at 40 V in the fluoride-containing electrolyte. A self-organized titania nanotubes layer was in situ grown on Ti foil by anodic oxidation, as shown in **Figure 3.10 (a).** After 20h, the voltage was changed into 20V and then anodized secondly for 2h, which is shown in **Figure 3.10 (b).** As describe elsewhere **[28]**, since the average diameter of the tube increases monotonically with the increasing

of the anodization voltage, an apparent interface could be clearly observed between the two nanotubes layers with different diameters corresponding to the different voltages, as shown in **Figure 3.11.**

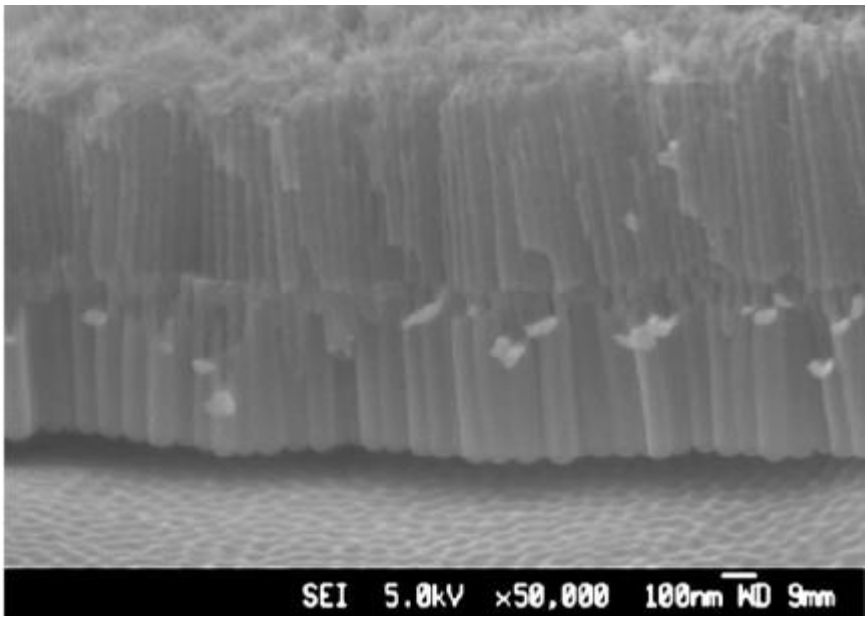

Figure 3.11 Bilayer structure of titania nanotubes formed by anodization under two different potential **[28].**

After the two-step anodization, a piece of FTO glass was stick to the anodized Ti foil by using titanium isopropoxide as the binder. A hot press was also introduced to compress them tightly with the heating temperature and compressive pressure about 250 ℃ and 1.5 MPa, respectively. Then both of them were under thermal annealing at 525 ℃ for 3 h with heating rate of 3 ℃/min. After the temperature had cooled, the FTO glass together with the anodized Ti foil was put into the 0.1 M HCl solution for 30 minutes. It could be seen that some bubbles were firstly produced between the FTO glass and Ti sheet and then split them from the middle. The reasons for this phenomenon can be explained as follows: As mentioned above, there was an apparent interface

between the two nanotubes layers. Due to the different diameters of the nanotubes in each layer, it was easy to produce stress at the interface which would finally split these two layers. The environment of high temperature treatment and aqueous HCl solution could help the detachment process **[27]**. When the two layers were separated, the titania nanotubes in the upper layer were penetrated which meant they were open-ended (**Figure 3.10 (c)**)**,** while the lower layer was still connected with the Ti sheet on which there was a barrier layer. The titanium ixopropoxide connected the top of the upper layer with the FTO glass. As a result, a thin layer of titania nanotubes film was covered on the FTO surface (**Figure 3.12 (a)**)**,** and then dip into the dye solution for 24 hours. After being rinsed with ethanol to remove nonchemisorbed dyes, the titania nanotubes film was sensitized into pink color **Figure 3.12 (b).**

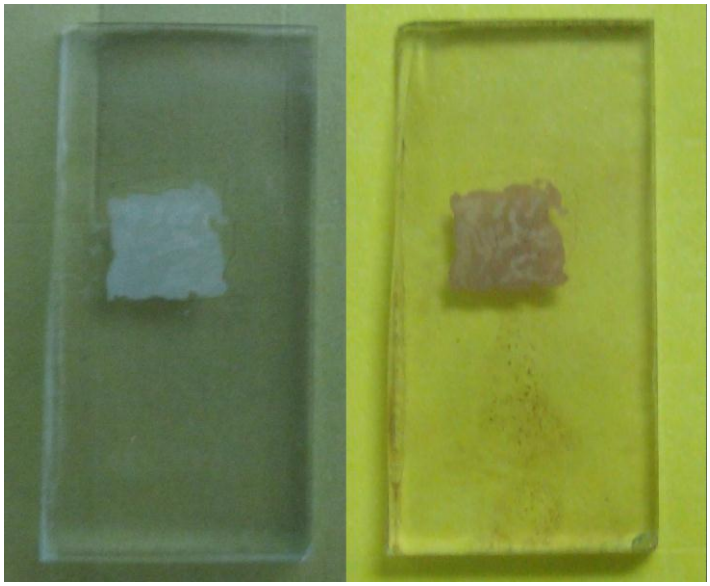

Figure 3.12 The titania nanotubes film coated on the FTO surface. (a) before (b) after sensitization.

The fabrication process of DSSC based on titania nanotubes layer is similar to that of the conventional DSSC based on titania nanoparticles. For brief, a piece of Surlyn 1702 hot melt film was sandwiched between the as prepared photoanode and counter electrode, and then pressed by the hot press for 100 seconds with positive press of 1.5 MPa under 100 ℃. The electrolyte, consisting of 0.6 M BMII (butylmethylimidazolium iodide), 0.03 M I_2, 0.5 M 4-tert-butylpyridine and 0.1M GuSCN (guanidinium thiocyanate) in the mixture of valeronitrile and acetonitrile (volume ratio: 85/15), was introduced through the hole of counter electrode employing vacuum backfilling method. Finally the hole in the counter electrode side was covered with a piece of glass and then sealed by the Surlyn 1702 film and resin.

3.4.1 Morphorlogy

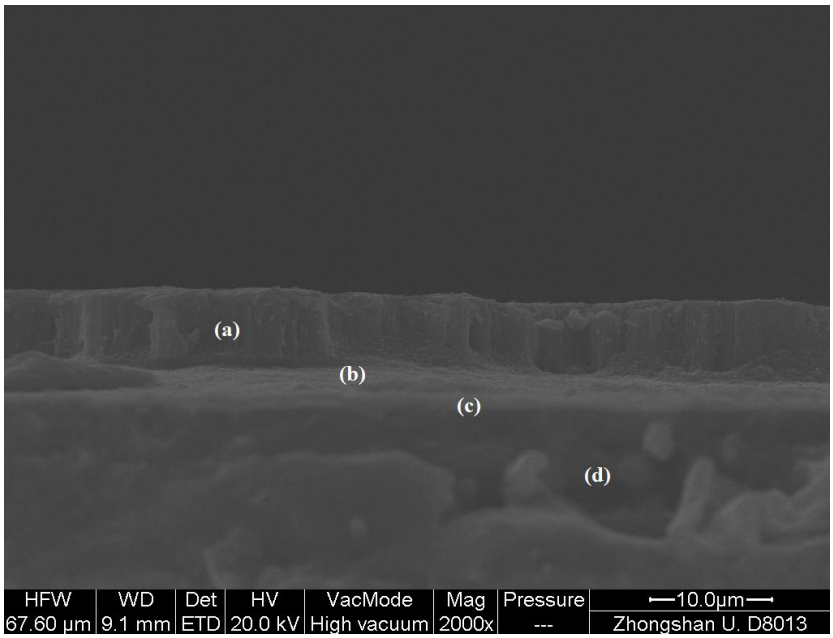

Figure 3.13 Cross-sectional SEM image of the FTO glass covered with titania nanotubes layer: (a) the titania nanotubes layer; (b) the binder layer formed by titanium isopropoxide; (c) the conductive layer of FTO glass; (d) The glass substrate

The cross-sectional SEM image of the as prepared photoanode is shown in **Figure 3.13**. There were 4 sections in the image. Section (a) represents the open-ended titania nanotubes layer with the thickness of 7 μm. The titania nanotubes arrays were vertically connected with the substrate. Section (b) is the binder layer formed by the titanium ixopropoxide. It connected the section (a) with section (c) which is the conductive layer of FTO glass. Section (d) is the bulk glass substrate. It is further demonstrated from **Figure 3.14** that the titania nanotube arrays were firmly rooted in the binder layer. Here the binder layer could not only ensure the transportation of the photo generated electrons from the titania nanotubes layer to the FTO glass, but also as the compact layer to prevent the direct contact between the substrate and the electrolyte.

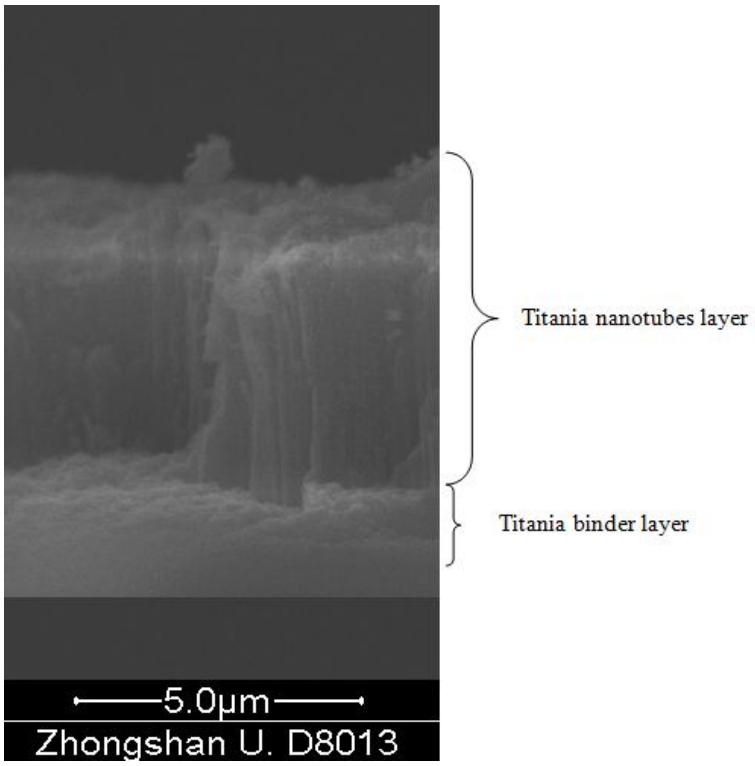

Figure 3.14 The joint between the titania nanotubes layer and the titania binder layer.

3.4.2 Influence of film thickness and device size

Table 3.4 The photovoltaic parameters of DSSCs based on different thickness of titania nanotubes layer.

Film thickness （μm）	V_{oc} (V)	J_{sc} (mA/cm^2)	*ff*	η (%)
5.2	0.80	6.35	0.73	3.71
10.6	0.79	10.06	0.73	5.80
14.8	0.79	12.37	0.72	7.04
21.1	0.77	14.65	0.72	8.12
25.6	0.75	14.88	0.68	7.59
32.4	0.68	16.54	0.63	7.08

We investigated a series of photoanodes based on different thickness of titania nanotubes layer by control the time of first anodization. As shown in **Table 3.4**, the optimal thickness fell in the range of 20–25 μm. By optimizing different parts of the device, the champion cell (**Figure 3.15**) in our laboratory could achieve the photovoltaic conversion efficiency up to 8.7% in a piece of 5mm × 6mm square titania nanotubes layer in the thickness of 23 μm, which was a bit higher than the corresponding DSSC (P25 type titania particles, η = 7.79%) in the nearly same size. The exceeded 0.91% conversion efficiency might attribute to the higher charge-collection efficiency of the highly ordered titania nanotube arrays. However, as the titania nanotubes layer is still based on FTO glass, it is predicted that the size effect would still influence the photovoltaic performance. To demonstrate this point, a piece of 2cm × 2cm square titania nanotubes layer in the same thickness (23 μm) was detached from the Ti sheet and covered on the FTO glass to fabricate the photoanode. From **Figure 3.16** it is obvious to see that the photovoltaic parameters decreased drastically, J_{sc}, *ff*, η changed from 15.72 mA/cm^2, 0.72, 8.7% to 8.6 cm mA/cm^2, 0.49, 3.0%, respectively. Only the

V_{oc} changed a little, from 0.77V to 0.71V. The predominance of titania natoubes was largely inhibited by the high resistance of FTO glass. This result indicates that it is better to cooperate titania nanotubes with low resistance substrates such as metal sheet.

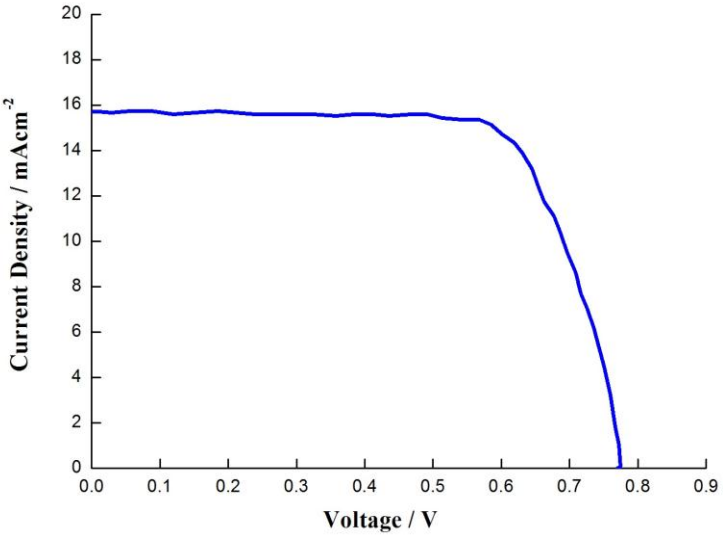

Figure 3.15 *I-V* curve of the champion DSSC using titania nanotubes layer. Device size: 0.3 cm^2, film thickness: 23.5 μm, *AM 1.5*, 100 mW/cm^2.

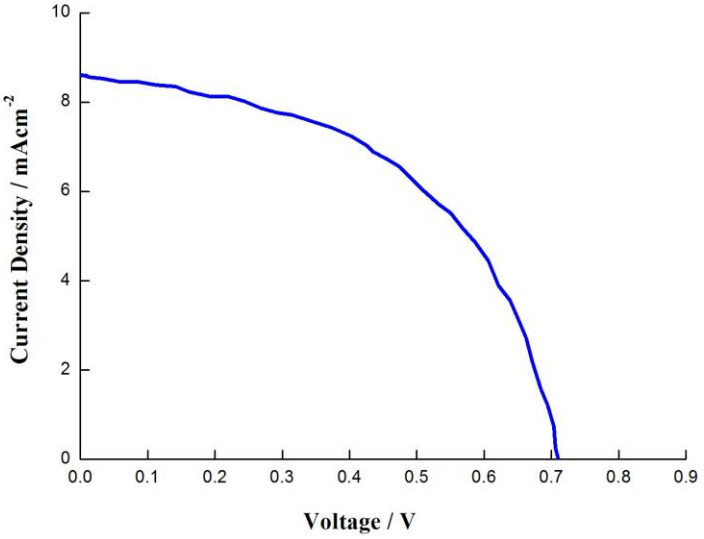

Figure 3.16 *I-V* curve of the DSSC using titania nanotubes layer. Device size: 4 cm^2, film thickness: 23.5 μm, *AM 1.5*, 100 mW/cm^2.

3.5 Conclusion

In summary, to master and optimize the basic fabrication techniques of the DSSCs, Grätzel's work has been further developed. The fabrication process of screen printing paste made by P25 type titania was simplified. By optimizing various parameters of the device such as film thickness, the highest conversion efficiency based on P25 type titania was 7.79%. However, the conversion efficiency decreased with the increase of device size due to the high resistance of FTO glass. For comparison, the DSSCs based on FTO glass with open-ended titania nanotubes layer was developed. By changing the anodization voltage, a bilayer titania nanotubes film was synthesized and finally parted in the middle. The champion cell based on open-ended titania nanotubes achieved conversion efficiency of 8.7% with the device size of 0.3 cm^2. However, the conversion efficiency dropped dramatically when the device size increased to 4 cm^2. Consequently the size effect is unavoidable for the DSSC based on FTO glass.

References:

1. B. Oregan, and M. Gratzel, A low-cost, high-efficiency solar cell based on dye-sensitized colloidal TiO_2 films. *Nature*, 1991. **353**: 737-40.
2. C.Y. Chen, M. Wang, J. Y. Li, N. Pootrakulchote, L. Alibabaei, C. H. Ngoc-le, J. D. Decoppet, J. H. Tsai, C. Gratzel, C. G. Wu, S. M. Zakeeruddin, and M. Gratzel, Highly Efficient Light-Harvesting Ruthenium Sensitizer for Thin-Film Dye-Sensitized Solar Cells. *ACS Nano*, 2009. **3**: 3103-09.
3. M. Adachi, Y. Murata, J. Takao, J. T. Jiu, M. Sakamoto, and F. M. Wang, Highly Efficient Dye-Sensitized Solar Cells with a Titania Thin-Film Electrode

Composed of a Network Structure of Single-Crystal-like TiO_2 Nanowires Made by the "Oriented Attachment" Mechanism. *J Am Chem Soc*, 2004. **126**: 14943-49.

4. J. Yoon, S. Jang, R. Vittal, J. Lee, and K. J. Kim, TiO_2 nanorods as additive to TiO_2 film for improvement in the performance of dye-sensitized solar cells. *J Photochem Photobiol A: Chem*, 2006. **180**: 184-188.
5. P. S. Archana, R. Jose, C Vijila, and S. Ramakrishna, Improved Electron Diffusion Coefficient in Electrospun TiO_2 Nanowires. *J Phys Chem C*, 2009. **113**: 21538-42.
6. S. M. Zakeeruddin, M. K. Nazeeruddin, R. Humphry-Baker, P. Pe´chy, P. Quagliotto, C. Barolo, G. Viscard, and M. Gra¨tzel, Synthesis, and Application of Amphiphilic Ruthenium Polypyridyl Photosensitizers in Solar Cells Based on Nanocrystalline TiO_2 Films. *Langmuir*, 2002. **18**: 952–54.
7. P. Wang, S. M. Zakeeruddin, J. E. Moser, M. K. Nazeeruddin, T. Sekiguchi, and M. Gra¨tzel, A Stable Quasi-Solid-State Dye-Sensitized Solar Cell with an Amphiphilic Ruthenium Sensitizer and Polymer Gel Electrolyte. *Nat. Mater*, 2003. **2**: 402-07.
8. P. Wang, S. M. Zakeeruddin, J. E. Moser, R. Humphry-Baker, P. Comte, V. Aranyos, A. Hagfeldt, M. K. Nazeeruddin, and M. Gra¨tzel, Stable new sensitizer with improved light harvesting for nanocrystalline dye-Sensitized solar cells. *Adv. Mater*, 2004. **16**: 1806-11.
9. I. Seigo, S. M. Zakeeruddin, P. comte. P. Liska, D. Kuang, and M. Grätzel, Bifacial dye-sensitized solar cells based on an ionic liquid electrolyte. *Nat Photonics*, 2008. **2**: 693-98.

10. Y. Bai, Y. Cao. J. Zhang, M. Wang, R. Li, P. Wang, S. M. Zakeeruddin, and M. Grätzel, High-performance dye-sensitized solar cells based on solvent-free electrolytes produced from eutectic melts. *Nat Mater*, 2008. **7**: 626-30.
11. I. Seigo, P. Chen, P. Comte, M. K. Nazeeruddin, P. Liska, P. Pe´chy, and M. Gra¨tzel, Fabrication of Screen-Printing Pastes From TiO_2 Powders for Dye-Sensitised Solar Cells. *Prog Photovoltaics*, 2007. **15**: 603-12.
12. A. Hagfeldt, G. Boschloo, L. Sun, L. Kloo, and H. Pettersson, Dye-Sensitized solar cells. *Chem Rev*, 2010. **110**: 6595–6663.
13. J. Nelson, Continuous-time random-walk model of electron transport in nanocrystalline TiO_2 electrodes. *Phys Rev B*, 1999. **59**: 15374-80.
14. Y. Suzuki, S. Ngamsinlapasathian, R. Yoshida, and S. Yoshikawa, Partially nanowire-structured TiO_2 electrode for dye-sensitized solar cells. *Cent Eur J Chem*, 2006. **4**: 476-88.
15. M. Adachi, Y. Murata, J. Takao, J. Jiu, M. Sakamoto, and F. Wang, Highly efficient dye-sensitized solar cells with a titania thin-film electrode composed of a network structure of single-crystal-like TiO_2 nanowires made by the "oriented attachment" mechanism. *J Am Chem Soc*, 2004. **126**:14943-49.
16. S. Uchida, R. Chiba, M. Tomiha, N. Masaki, and M. Shirai, Application of titania nanotubes to a dye-sensitized solar cell. *Electrochemistry*, 2002. **70**: 418-20.
17. J. T. Jiu, S. Isoda, F. M. Wang, and M. Adachi, Dye-sensitized solar cells based on a single-crystalline TiO_2 nanorod film. *J Phys Chem B*, 2006. **110**: 2087-92.

18. J. R. Jennings, A. Ghicov, L. M. Peter, P. Schmuki, and A. B. Walker, Dye-Sensitized Solar Cells Based on Oriented TiO_2 Nanotube Arrays: Transport, Trapping, and Transfer of Electrons. *J Am Chem Soc*, 2008. **130**:13364-72.
19. D. Kim, A. Ghicov, S. P. Albu, and P. Schimuki, Bamboo-Type TiO_2 Nanotubes: Improved Conversion Efficiency in Dye-Sensitized Solar Cells. *J Am Chem Soc*, 2008. **130**:16454-55.
20. J. M. Macak, H. Tsuchiya, and P. Schmuki, High-aspect-ratio TiO_2 nanotubes by anodization of titanium, *Angew Chem Int Edit*, 2005. **44**: 2100-02.
21. K. Zhu, N. Kopidakis, N.R. Neale, J. van de Lagemaat, and A.J. Frank, Influence of Surface Area on Charge Transport and Recombination in Dye-Sensitized TiO_2 Solar Cells. *J Phys Chem B*, 2006. **50**: 25174-80.
22. K. Zhu, N. R. Neale, A. Miedaner, and A. J. Frank, Enhanced Charge-Collection Efficiencies and Light Scattering in Dye-Sensitized Solar Cells Using Oriented TiO_2 Nanotubes Arrays. *Nano Lett*, 2007. **7**: 69-74.
23. G. K. Mor, K. Shankar, M. Paulose, O. K. Varghese, and C. A. Grimes, Use ofhighly-ordered TiO2 nanotube arrays in dye-sensitized solar cells. *Nano Lett*, 2006. **6**: 215-18.
24. O. K. Varghese, M. Paulose, and C. A. Grimes, Long vertically aligned titania nanotubes on transparent conducting oxide for highly efficient solar cells. *Nat Nanotechnol*, 2009. **9**: 592-97.
25. H. Park, W. R. Kim, H. T. Jeong, J. J. Lee, H. G. Kim, and W. Y. Choi, Fabrication of dye-sensitized solar cells by transplanting highly ordered TiO_2 Nanotube arrays. *Sol Energ Mat Sol C*, 2011. **1**: 184-89.

26. N. K. Allam, S. Karthik, and A. G. Craig, A general method for the anodic formation of crystalline metal oxide nanotube arrays without the use of thermal annealing. *Adv Mater*, 2008. **20**: 3942-46.
27. J. H. Park, T. W. Lee, and M. G. Kang, Growth, detachment and transfer of highly-ordered TiO_2 nanotube arrays: use in dye-sensitized solar cells. *Chem Commun*, 2008. **25**: 2867-69.
28. X. Y. Wang, S. Zhang, and L. D. Sun, A Two-step anodization to grow high-aspect-ratio TiO_2 nanotube. *Thin Solid film*, 2011.

CHAPTER 4 Development of mesh-like DSSCs

4.1 Introduction

As we know, it is very universal in the nature that mesh structure is utilized, for example, the spider web to catch the insects, the capillary network in the lung to exchange oxygen with the cells, and the network of leaf vein to transport water and nutrient to the plant. Nowadays more and more mesh structures are utilized in the human world, such as screen windows, fishing net and so on. Compared with the opaque sheet structure, mesh structure could not only connect all parts together with the wires, but also offer certain size of holes for objects to pass through. In this chapter, in terms of bionic viewpoint, we make use of mesh structure to modify the traditional structure of DSSC into a brand new one.

As discussed in Chapter 1, conventional type DSSC adopts conductive glass such as FTO glass as the substrates. Due to the relatively high sheet resistance and expensive fabrication cost of it, more and more efforts are putting into finding other substrates to replace it. Toivola et al. **[1]** tried to use stainless steel and carbon steel as the substrates of counter electrodes and achieved photovoltaic conversion efficiencies of 3.6% and 3.1%, respectively. Fang et al. **[2]** investigated the photovoltaic parameters of DSSCs employing stainless steel as the substrate of counter electrode. By reducing the internal resistance of device, the large scale DSSC increased its conversion efficiency by 20%. However, as the counter electrode is not the most critical component of DSSC, people turned to find suitable substrates for the photoanodes. Yoshikawa et al. **[3]** tried to

replace the photoanode TCO substrate with a Ti metal plate because of its low resistivity, low production cost and high temperature sinterability. Their research result indicated that the Ti plate had superiority for producing large scale DSSCs without metal track and reducing the cost of DSSCs. Kang **[4-5]** and his coworkers fabricated individual DSSCs and modules by using stainless steel as the photoanode substrates and obtained the conversion efficiency of 6.1% and 3%, respectively. Onoda et al. **[6]** had demonstrated the photovoltaic parameters of DSSCs based on FTO, Ti sheet and stainless steel as the substrates of photoanode. The final result implied that the efficiency of DSSCs based on Ti substrate was superior to the ones using stainless steel and FTO. They also investigated the corrosion resistivity of different metal and only the Ti, Ta, Nb, Ni and Pt could endure the long term corrosion resistance of iodine in the electrolyte **[7-9]**. Although all these work confirmed the superiority of metal substrate, the resistance limitation problem has not been totally resolved since there was still a TCO glass as the substrate of counter electrode or photoanode. The sheet resistance is only half reduced. Most of all, for the photoanode based on metal substrate, the DSSC was composed of a Ti sheet coated with titania porous layer, electrolyte, and a platinized TCO glass. As the Ti sheet could not transmit light, sunlight has to irradiate through the counter electrode side which is at opposite side to traditional DSSC and this type of cell is also named as backside illuminated DSSC **[10]**. The sunlight intensity absorbed by the active layer of photoanode was poor due to the low transmittance of the platinized TCO glass and the high absorbance of the redox electrolyte. It has been investigated that compared with the frontside illuminated DSSC, there will be 40% loss for the backside illuminated DSSC **[11]**.

Among the metals that could be used as the substrates of DSSCs, Ti has the biggest advantage because it can directly in situ synthesize highly ordered, self-organized titania nanotube arrays which offer direct electrical pathways for rapid collection of electrons and lower the recombination process **[12-14]**. Through the electrochemical anodization method, the highly ordered titania nanotube arrays can be in situ synthesized on the surface of Ti foil. The anodized Ti foil can be directly used as the photoanode after sensitized by the dye solution. Here the Ti foil serves as both the substrate and the source material. However, the same as the previous work, due to the opaque of Ti foil, the DSSC based on highly ordered titania nanotube arrays can only be limited in the backside illuminated DSSC, which largely thwarts the benefits of highly ordered titania nanotube arrays.

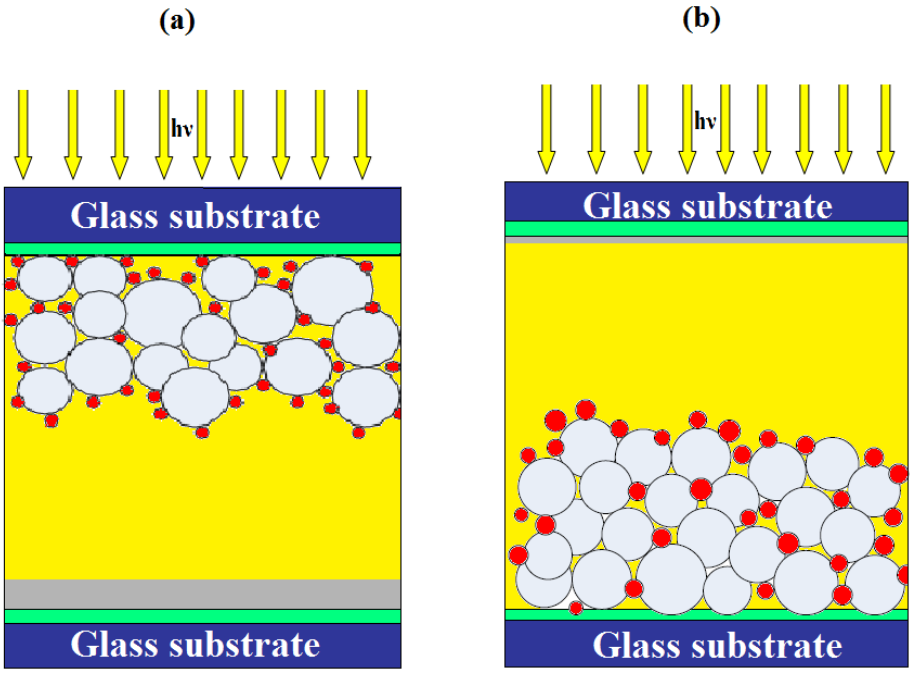

Figure 4.1 The schematic diagram of two illumination patterns: (a) Frontside illumination. (b) Backside illumination

Figure 4.1 shows the schematic digram of light illumination patterns in DSSCs. **Figure 4.1(a)** and **Figure 4.1(b)** represent the conversional frondside illuminated and the backside illuminated ways. If we still want to use the frondside illuminated method to fabricate DSSC whose photoanode is based on opaque Ti sheet, then the oxidized triiodide ions on the front side surface of the substrate have to diffuse a long way to round the photoanode substrate and then finally get to the counter electrode, as depicted in **Figure 4.2(a).** The long distance of diffusion would lower the electrolyte regeneration process and reduce the photovoltaic performance of the device. Is there a way to shorten the diffusion path of the triiodide irons? One idea comes out through borrowing the bionic idea to use the mesh structure, as illustrated in **Figure 4.2(b).** By drilling holes on the Ti sheet, instead of bypassing the photoanode to reach the counter electrode, the oxidized triiodide ions can directly diffuse through the holes to the counter electrode, which largely save the diffusion length. As Ti mesh is just the outcome of drilling holes on a Ti sheet, in this chapter we choose Ti mesh as the substrate of photanode. Besides, another reason to choose anodization as the coating method is mainly due to its completely coverage of titania nanotubes on the mesh surface. It is hard to cover titania nanoparticles completely on the Ti mesh without blocking the mesh holes.

Generally, the Ti mesh is classified by the holes number on the mesh per square inch. For example, if the mesh has 60 holes per square inch, then it is sorted as 60-mesh. With the increase of the holes number per square inch, the diameter of the holes decreases while the roughness factor rises due to the increased actual surface area. This feature is thus often utilized by the catalysis field as the loading of catalysts. In this chapter, we will adopt three types of Ti meshes as the substrates: 60-mesh, 90-mesh and 120-mesh.

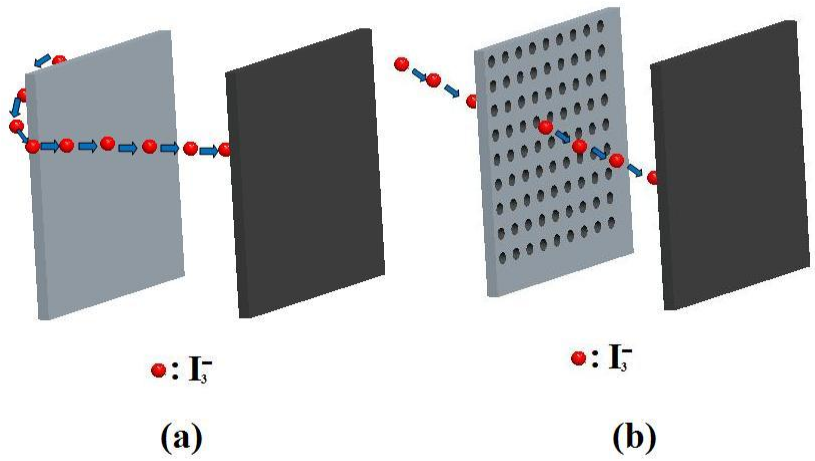

Figure 4.2 The diffusion path of the electrolyte: (a) Ti sheet without holes. (b) Ti sheet with holes.

4.2 Experimental materials and equipment

4.2.1 Experimental materials

All the materials used in the experiments are listed in Table 4.1.

Table 4.1 Experimental materials

Name	Remark	Manufactory
Ti sheet and Ti mesh	commercially pure titanium	Hebei anping netting screen production ltd.
Ammonium fluoride	AR. 98+%	Tianjin fuchen chemical reagent factory
Ethylene glycol	AR.	Guangzhou chemical reagent factory
Titanium tetrachloride	AR. 99%	Guangzhou chemical reagent factor
Chloroplatinic acid	AR.	Shenyang research institute of nonferrous metals

Ru complex dye	N719	Solaronix
Ethanol	AR.	Guangzhou chemical reagent factory
Anhydrous LiI	AR. 98+%	Fluka
I_2	AR. ≥99.55(RT)	Fluka
Acetonitrile	AR.	Tianjin damao chemical instrument supply station
4-tertbutylpyridine	AR. 99%	Aldrich
Surlyn 1702 film and resin	30μm-100 μm	Dupont
AB epoxy transparent glue	15s	Singapore miradur specialty chemicals ltd.

4.2.2 Equipment

All the equipment is listed in Table 4.2.

Table 4.2 Equipment list

Name	Model	Manufactory
DC Power Supply	GPC-6030D	Guangzhou xinhong trading co., ltd
Keithley 2400		Keithley instruments inc.
Low-temperature resistance furnace	SX-2.5-10	Shanghai wuyangshan international trading co., ltd
Table-type electrothermal constant-temperature dry box	DHG-9023A	Guangzhou kerun electronics co., ltd
Solar simulator	Newport-Oriel 91192	Newport co., ltd
Hot press	JCH-C602H	Dongguan electronic equipmnet factory

4.3 The rigid mesh-like DSSC

4.3.1 Sheet resistance of various substrates at different temperature

In order to achieve high conversion efficiency, it is important to anneal the titania layer at 450–550 ℃ to form the necking structure. Therefor the substrates should withstand the high temperature. The sheet resistance of Ti mesh, Ti sheet, FTO and ITO is recorded by electrometer with four point probes, as listed in **Table 4.3**.

Table 4.3 The sheet resistance of Ti mesh, Ti sheet, FTO and ITO before and after annealing at 450 ℃

Substrates	Before annealing	After annealing at 450 ℃
Ti mesh (Ω/□)	0.92×10^{-3}	0.93×10^{-3}
Ti sheet (Ω/□)	0.55×10^{-3}	0.55×10^{-3}
FTO (Ω/□)	12.8	25.7
ITO (Ω/□)	9.0	40.3

It is clear that the sheet resistance of both FTO and ITO dramatically rises with the increase of the sintering temperature. This phenomenon can be explained as follows: When the FTO or ITO is heated, the oxygen in the air bonds a fraction of oxygen vacant and consequently decrease the oxygen vacancies **[15-16]**. As the vacancies play a role to supply electrons, the decrease of vacancies would accordingly increase the sheet resistance. On the contrary, the sheet resistance of Ti sheet and Ti mesh changed little with the increase of sintering temperature due to the different conduction mechanisms of metal. Furthermore, the sheet resistance of Ti mesh are lower than that of FTO by nearly 1/27000 time after annealing at 450 ℃.

4.3.2 Preparation of the photoanode

3 types of Ti mesh (60-mesh, 90-mesh, and 120-mesh) were applied as the substrates of photoanodes. Prior to anodization, the Ti mesh was degreased and cleaned by sonicating in acetone, ethanol and methanol successively, followed by rinsing with deionized water and drying the samples in a nitrogen stream. Anodization was performed in a two-electrode configuration with Ti mesh as the working electrode and platinum foil as the counter electrode under constant potential (30 V) at room temperature (23 ℃). A direct current power supply (GPC-6030D) was used as the voltage source to drive the anodization. The Ti mesh was anodized in the electrolyte containing a mixture of ethylene glycol (48.86 wt%), polyethylene glycol 600 (49.38 wt%), H_2O (1.31 wt%) and NH_4F (0.43 wt%). In the first 5 minutes of anodization, lots of bubbles were produced from the surface of Ti mesh and afterwards less gradually. The color of the Ti mesh changed from silvery white to light red and then finally white. In order to achieve different thickness of nanotube arrays layer, anodization time was ranged from 10 h to 80 h. After anodization, the sample was carefully taken out from the electrolyte and rinsed with deionized water to remove the fluorine irons at 23 ℃ for three times. Each time after the sample was rinsed for 3 minutes, it should be dried in a gently steam of nitrogen gas. Finally the cleaned sample was sintered at 450 ℃ (heating/cooling rate of 10 ℃ / minutes) in air.

Each time after the sample being rinsed, it should be make sure that the sample was dried completely; otherwise its surface oxide layer would peel off when it was rinsed again. Besides the velocity of nitrogen flow should be controlled well to avoid blowing the oxide layer off. Only after annealing at 450 ℃, the surface oxide layer could be firmly attached on the surface of Ti mesh.

4.3.3 Preparation of the counter electrode

The Ti sheet, cut into the same size of Ti mesh, was used as counter electrode substrate. To increase the roughness factor of the substrate, by exposing the Ti sheet to an etching electrolyte comprising the hydrofluoric acid and nitric acid, the textured surface was produced. Then the Ti sheet was washed with acetone and ethanol in an ultrasonic bath for 3 minutes. Finally it was rinsed with deionized water and dried in a steam of nitrogen gas

The counter electrode was prepared on Ti sheet by the electrodeposition process which was carried out using an aqueous solution of 5×10^{-3} mol/L H_2PtCl_6 at room temperature. A digital sourcemeter (Keithley, 2400) was used as a power supply. Here, the platinized Ti sheet was prepared in a two-electrode configuration with Ti sheet as the cathode and platinum foil as the anode with 15 mA cm^{-2} current density from 10 s to 90 s and then calcined at 350 ℃ for 30 minutes.

It is also investigated to use the thermal decomposition of $H_2PtCl_6 \cdot 6H_2O$ aqueous solution to platinize the Ti sheet. However, due to the incompatibility of $H_2PtCl_6 \cdot 6H_2O$ aqueous solution and Ti sheet, the Pt was not coated onto the surface of Ti sheet uniformly, just like Pt islands.

4.3.4 Fabrication process

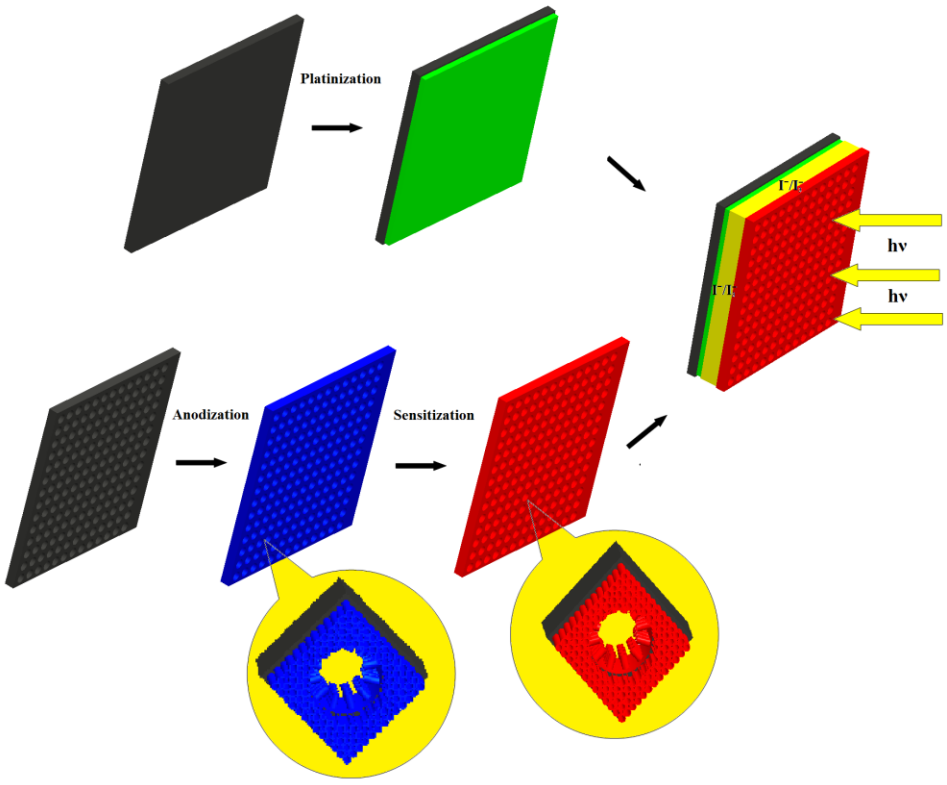

Figure 4.3 Fabrication process of the rigid mesh-like DSSC

For solar cell fabrication, the anodized Ti mesh was sensitized overnight for 24 h by soaking in N719 dye dissolved in ethanol. After soaking, the sample was rinsed with ethanol to remove nonchemisorbed dyes. The fabrication process of the cell is shown in **Figure 4.3.** The sensitized mesh-like photoanode was situated between the super white glass and the platinized Ti sheet. The super white glass here had two main functions: (i) To connect with the platinized Ti sheet by sealing material to seal the electrolyte and Ti mesh. (ii) To let sunlight pass through to reach the mesh-like photoanode. The Surlyn1702 hot melt film was used as the spacer and sealant to separate and seal the electrodes just like in the TCO-based DSSC. We used the hot press to melt the Surlyn 1702 film with thickness of 80 μm at its melting point of 90 °C. To planish the mesh-like photoanode, the positive pressure was set at 1.5 MPa to guarantee the contact

between super white glass and platinized Ti sheet. Then the Surlyn resin and epoxy were used to further seal the edges of the cell. The electrolyte, consisting of 0.5 mol/L LiI, 0.05 mol/L I_2, and 0.5 mol/L 4-tert-butylpyridine in acetonitrile, was introduced with the help of two holes in the sealed film by capillary action. Finally the holes were sealed using epoxy. To accurate determine the photovoltaic parameters, by using a black mask, the active area of the cell was 2 cm^2.

One of the advantages to use Ti mesh and Ti sheet as the substrates is their low sheet resistance. Consequently unlike most of the TCO related study which emphasized on a very tiny scale device (0.1cm^2 to 0.5 cm^2), all the DSSCs fabricated in this chapter are in the size of 2 cm^2 unless specially notified. It would be best to planish the Ti mesh before anodization. After annealing it is hard to press it smoothly.

The operation principles of rigid mesh-like DSSC are briefly summarized as follows (**Figure 4.4**): When the sunlight irradiates through the super white glass to the dye molecules anchored on the highly ordered titania nanotube arrays, the dye molecules in the original state are stimulated to the excited state (Excitation). The unstable excited dye molecules inject their electrons into the conduction band of highly ordered titana nanotubes (Injection). The injected electrons subsequently transport through the vertically ordered pathways to the Ti mesh substrate（percolation）. This step is much different with that of the nanoparticle based networks in which electrons transport randomly through the particle-particle interfaces, grain-grain boundaries. Then they were collected to the external circuit. Finally through the external circuit, the electrons are gathered on the platinized Ti sheet (counter electrode). Concurrently the oxidized

dye cations are reduced by iodide ions and iodide ions are oxidized into the triiodide ions (Dye regeneration). The triiodide ions diffuse through the mesh holes as channels to the counter electrode in which triiodide ions are reduced into iodide ions again by the Pt catalysis (Electrolyte regeneration). Similar as conventional DSSC, there is no permanent change of chemicals in the mesh-like DSSC. The only differences are the electrons transportation ways and the electrolyte diffusion pathways.

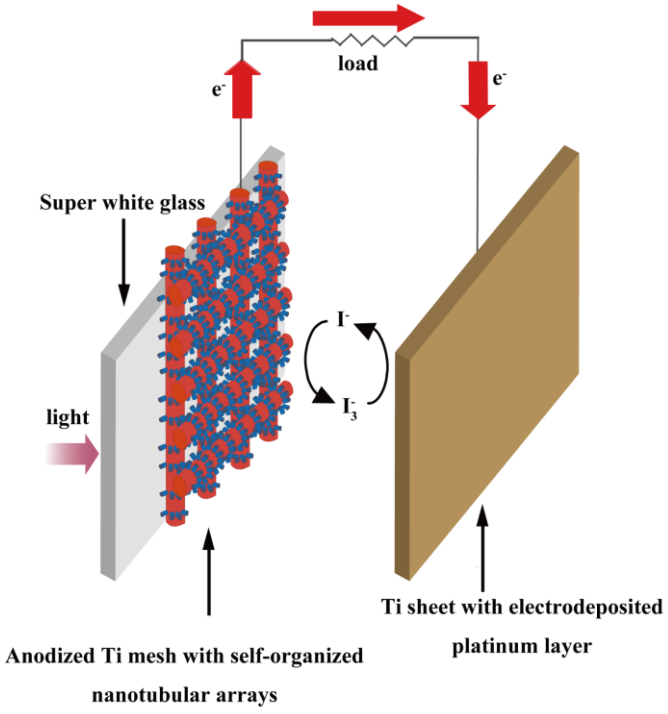

Figure 4.4 Operation principles of rigid mesh-like DSSC

4.3.5 Morphology

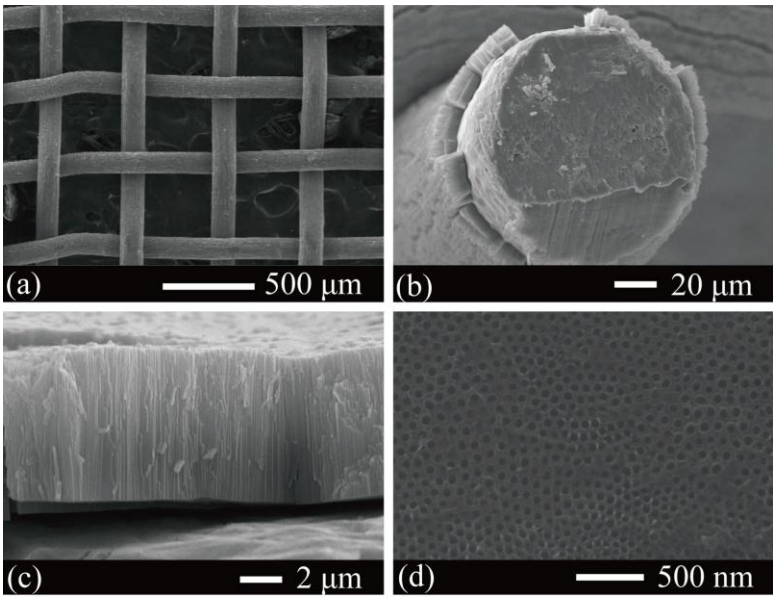

Figure 4.5 SEM images of anodized Ti mesh with a highly ordered self-organized titania nanotubu arrays: (a) 60-mesh Ti substrate; (b) and (c) cross-sectional view; (d) top view

Figure 4.5 (a) shows the SEM image of the Ti mesh which had 60 mesh holes per square inch. The diameter of one Ti wire was about 0.1mm and the length of the hole is about three times of the wire diameter. **Figure 4.5 (b)** is the cross-sectional SEM image of the Ti wire anodized for 15 h. It is obviously that after anodization the highly ordered titania nanotube arrays grew thoroughly round the surface of the wire with average length of 7.31 μm, as shown in **Figure 4.5 (c)**. **Figure 4.5 (d)** is the top view SEM image of the anodized Ti wire. Nanotubes were packed in approximately cylindrical symmetry with an average inner diameter and wall thickness of 57 ± 3 and 11 ± 1 nm, respectively. It can be seen from XRD pattern (**Figure 4.6**) that the nanotube array layer had been transformed from amorphous material to anatase phase after annealing.

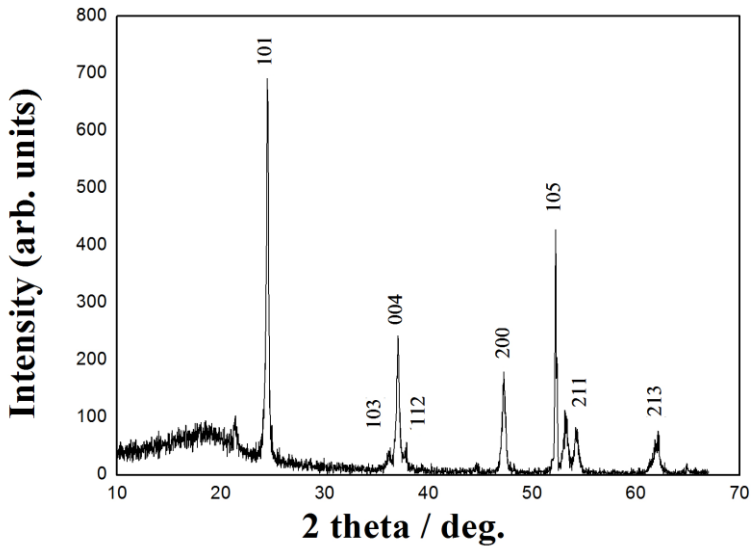

Figure 4.6 XRD pattern of anodized Ti mesh after calcination at 450 ℃

4.3.6 Dye loading of the photoanode

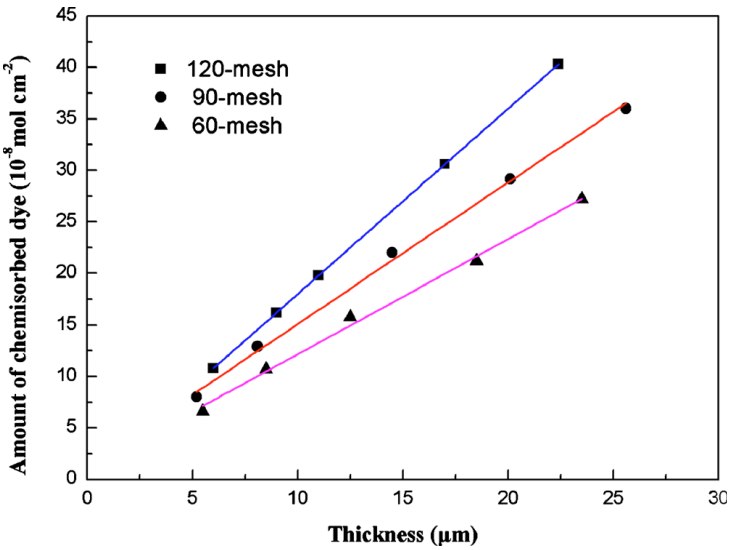

Figure 4.7 Dependence of the amount of chemisorbed dye on the thickness of titania nanotube film based on three types of photoanodes (60-mesh, 90-mesh, and 120-mesh)

Dye loading is one of the key factors to increase the light harvesting efficiency. The dependence of the dye adsorption on different thickness of titania nanotube film based

on three types of photoanodes is illustrated in **Figure 4.7**. It is demonstrated that the amount of dye adsorption increased linearly with the thickness of titania nanotube film. Furthermore, when the thickness of titania nanotube film was fixed, the dye loading of 120-mesh photoanode was the highest, followed by the one based on 90-mesh and then the one based on 60-mesh. As illustrated before, with the increase of mesh number, the roughness factor is also enhanced due to the increased surface area of Ti mesh. That means there will be more surface area to in situ synthesize the titania nanotubes. As the amount of dye adsorption partly depends on the surface area of the titania nanotube film, the dye loading is enhanced.

4.3.8 Influence of film thickness on photovoltaic performance

In order to investigate the influence of film thickness on the photovoltaic performance, a series of 60-mesh photoanodes with different anodization time were used to fabricate DSSCs. The photocurrent-voltage characteristics of the cells are shown in **Figure 4.8**. It was demonstrated that the DSSC with 14.3 μm thick nanotube array layer exhibited the highest conversion efficiency of 3.4%. The existence of optimal film thickness can be explained as follows: when the nanotube array layer was not too thick, dye absorption quantity would increase linearly as the tube length increases (as shown in **Figure 4.7**) leading to the enhancement of short current density. However, when the layer was too thick, the diameter of the mesh hole decreased, restricting the transportation of electrolyte. Besides the electron diffusion length is also increased, which increase the recombination rate. All of this would finally reduce the efficiency of

the cell. This result suggests a proper length of nanotube array layer is essential to optimize the performances of the cell.

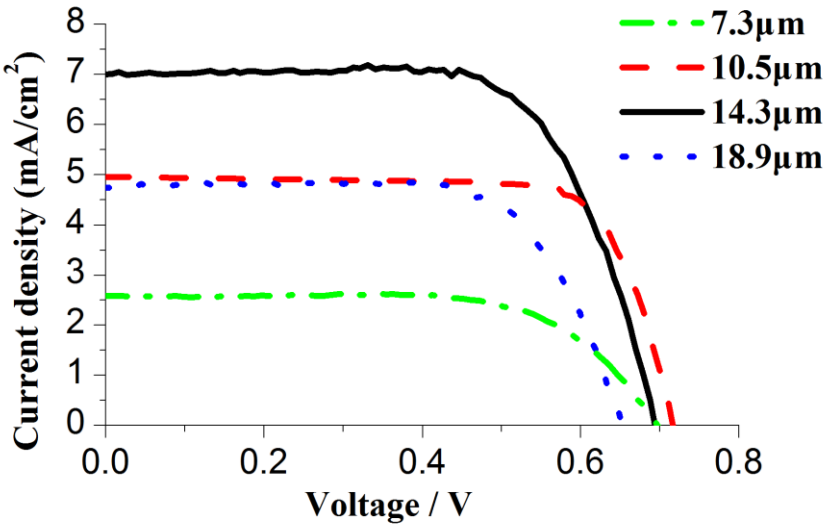

Figure 4.8 *I-V* performances of the DSSCs with different length of nanotube array layer. *AM 1.5*, 100 mW/cm^2

4.3.9 Influence of deposition time of Pt on the counter electrode

As Pt is a kind of noble metal, it is essential to save the amount of Pt in accordance with the low fabrication cost of DSSCs. By controlling the electrodeposition time from 10s to 90s with each 10s as an interval, 9 pieces of platinized Ti sheets were fabricated as counter electrodes with one piece of 60-mesh photoanode. For convenience, all these devices were not seal for the sake of changing counter electrodes.

Table 4.4 Conversion efficiencies of DSSCs with different deposition time of Pt

Time	10	20	30	40	50	60	70	80	90
Conversion	0.56%	1.1%	2.5%	3.3%	3.3%	3.5%	3.2%	3.2%	3.2%

Efficiency

It is apparent from **Table 4.4** when the deposition time was 10 s, the conversion efficiency was only 0.56% because of the insufficient amount of Pt to catalyze the redox couple. When the deposition time was up to 40 s, the conversion efficiency was around 3.3% and changed little with more deposition time. As a result, we platinized all the Ti sheets with the deposition time for 40 s.

It is not accurate that the more amount of Pt, the better of the catalytic activity. As the catalytic reaction is based on surface reaction, only the Pt atoms on the surface can be used as the catalysts. With the increase of deposition time, the Pt deposited onto the Ti surface first appeared as gray color, then gradually changed to black and finally turn to silver white just like a Pt mirror. Pt black is the best catalyst due to its higher dispersion. When the Pt black changed into Pt mirror, the dispersion of Pt was reduced due to the agglomeration of Pt clusters.

4.3.10 Influence of mesh number and device size

Table 4.5 The photovoltaic parameters of different-sized DSSCs based on 60-mesh photoanode, 90-mesh photoanode, 120-mesh photoanode and FTO-based photoanode

Holes number per square inch	Area (cm^2)	V_{oc} (V)	J_{sc} (mA/cm^2)	*ff*	η (%)
60	2	0.69	7.01	0.70	3.4
60	4	0.70	6.89	0.69	3.3
90	2	0.68	11.30	0.69	5.3
90	4	0.67	10.95	0.68	5.0
120	2	0.65	11.80	0.56	4.3

120	4	0.66	11.50	0.53	4.0
FTO	0.283	0.78	15.14	0.66	7.79
FTO	1	0.77	10.1	0.63	4.90
FTO	2	0.72	7.3	0.50	2.63
FTO	4	0.70	6.2	0.44	1.91

To compare the influence of holes number on the photovoltaic parameters, three types of photoanodes in two different areas (2 cm^2 and 4 cm^2) were fabricated into DSSCs. In order to make sure other conditions remaining unchanged, all the Ti meshes were anodized simultaneously in one electrolytic cell for 30 h, which finally resulted in nearly the same length (14.3 μm) nanotube array layer. To further demonstrate the advantage of Ti metal substrates, we also fabricated FTO based DSSCs in 4 different areas, from 0.283 cm^2 to 4 cm^2. **Table 4.5** summarizes the photovoltaic performances of different-sized DSSCs based on three types of Ti meshes and FTO glass. It could be observed that when the area of the cell was 2 cm^2, the efficiency (η) of the cell based on 90-mesh photoanode was the highest, about 5.3% while the others based on 60-mesh photoanode and 120-mesh photoanode were 3.4% and 4.3%, respectively. It is believed the short current density (J_{sc}) and fill factor (*ff*) are the dominant factors to affect the conversion efficiencyiy since the open circuit voltages (V_{oc}) changed only a little. This phenomenon can be explained as follows: with the increase of holes number per square inch, the adsorption quantity of dye molecules was also enhanced in virtue of more titania surface area appeared, as shown in **Figure 4.7**.

However, the diffusion of the electrolyte was more and more difficult since the diameter of the holes decreased. As a result, lots of triiodide irons accumulated at the photoanode side, which caused the polarization of the photoanode and negatively

influenced the photovoltaic performances such as the fill factor. This result indicates a proper number of mesh holes is very important for the mesh-like photoanode. Moreover, it can also be observed that the device size of mesh-like DSSCs had only a little impact on the performances of the cell, which showed the advantage of low resistance by using Ti mesh and Ti sheet as the substrates. However, the efficiencies of FTO based DSSCs decreased drastically, from 7.79% in 0.25 cm^2 area to 1.91% in 4 cm^2 area. This result implies the potential to produce mesh-like DSSCs in large scale.

4.4 Flexible mesh-like DSSC

The flexibility of DSSC has been one of the research hotspots recent years due to its potential to fabricate portable, lightweight DSSCs through roll-to-roll mass production. Until now in most of the reported research conductive plastic substrates, such as ITO/PET are used as the flexible substrates **[17-21]**. As the plastic substrate could not stand high temperature calcination, usually the porous nanocrystalline titania film was coated onto the substrate by low-temperature sintering **[22-24]**, mechanical pressing **[25]**, chemical vapor deposition **[26]**, etc. However the conversion efficiencies of these flexible DSSCs are usually lower than that of the DSSCs based on TCO glass. The main reason is due to the poor necking of titania nanoparticles under low-temperature heat treatment. In this chapter to overcome this weakness, we utilize Ti mesh and Ti sheet as the substrates as both of them are flexible, conductive and high temperature resistant. It is expected that these features could improve the photovoltaic performance of the flexible DSSCs.

4.4.1 Fabrication process of the flexible mesh-like DSSC

The fabrication process of flexible mesh-like DSSCs is similar to that of the rigid devices. The only difference is by using two pieces of transparent thermoplastic film as the outer sealing materials to replace the super white glass. The structure of flexible mesh-like DSSC is a piece of transparent thermoplastic film, mesh-like photoanode, surlyn film, electrolyte, platinized Ti sheet and another piece of transparent thermoplastic film. The two pieces of transparent thermoplastic film were finally sealed by thermoplastic machine.

4.4.2 Influence of bending

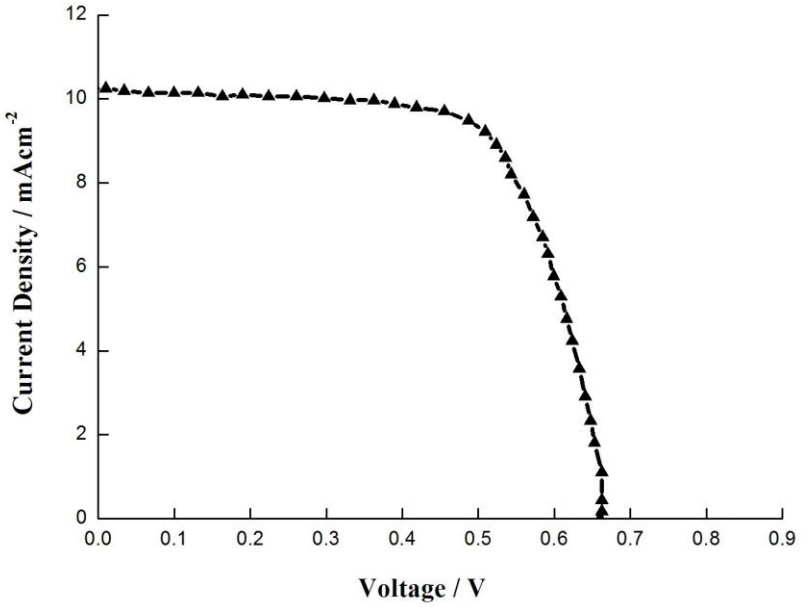

Figure 4.9 *I-V* performances of the flexible mesh-like DSSCs. Photoanode: 90-mesh, Area: 2cm^2

The photovoltaic performance of the flexible mesh-like DSSC (90-mesh photoanode, 2cm2) is shown in **Figure 4.9**. The conversion efficiency was about 4.6%, a little lower than that of the same photoanode in the rigid mesh-like DSSC. This is mainly due to the

lower transmittance of the transparent thermoplastic film (79%), compared with the super white glass (91.5%). As the bendability is one of the important factors for flexible DSSCs, we measured the photovoltaic parameters according to the bending times with bending angle about 90 °, as shown in **Figure 4.10**. It can be seen from **Table 4.6** that there is no obvious decrease in these photovoltaics parameters after 200 times of bending. Thus, this flexible mesh-like DSSC has good mechanical bendability to be a promising device for industry production.

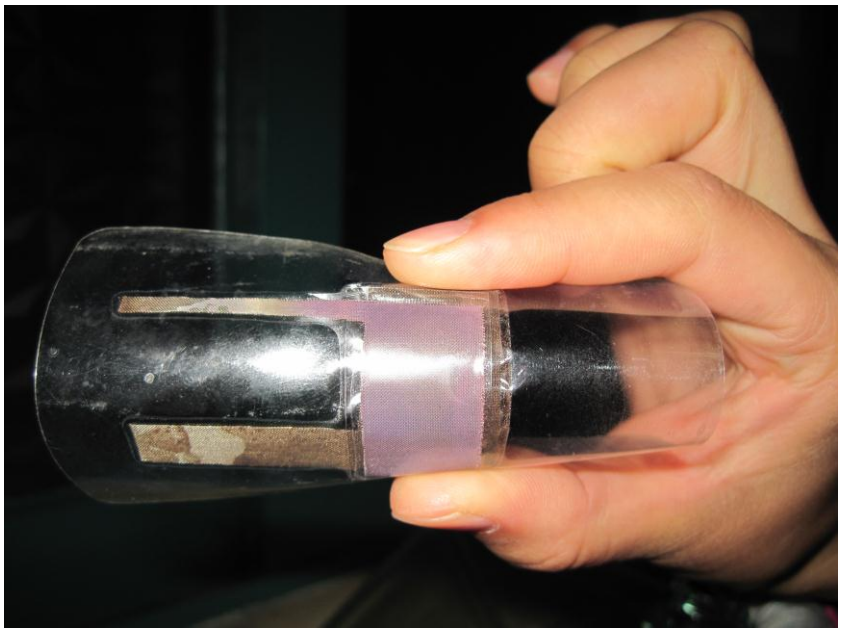

Figure 4.10 A prototype of a flexible mesh-like DSSC with bending angle of 90 °.

Table 4.6 The photovoltaic parameters of a flexible mesh-like DSSC as a function of bending times

Bending times	V_{oc} (V)	J_{sc} (mA/cm^2)	*ff*	η (%)
40	0.66	10.06	0.69	4.58
80	0.67	10.55	0.66	4.66

120	0.66	10.21	0.68	4.58
160	0.68	10.36	0.68	4.79
200	0.66	10.40	0.66	4.53

4.5 Further improvements

Although this new structured mesh-like DSSC has showed some advantages over traditional ones, there are still lots of problems remained to be solved. For example, the short current density is lower than the-state of the art (>15mA/cm^2) even if we have utilized the TiO_2 nanotubes as the photoanode material and low-resistance Ti mesh and Ti sheet as the substrates. One of the main reasons is the thickness of the Ti mesh. In the traditional TCO-based dye-sensitized solar cell, the diffusion length of the ions is controlled by the surlyn film which is usually 20 to 50 μm **[27]**. However, the diffusion length in our device is mainly controlled by the Ti mesh which is more than 100 μm. If we could make a thinner Ti mesh, the diffusion length will be shortened, which is beneficial for the current density. At present, we try to use the laser drilling machine to drill tiny holes on a thin Ti sheet (about 50 μm) to produce Ti mesh and then use it to fabricate the cell. This work is currently in progress. Moreover, for the flexible mesh-like DSSCs, it is necessary to find high transparency thermoplastic film as the sealing materials. By utilizing a thinner Ti mesh and higher transparent thermoplastic film, the flexible mesh-like DSSC could increase its conversion efficiency to a higher value.

4.6 Conclusion

As a summary, a new type of mesh-like DSSC is developed by using Ti mesh and Ti sheet as the substrates of photoanode and counter electrode, respectively. The structure of this DSSC showed some advantages such as low sheet resistance over the traditional ones. Besides, according to the data of Alibaba Limited, the current price of TCO glass suitable for the DSSC is 25-40 USD/m^2, while the price of Ti mesh, Ti sheet and the super white glass is 15-20 USD/m^2, 12-18 USD/m^2 and 6-12 USD/m^2, respectively, which means the cost of the proposed DSSC is comparable with the traditional one and has a little advantage. The Ti mesh was anodized to directly synthesize the highly ordered self-organized titania nanotube array layer on its surface. Different length of nanotube array layers was investigated to find their influence on the photovoltaic performances. The experiment indicated that a proper length of the layer is a key factor to achieve high conversion efficiency. The influence of the mesh numbers is considered and it was found that the cell with 90-mesh photoanode exhibited the highest conversion efficiency of 5.3%, which showed superiority compared with the backside illuminated DSSC and other metal-substrate-based DSSC. The most important is that the size of the cell had only a little impact on the photovoltaic parameters, e.g. the conversion efficiency of the DSSC in 4 cm^2 area was 5.0%, only a little lower than 5.3% in 2 cm^2 area. The flexible mesh-like DSSC were also fabricated by using transparent thermoplastic film as the sealing materials. The bendability was investigated and showed good mechanical and photovoltaic stability. Further work is essential to optimize the sealing material and the thickness of the mesh.

References:

1. M. Toivola, F. Ahlskog, and P. Lund, Industrial sheet metals for nanocrystalline dye-sensitized solar cell structures. *Sol Energ Mater Sol C*, 2006. **90**: 2881-93.
2. X. M. Fang, T. L. Ma, M. Akiyama, G. Q. Guan, S. Tsunematsu, and E. Abe, Flexible counter electrodes based on metal sheet and polymer film for dye-sensitized solar cells. *Thin Solid Films*, 2005. **472**: 242-45.
3. K. Onoda, S. Ngamsinlapasa, T. Fujieda, S. Yoshikawa, The superiority of Ti plate as the substrate of dye-sensitized solar cells. *Sol Energ Mater Sol C*, 2007. **13**: 1176-81.
4. Y. Jun, J. Kim, and MG. Kang, A study of stainless steel-based dye-sensitized solar cells and modules. *Sol Energ Mater Sol C*, 2007. **91**: 779-84.
5. M. G. Kang, N. G. Park, K. S Ryu, S. H. Chang, and K. J. Kim, 4.2% efficient flexible dye-sensitized TiO2 solar cells using stainless steel substrate. *Sol Energ Mater Sol C*, 2006. **90**: 574-81.
6. K. Onoda, S. Ngamsinlapasa, T. Fujieda, and S. Yoshikawa, The superiority of Ti plate as the substrate of dye-sensitized solar cells. *Sol Energ Mater Sol C*, 2007. **91**: 1176-81.
7. S. Kayama, Y. Wakizaka, and K. Kondo, Metal Oxide Dispersion, Metal Oxide Electrode Film, and Dye Sensitized Solar Cell, photoactive electrode. US Patent No 7, 157, 788, 2002.
8. H. Sugihara, K. Hara and K Sayama, et al. Platinum complex for use as sensitizer for semiconductor electrode of solar cell. US Patent No 6, 274, 806, 2000.

9. K. Okada, H. Matsui, T. Kawashima, T. Ezure, and N. Tanabe, 100mm ×100 mm large-sized dye sensitized solar cells. *J Photochem Photobiol A: Chem*, 2004. **164**: 193-98.
10. M. Paulose, K. Shankar, O. K. Varghese, G. K. Mor, B. Hardin, and C. A. Grimes, Backside illuminated dye-sensitized solar cells based on titania nanotube array electrodes. *Nanotechnology*, 2006. **17**: 1446-48.
11. S. Ito, NLC. Ha, G. Rothenberger, P. Liska, P. Comte, S. M. Zakeeruddin, P. Pechy, M. K. Nazeeruddin, and M. Graetzel, High-efficiency (7.2%) flexible dye-sensitized solar cells with Ti-metal substrate for nanocrystalline-TiO_2 photoanode. *Chem Commun*, 2006. **38**: 4004-06.
12. G. K. Mor, O. K. Varghese, M. Paulose, and C. A. Grimes, Transparent highly ordered TiO_2 nanotube arrays via anodization of titanium thin films. *Adv Funct Mater*, 2005. **15**: 1291-96.
13. O. K. Varghese. M. Paulose, K. Shankar, G. K. Mor, and C. A. Grimes, Water-photolysis properties of micron-length highly-ordered titania nanotube-arrays. *J Nanosci Nanotechno*, 2005. **5**: 1158-65.
14. S. Yamanaka, T. Hamaguchi, H. Muta, K. Kurosaki, and M. Uno**,** Fabrication of oxide nanohole arrays by a liquid phase deposition method. *J Alloy Compd*, 2004. **373**: 312-15
15. T. Kawashima, H. Matsui, and N. Tanabe, New transparent conductive films: FTO coated ITO, *Thin Solid Films*, 2003. **445**: 241-44.

16. T. Kawashima, T. Ezure, K. Okada, H. Matsui, K. Goto, and N. Tanabe, FTO/ITO double-layered transparent conductive oxide for dye-sensitized solar cells. *J Photochem Photobiol A: Chem*, 2004. **164**: 199-202.
17. M. A. Depolima, A. F. Nogueira, D. A. Machado, and C. Longo, All-polymeric electrochromic and photoelectrochemical devices: new advances. *Electrochim Acta*, 2001. **46**: 4243-49.
18. M. Durr, A. Schmid, M. Obermaier, S. Rosselli, A. Yasuda, and G. Nelles, Low-temperature fabrication of dye-sensitized solar cells by transfer of composite porous layers. *Nat Mater*, 2005. **4**: 607-11.
19. S. Uchida, M. Timiha, H. Takizawa, and M. Kakizawa, Flexible dye-sensitized solar cells by 28 GHz microwave irradiation. *J Photochem Photobiol A: Chem*, 2004. **164**: 93-96.
20. J. H. Xiang, P. X. Zhu, Y. Masuda, M. Okuya, S. Kaneko, and K. Koumoto, Flexible solar-cell from zinc oxide nanocrystalline sheets self-assembled by an in-situ electrodeposition process. *J Nanosci Nanotechno*, 2006. **6**: 1797-1801.
21. D. S. Zhang, T. Yoshida, T. Oekermann, K. Furuta, and H. Minoura, Room-temperature synthesis of porous nanoparticulate TiO_2 films for flexible dye-sensitized solar cells. *Adv Funct Mate*, 2006. **16**: 1228-34.
22. C. Longo, A. F. Nogueira, M. A. De Paoli, and H. Cachet, *Cloning of a novel receptor expressed in rat prostate and ovary, J Phys Chem B*, 2002. **106**: 5925-30.

23. P. M. Sommeling, M. Spa ¨ th, J. Kroon, R. Kinderman, and J. A. M. van Roosmalen, Dye-sensitized nanocrystalline TiO_2 solar cells on flexible substrates, ECN- RX—98-040, 1998.

24. F. Pichot, J.R. Pitts, and B. A. Gregg, Low-temperature sintering of TiO_2 colloids: application to flexible dye-sensitized solar cells, *Langmuir*, 2000. **16**: 5626-30.

25. H. Lindstro ¨m, A. Hormberg, E. Magnusson, L. Malmqvist, and A. Hagfeldt, A new method to make dye-sensitized nanocrystalline solar cells at room temperature, *J Photochem Photobiol*, 2001. **A145**: 107-112.

26. T. N. Murakami, Y. Kijitori, N. Kawashima, and T. Miyasaka, Low Temperature Preparation of TiO_2 Mesopores for Efficient Dye-Sensitized Photoelectrode by Chemical Vapor Deposition Combined with UV Light Irradiation. *J Photochem Photobiol*. 2004. **A 164**: 187-91.

27. M. K. Nazeeruddin, F. De Angelis, S. Fantacci, A. Selloni, G. Viscardi, P. Liska, S. Ito, B. Takeru, and M. Gratzel, Combined Experimental and DFT-TDDFT Computational Study of Photoelectrochemical Cell Ruthenium Sensitizers. *J Am Chem Soc*, 2005. **127:** 16835-47

CHAPTER 5 Development of the DNA-like DSSCs

5.1 Introduction

Spiral-like structure exists universally in the nature. From the smallest cell to the infinite universe, the spiral structure could be seen everywhere. Especially in 1953 when James D. Watson and Francis Crick **[1]** announced the discovery of DNA double helix structure (**Figure 5.1**) to the world, more and more efforts were dedicated to extensively investigate this marvelous structure. The question is raised: why does the universe choose double helix structure as the basic architecture of hereditary material and what is its advantage? Although this question is still under investigation, one of the superiority of the double helix structure is that it can utilize the 3D space sufficiently. As we know, the space in a cell is very limited, it is necessary to choose a compact structure. Due to this merit, recent years the double helix structure is widely used in many other fields such as the architecture design. Is it possible to utilize this novel structure to the photovoltaic field especially DSSCs?

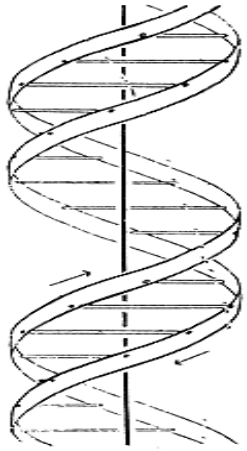

Figure 5.1 The double helix structure of a DNA molecule **[1]**

So far the commercialized solar cells are all based on 2D planar substrate including the DSSCs. Although planar DSSCs have achieved conversion efficiency up to 11.5% **[2]**, the 2D structures have shortcomings that they largely occupy land and cannot utilize the spatial scattered light. It was not until recent years a few research groups paid attention to building DSSCs based on 3D substrates, such as wire-like DSSCs **[3]**, bifacial DSSCs **[4]**, photovoltaic fibers **[5]**, 3D DSSC based on optical fibers **[6]**, and all Ti based 3D DSSC **[7-8]**. Among them, Dr. Liu's research group designed an all Ti based 3D DSSCs which could absorb sunlight from all directions. Compared with the planar substrate based DSSCs, by using the same land occupancy, this type of DSSC could further increase its absorption area to utilize the spatial scattered light and thus increased the light harvesting efficiency. Besides, due to the low resistance of Ti wires, the sheet resistance of 3D DSSC was largely reduced. However, this type of 3D DSSC adopted titania nanoparticles film as the active layer of photoanode by dip coating method. As introduced in Chapter 1, there were lots of grain boundaries between the nanoparticles which acted as trap sites to block the electrons transport and finally increase the recombination process **[9-10]**. The affinity between the Ti substrate with the titania nanoparticles film was not compact enough **[7-8]**. The active layer of photoanode was easy to be peeled off from the support substrate. Moreover, dip-coating method could not precisely control the thickness of the film hence it was hard to investigate the influence of film thickness to optimize the device. If the film was too thick, it was easy to produce deep cracks on the film, resulting in the direct contact between the substrate and the electrolyte. Finally the triiodide ions were reduced by the electrons of the substrate and lowered the charge collection efficiency. Furthermore, the distance

between photoanode and counter electrode was longer than the traditional ones, thus increased the electrolyte diffusion resistance.

In order to overcome the deficiencies mentioned above, by the inspiration of double helix structure, a new 3D structured DSSC is developed which is named as the DNA-like DSSC according to its appearance. It is also a TCO-free device which is based on Ti wires with low resistance. Instead of dip-coating, we still adopt electrochemical anodization method to directly synthesize highly ordered titania nanotube arrays on the surface of Ti wires. As a result, not only the affinity between the Ti substrate and titania film is improved, but also it is more easy to control the film thickness by adjusting the anodization time.

5.2 Experimental materials and equipment

5.2.1 Experimental materials

All the materials used in the experiments are listed in Table 5.1.

Table 5.1 Experimental materials

Name	Remark	Manufactory
Ti wires	commercially pure titanium	Hebei anping netting screen production ltd.
Ammonium fluoride	AR. 98+%	Tianjin fuchen chemical reagent factory
Ethylene glycol	AR. 98+%	Guangzhou chemical reagent factory
Chloroplatinic acid	AR.	Shenyang research institute of nonferrous metals

Silicon dioxide hydrosol	AR. 98+%	Fluka
Ru complex dye	N719	Solaronix，sa
Ethanol	AR.	Guangzhou chemical reagent factory
Anhydrous LiI	AR. 98+%	Fluka
I_2	AR. ≥99.55(RT)	Fluka
Acetonitrile	AR.	Tianjin damao chemical instrument supply station
4-tertbutylpyridine	AR. 99%	Aldrich
Surlyn 1702 resin		Du pont
AB epoxy transparent glue	15s	Singapore miradur specialty chemicals ltd.

5.2.2 Equipment

All the equipment is listed in Table 5.2.

Table 5.2 Equipment list

Name	Model	Manufactory
UV–Vis–NIR spectrometer	U-4100	Hitachi
DC Power Supply	GPC-6030D	Guangzhou xinhong trading co., ltd
Keithley 2400		Keithley instruments inc.
Low-temperature resistance furnace	SX-2.5-10	Shanghai wuyangshan international trading co., ltd
Solar simulator	Newport-Oriel 91192	Newport co., ltd
Hydrothermal tank	HSRL-400	Jinan henghua technology co., ltd.

5.3 DNA-like DSSC based on highly ordered nanotube arrays

5.3.1 Preparation of the photoanode

The Ti wire with diameter of 0.4 mm was twined around a steel screw to make a spiral-like electrode, which can be seen from **Figure 5.2 (a)**. Prior to anodization, the spiral-like electrode was ultrasonically cleaned and degreased in acetone and ethanol successively, followed by rinsing with deionized water and drying the sample in a nitrogen stream. Anodization was performed in a two-electrode configuration with the spiral-like Ti wire as the working electrode and Pt foil as the counter electrode under constant potential (30 V) at room temperature (23 ℃). A direct current power supply (GPC-6030D) was used as the voltage source to drive the anodization. The electrode was anodized in the electrolyte containing a mixture of ethylene glycol (48.86 wt%), polyethylene glycol 600 (49.38 wt%), H_2O (1.31 wt%) and NH_4F (0.43 wt%). Similar to the electrochemical anodization of Ti mesh, the thickness of titania nanotube arrays layer around the Ti wire can be controlled by changing the anodization time. In the first 60 seconds, it was apparent to see lots of bubbles come from the wire surface, while only a little bubble produced from the Pt foil. After 10 minutes, no bubbles could be seen from the Ti wire since the over oxidized titania layer was covered on the Ti surface. When the anodization process was finished, the samples were carefully taken out from the electrolyte and rinsed with deionized water to remove the fluorine irons at 23 ℃ for three times. Each time after the sample was rinsed for 3 minutes, it should be dried in a gently steam of nitrogen gas. Finally the cleaned sample was sintered at 450 ℃ (heating/cooling rate of 10 ℃ / minutes) in air.

The Ti wire should be made to spiral shape first and then anodized. On the contrary, if the Ti wire was anodized first, then when it was twisted into the spiral-like, the oxide layer on the turnings of the wire would be peeled off due to the bending stress of these points. It is very important to anneal these samples at 450 ℃ to fix the surface oxide layer.

5.3.2 Preparation of the counter electrode

The substrate of counter electrode was also a Ti wire. In order to enhance the adherence of Pt layers onto the substrate, the Ti wire was polished with sand paper to produce a much rougher surface. Then it was washed with acetone and ethanol in an ultrasonic bath for 3 minutes. Finally the cleaned Ti wire was platinized by the electrodeposition process which was carried out using an aqueous solution of 5×10^{-3} mol/L $H_2PtCl_6 \cdot 6H_2O$ at room temperature. A digital sourcemeter (Keithley, 2400) was used as a power supply. Here, the Pt electrode was prepared with 15 mA cm^{-2} current density for 60 s and then sprayed with a porous SiO_2 layer as an electrical insulator and calcined at 150 ℃ for 30 minutes.

The function of the porous SiO_2 layer is to electrical insulate the platinized Ti wire from the anodized Ti wire. Although the direct contact between the platinized Ti wire with the oxide surface of the anodized Ti wire cannot lead to short circuit, this step is prepared as a precaution if at one time a piece of oxide layer peels off from the substrate.

5.3.3 Fabrication process

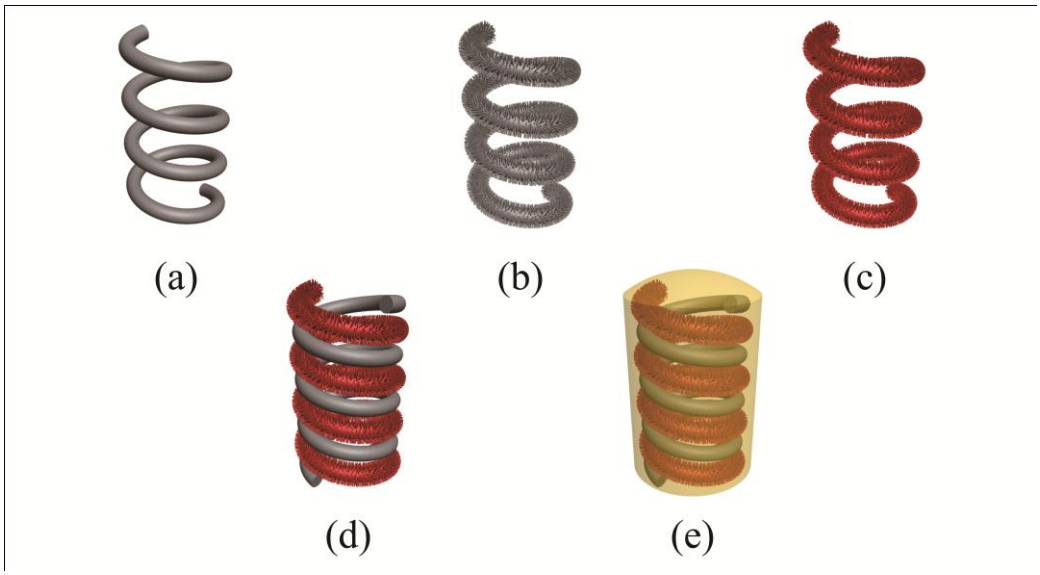

Figure 5.2 Fabrication process of the DNA-like DSSC: (a) Spiral-like electrode based on Ti wire; (b) Anodized spiral-like electrode; (c) Sensitized spiral-like electrode; (d) DNA-like electrodes; (e) Sealed DNA-like DSSC

For solar cell fabrication, the anodized spiral-like Ti wire (**Figure 5.2 (b)**) was sensitized overnight for 24 hours by soaking in the solution of N719 dye dissolved in ethanol. After soaking, the sensitized wire (**Figure 5.2 (c)**) was rinsed with ethanol to remove nonchemisorbed dyes. The anodized spiral wire was then twisted with the platinized Ti wire to make the DNA-like structure which is shown in **Figure 5.2 (d).** If not illustrated specially, all the cells in this paper have 14 screw threads with the length about 1.5 cm. Then they were all put into a small glass tube with the electrolyte consisting of 0.5 mol/L LiI, 0.05 mol/L I_2, and 0.5 mol/L 4-tert-butylpyridine in acetonitrile. Finally the tube was sealed with Surlyn 1702 resin and epoxy, as shown in **Figure 5.2 (e).**

The operation principles of DNA-like DSSC are briefly summarized as follows (**Figure 5.3**): When the sunlight irradiates through the small glass tube to the sensitized

spiral-like Ti wire, the dye molecules anchored on the highly ordered titania nanotube arrays are stimulated from the original state to the excited state (Excitation). The unstable excited dye molecules inject their electrons into the conduction band of highly ordered titana nanotubes (Injection). The injected electrons subsequently transport through the vertically ordered pathways to the Ti wire substrate（percolation）. Then they were collected through the Ti wire to the external circuit. Finally through the external circuit, the electrons are gathered on the platinized spiral-like Ti wire (counter electrode). Concurrently the oxidized dye cations are reduced by iodide ions and iodide ions are oxidized into the triiodide ions (Dye regeneration). The triiodide ions can diffuse up or down to the nearest platinized Ti wire in which triiodide ions are reduced into iodide ions again by the Pt catalysis (Electrolyte regeneration), and then the iodide ions can also diffuse up or down to the nearest sensitized Ti wire. This step is the most different with the conventional one that the triiodide ions have two choices to diffuse. Similar as conversional DSSC, there is no permanent change of chemicals in the DNA-like DSSC. The only differences are the electrons transportation ways and the electrolyte diffusion pathways.

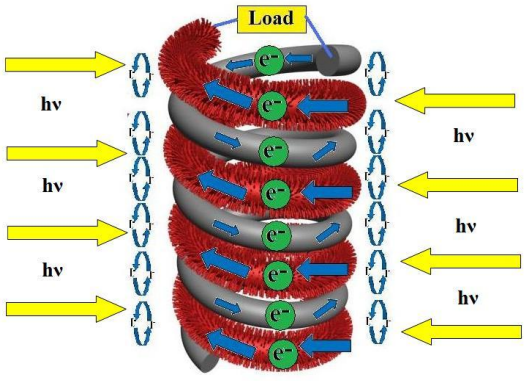

Figure 5.3 Operation principles of the DNA-like DSSC

5.3.4 Morphology

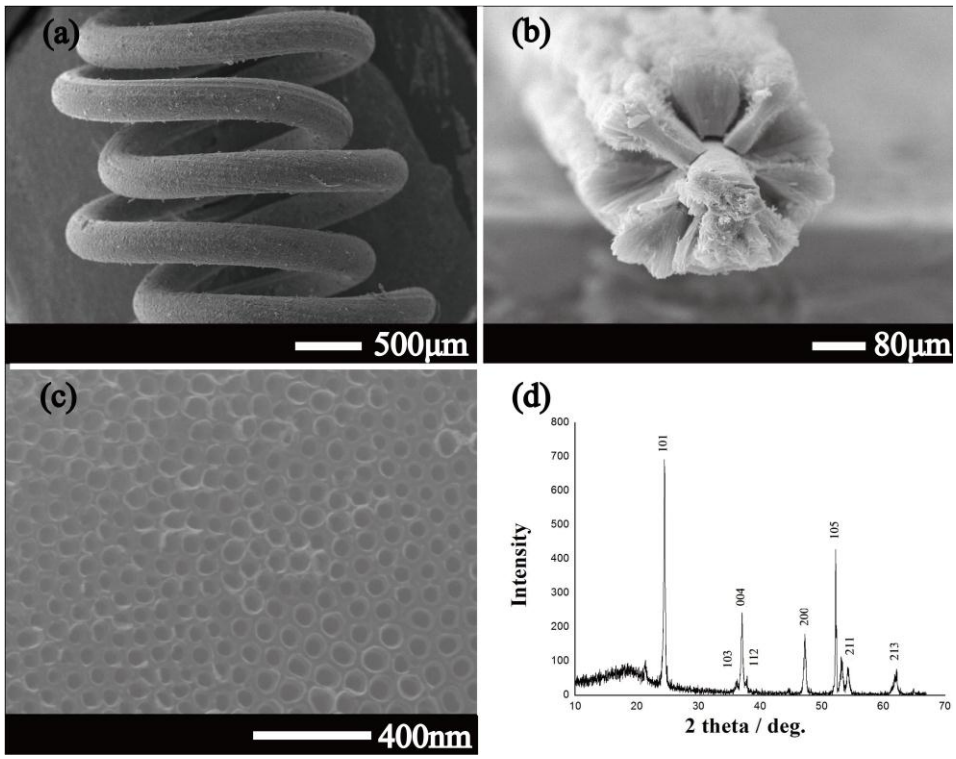

Figure 5.4 The morphology information of DNA-like DSSCs: (a) SEM image of the DNA-like dye-sensitized solar cell (not sealed). (b) Cross-sectional view SEM image of the anodized Ti wire. (c) Top view SEM image of the anodized Ti wire. (d) XRD pattern of the anodized Ti wire after annealing

Figure 5.4 (a) shows the SEM image of the DNA-like DSSC (not sealed) which is a left-handed double-helix structure. Two electrodes wind around each other with gaps for the diffuse of electrolyte. **Figure 5.4 (b)** is the cross-sectional SEM image of the anodized Ti wire. It is evident that after anodization the self-organized titania nanotube arrays grew perpendicularly around the Ti wire substrate. **Figure 5.4 (c)** is the top view SEM image of the anodized Ti wire. Nanotubes were packed in approximately cylindrical symmetry with an average inner diameter and wall thickness of 73 ± 5 and

10 ±2 nm, respectively. It can be seen from the XRD patterns (**Figure 5.4 (d)**) that after annealing the nanotubular arrays layer has anatase phase.

5.3.5 Influence of film thickness

In order to compare the cells with different length of nanotubular arrays, the anodized spiral-like Ti wires with different anodization time were used to fabricate the DSSCs. **Figure 5.5** shows the *I-V* features of the cell with different thickness of nanotube layers. The 15.3 μm length nanotubular layer DSSC exhibited the highest peak output power (P_{max}), about 0.49 mW. This is because the dye adsorption in the film is enhanced when the length of the nanotubular arrays is longer and an increased short circuit current (I_{sc}) would be expected. The charge recombination between electrons and triiodide ions in the electrolyte would, however, become more serious in thicker films as the electron transportation and the electrolyte diffusion in the titania layer are harder, which was detrimental to electron collection efficiency, and hence, lowered the photocurrent. It could be seen that from the trend of I_{sc} the dye adsorption dominated the photocurrent generation below 15.3 μm, resulting in an increase in I_{sc} until 15.3 μm. On the contrary, charge recombination played a key role in the photovoltaic performance when the thickness was more than 15.3 μm. The open circuit voltage (V_{oc}) showed almost no variation at least within the length range of our experiments. Balanced from these factors, P_{max} increased with thickness until 15.3 μm followed by a decrease. It was concluded from **Figure 5.5** that the optimal thickness fell in the range of 14–16 μm. The titania films presented in this article had a thickness in the optimal range.

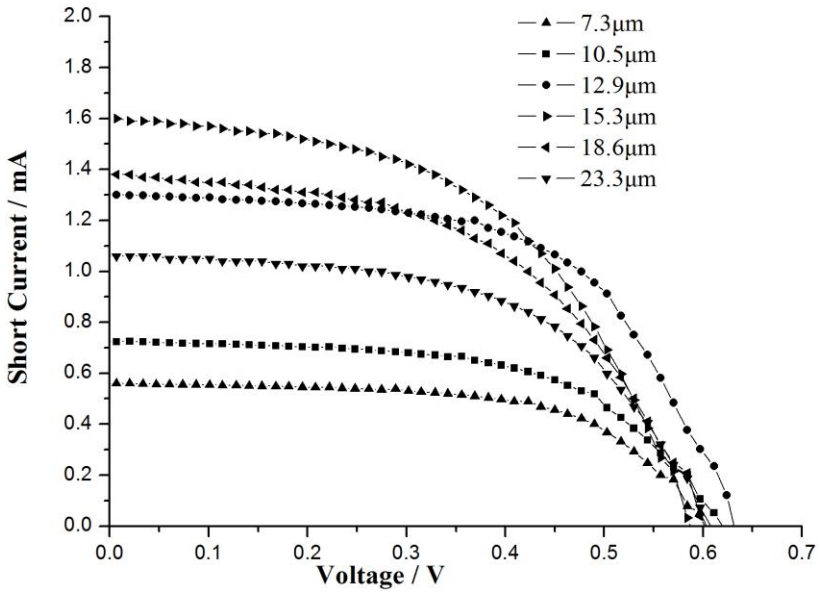

Figure 5.5 *I-V* performances of the DSSCs with different length of the nanotubular array layer. *AM 1.5*, 100 mW/cm^2

5.3.6 Sunlight utilization

Given that the sunlight contains 10% to 20% diffuse light in a clear day and even more than 50% in a cloudy day, the DNA-like DSSCs in our work have superiority of light utilization as its 3D symmetrical double-helix structure could effectively capture spatial diffuse sunlight from any directions normalized to the center axis, compared to the traditional flat-type DSSC. In order to verify this point, we fixed the DNA-like DSSC in the center of a circle and moved the light source around the circumference from 0 °to 360 °. **Figure 5.6** shows the photovoltaic parameters of the cell illuminated in different degrees of light source. The figure shows that the I_{sc} and V_{oc} changed little with

the changes of angles of the light source, which indicates that the DNA-like DSSC has the ability of passive tracking light source and is more suitable to practical application.

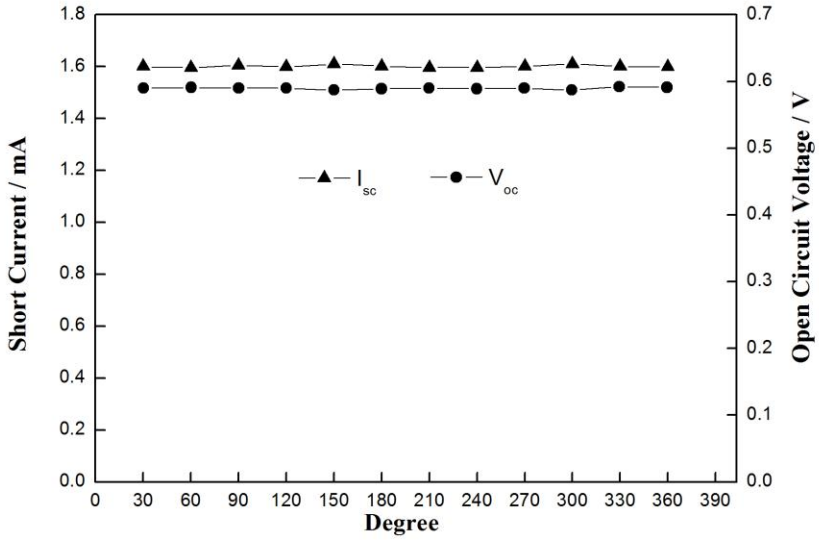

Figure 5.6 The photovoltaic parameters of the cell illuminated in different degrees of light source.

5.3.7 DNA-like DSSC modules

As the output of single DNA-like DSSC is very small, it is necessary to assemble the cells into a module. The photovoltaic performance of the DNA-like DSSCs had also been studied when they were connected in parallel or series. **Figure 5.7** shows the *I-V* curves of two such cells separated and combined in series or in parallel. The total V_{oc} equaled the sum of the two cell's V_{oc} when they were in series and the total I_{sc} equaled the sum of the two cell's I_{sc} when they were in parallel. We even tried to fabricate a module with 10 cells in parallel (**Figure 5.8**) and found the I_{sc} still nearly equaled the sum of the separate cells' I_{sc}. Furthermore, as the conventional solar cells utilize the grid

lines on their surface to collect electrons, there will be 7% light loss. In the DNA-like DSSC modules, as the lead wires are under the cells, they will not block the incident sunlight. This result implies the possibility of larger modules with lots of DNA-like DSSCs assembled by integrated circuit method.

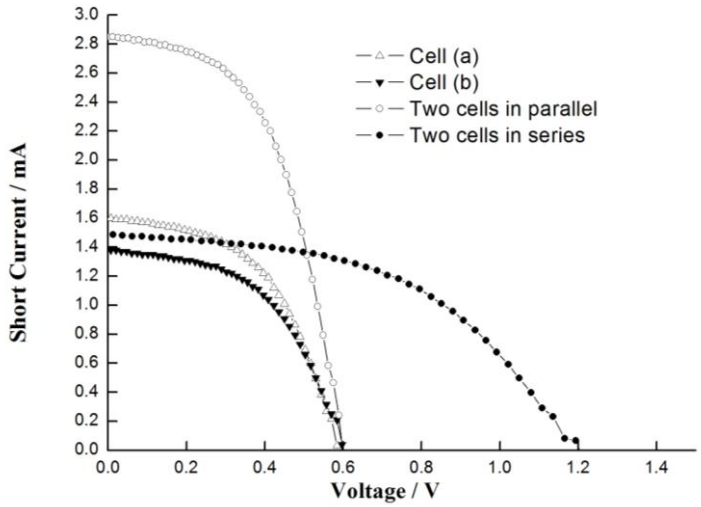

Figure 5.7 *I-V* curves of two DNA-like devices separated and combined in series or in parallel.

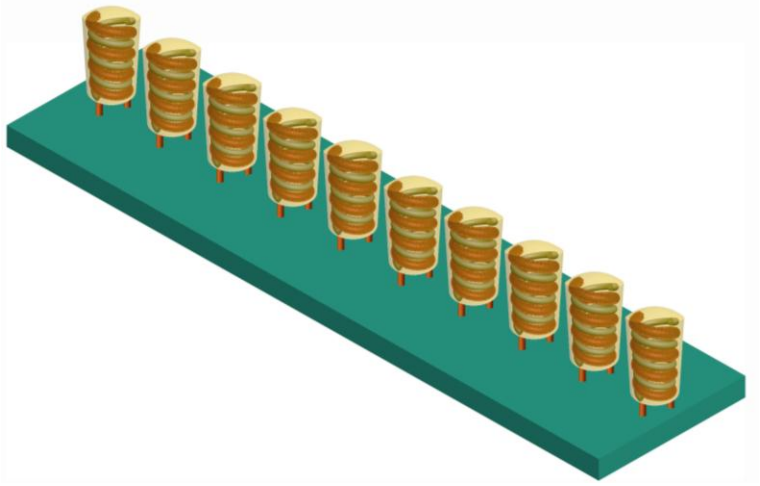

Figure 5.8 PV module with 10 DNA-like DSSCs in parallel

5.4 DNA-like DSSC based on titania nanowire-covered nanotube bilayer film electrodes

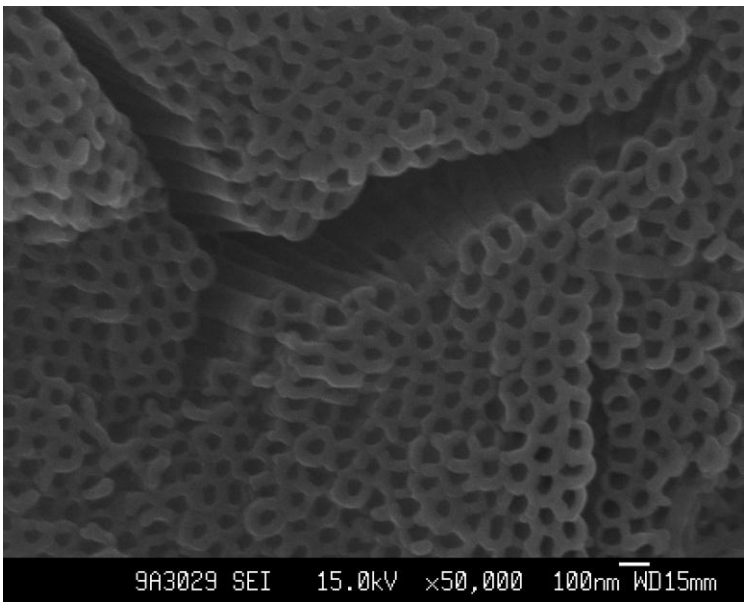

Figure 5.9 Cracks on the photoanode film

The idea of coating one more layer of titania nanowire onto the top of titania nanotube come from an tentative experiment: we put a anodized Ti sheet into the hydrothermal reactor to see where the nanowires would grow. After reaction, through the SEM observation it was interested to see that nanowires grew everywhere, including the top and side of nanotubes and even the uncovered substrate. As we know it was a common phenomenon to see micron-wide cracks on the photoanode film, as shown in **Figure 5.9**. This was mainly due to the uneven coefficient of heat expansion and hard to avoid. If the crack was deep enough to the substrate, then the triiodide ions in the electrolyte could directly contact with the substrate and be reduced by the electrons in the substrate, which would directly reduce the electrons collection efficiency. By the inspiration of nanowires covered nanotube result, we applied this two-step formation of

titania nanowires-covered nanotube bilayer technique on the photoanode of DNA-like DSSC to further optimize this device.

5.4.1 Preparation of titania nanowires-covered nanotubes bilayer film

First a Ti sheet was exposed to an etching fluid comprising of hydrofluoric acid and nitric acid to get a textured surface and then it was washed with acetone and ethanol in an ultrasonic bath for 3 minutes. The anodization was performed in a two-electrode configuration with the Ti sheet as the working electrode and a platinum foil as the counter electrode under constant potential (30 V) at room temperature (23 ℃) for about 20 h. The Ti sheet was anodized in the electrolyte containing a mixture of ethylene glycol (50.86 wt.%), polyethylene glycol 600 (47.38 wt.%), H_2O (1.31 wt.%) and NH_4F (0.43wt.%) to grow the nanotube arrays layer. After anodization, the anodized sample was rinsed with deionized water and dried in a nitrogen stream. The titania nanowires were directly grown onto the titania nanotube arrays layer by putting the anodized Ti sheet into a Teflon reactor (50 mL), containing 27 mL of 1.0 mol/L NaOH solution. Then the reactor was sealed and hydrothermally heated at 230 ℃ for 4 h to grow the titania nanowires. When the reaction period ended, the sample was immersed into a 0.1 M HCl aqueous solution for 10 h and then washed with deionized water. Finally, the sample was sintered at 450 ℃ for 30min.

By replacing the Ti sheet with a spiral-like Ti wire with other conditions remaining unchanged, we applied the titania nanowire-covered nanotube bilayer film as the photoanode material to fabricate the DNA-like DSSCs. For comparison, titania

nanotube-based electrodes and titania nanowire-based electrodes were also made to fabricate the reference devices, as shown in **Figure 5.10.**

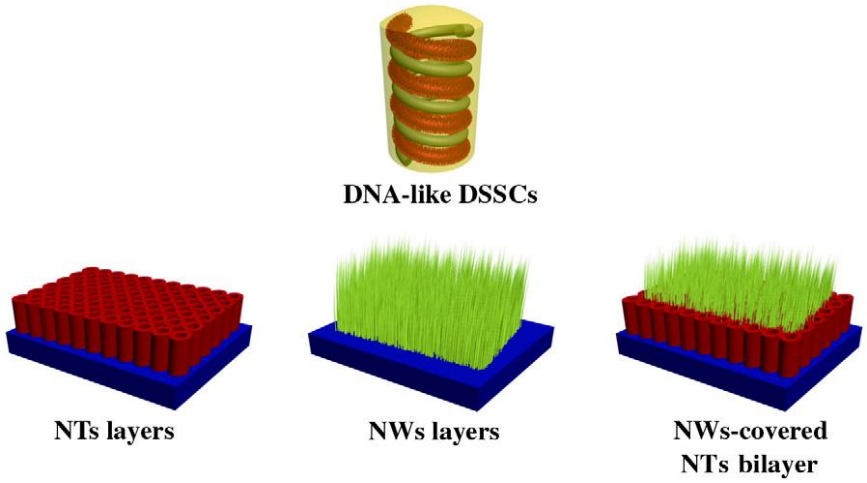

Figure 5.10 Schematic diagram of the DNA-like DSSCs based on the nanotube film, nanowire film and nanowire-covered nanotube bilayer film electrodes

5.4.2 Morphology

Figure 5.11 shows the representative SEM images of the as-prepared titania nanowire-covered nanotube bilayer film. As shown in **Figure 5.11(a)**, highly well oriented titania nanowires entangled each other to form a macroporous structure. From the cross-section view (**Figure 5.11(b)**) we could see the titania nanowires rooted firmly from the top of the titania nanotube layer. The titania nanowires are 0.15–0.3 μm in width and 1–3 μm in length. Here we also find something interesting. It is common that there would be some cracks in the film due to the difference of the expansion coefficients between the substrate and the film. It is observed from **Figure 5.11(c)** that the titania nanowires could also be directly synthesized from the sides of the crack and connected together. To observe the crack more clearly, the nanowire layer on the top

was removed by the ultrasonic treatment. As shown in **Figure 5.11(d)**, a high density of nanowires filled the crack and connected the cracks like bridges. It is attributed to the deep penetration of NaOH solution into the cracks and reacted with the titania nanotubes. This phenomenon indicates that the nanowires may play a role to modify the surface cracks of the lower layer (nanotube layer), which is beneficial to avoid the direct contact between the substrate and the electrolyte and lower the dark current of the DSSCs.

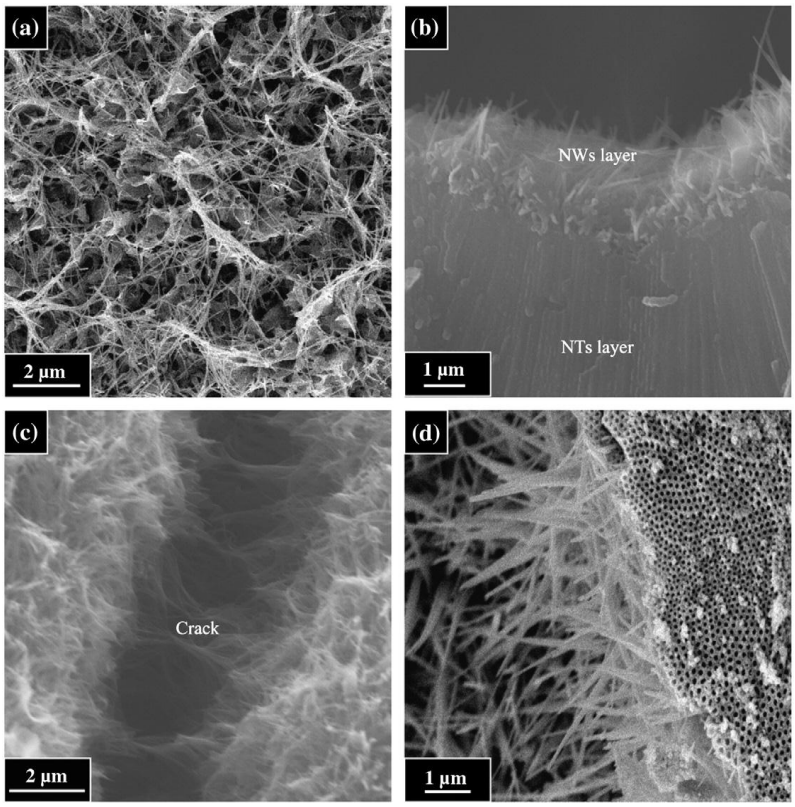

Figure 5.11 SEM images of the nanowire-covered nanotube bilayer film: (a) top view; (b) cross-section view; (c) and (d) cracks

5.4.3 Reflectance spectra of films

The reflectance spectra of the titania nanowire-covered nanotube bilayer film, the titania nanowire film and the titania nanotube film are shown in **Figure 5.12**, which

were respectively measured by the UV–Vis–NIR spectrometer. It can be observed that in the spectral range from 430 to 1100 nm, the nanowire film exhibited the highest diffuse reflectance, followed by the nanotube film and finally the nanowire-covered nanotube bilayer film. This result explains two important issues. First, only the nanowire film cannot effectively reduce the reflectance of the substrate since the coverage of nanowires on the substrate is not enough. Second, the nanowires could go on decreasing the reflectance of the nanotube film because they could reflect the incident light several more times, which would further increase the light harvesting efficiency. Consequently, compared with the titania nanowire film and the titania nanotube film, the titania nanowire-covered nanotube bilayer film is more suitable as a light trapping layer.

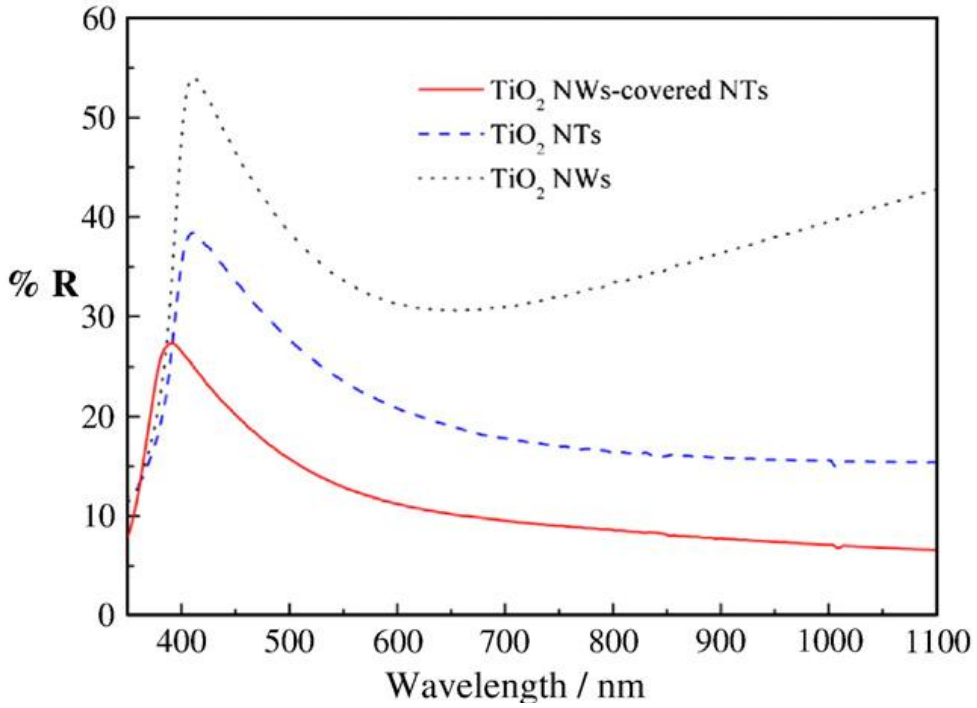

Figure 5.12 Reflectance spectra of the nanotube film, nanowire film and nanowire-covered nanotube bilayer film

5.4.4 *I-V* measurement

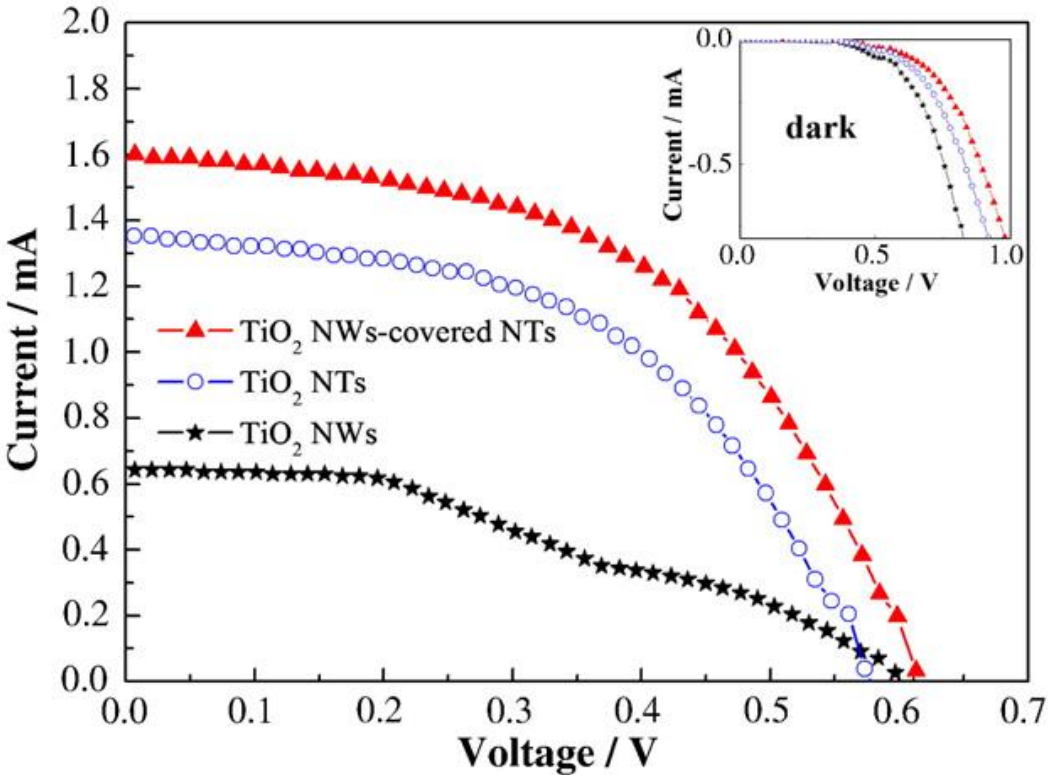

Figure 5.13 *I–V* performance of the DSSCs based on nanotube film, nanowire film and nanowire-covered nanotube bilayer film under *AM 1.5* illuminations (100 mW/cm^2) and in the dark (insert)

The photovoltaic characteristics of the DNA-like DSSCs based on titania nanowire film, nanotube film and nanowire-covered nanotube bilayer film are shown in **Figure 5.13**. It could be seen that the cell based on the titania nanowire-covered nanotube bilayer film generated an open-circuit voltage (V_{oc}) of 0.62 V, a short-circuit current (I_{sc}) of 1.6 mA, a fill factor (*ff*) of 52% and a maximum power (P_{max}) of 0.51 mW, which is a remarkably improved result compared with those resulting from the nanotube cell (V_{oc} =0.58 V, I_{sc} =1.35 mA, *ff* =0.51%, P_{max} =0.4 mW) and the nanowire cell (V_{oc} =0.6 V, I_{sc} =0.64 mA, *ff* =36.5%, P_{max} =0.14 mW). It is partially due to the relatively high light harvesting efficiency of the bilayer film. Besides, from the dark current measurement of

the cells in the upper right corner of **Figure 5.13**, we could see the dark current of the DSSC based on a bilayer film is the lowest, which could be attributed to the modification of the film cracks by the nanowires. With the decrease of the dark current, the charge recombination between the electrolyte and the substrate could be reduced and the photovoltaic performance is improved.

5.5 Conclusion

In this chapter several brand new 3D DNA-like DSSCs were developed based on low resistance Ti wires. The optimal thickness of the titania nanotube film was investigated to achieve the best photovoltaic performance and the length in the range of 14-16 μm was favorable. It was demonstrated that the symmetrical double-helix structure had the characteristics of a passive tracking light source. The study on connecting cells in series and parallel indicated that the total open circuit voltage and the total short circuit current equaled the sum of each cell's in series and in parallel, respectively. This result suggested that it was possible to manufacture large modules based on lots of DNA-like DSSCs through integrated circuit technique. By covering one more layer of titania nanowires onto the surface of titania nanotube film, the cracks on the original film was modified, which could prevent the direct contact between the substrate and the electrolyte and lowered the dark current of the device. Additionally, the bilayer film could further increase the light harvesting efficiency as the upper nanowire layer played a role as the light trapping layer. However, one of the key issues of the DNA-like DSSC is its low fill factor. This is partially due to the material properties, such as the length proportion of nanowire with nanotube, and partially due to

the device structure, for example, the optimal length of thread pitch. Further work is essential to optimize the device through the material synthesis and structure design, and higher conversion efficiency is expected.

References:

1. J. D. Watson, F.H.C. Crick, A structure for Deoxyribose Nucleic Acid, Nature, 1953. **171**: 737-38.
2. C.Y. Chen, M. Wang, J. Y. Li, et al. Highly Efficient Light-Harvesting Ruthenium Sensitizer for Thin-Film Dye-Sensitized Solar Cells, ACS Nano, 2009. **3**: 3103-09.
3. X. Fan, Z. Z. Chu, F. Z. Wang, et al. Wire-shaped flexible dye-sensitized solar cells, Advanced Materials, 2008. **20**: 592-95.
4. S. Ito, S. M. Zakeeruddin, P. Comte, et al. Bifacial dye-sensitized solar cells based on an ionic liquid electrolyte, Nature Photonics, 2008. **2**: 693-98.
5. J. Ramier, C. Plummer, Y. Leterrier, et al. Mechanical integrity of dye-sensitized photovoltaic fibers, Renewable Energy, 2008. **33**: 314-19.
6. M. Toivola, M. Ferenets, P. Lund, et al. Photovoltaic fiber, Thin Solid Films, 2009. **517**: 2799-2802.
7. Y. Liu, H. Shen, Y. Deng. A novel solar cell fabricated with spiral photo-electrode for capturing sunlight 3-dimensionally, Science in China Series E-Technological Sciences, 2006. **49**: 663-73.

8. H. Wang, Y. Liu, H. M. Xu, et al. An investigation on the novel structure of dye-sensitized solar cell with integrated photoanode, Renewable Energy, 2009. **34**: 1635-38.
9. J. Nelson. Continuous-time random-walk model of electron transport in nanocrystalline TiO_2 electrodes, Physical Review B, 1999. **59**: 15374-80.
10. Y. Suzuki, S. Ngamsinlapasathian, R. Yoshida, et al. Partially nanowire-structured TiO_2 electrode for dye-sensitized solar cells, Central European Journal of Chemistry, 2006. **4**: 476-88.

CHAPTER 6 Development of the three-dimensional double deck mesh-like DSSCs

6.1 Introduction

As discussed in Chapter 4, the mesh-like DSSC has the advantages of low sheet resistance, fast electron transportation and cheap fabrication cost. Besides, the DNA-like DSSC introduced in chapter 5 shows the superiority of sunlight utilization and series-parallel connection. Combined these merits together, in this chapter a brand new structured DSSC is further developed and investigated. As this device is based on three-dimensional double deck cylindrical Ti meshes as the substrates, it is named as three-dimensional (3D) double deck mesh-like DSSC. For the same reason as before, the electrochemical anodization is employed to in situ synthesize the titania nanotube layer on the Ti substrate. It is expected that this type of DSSC could inherit the merits of mesh-like DSSC and DNA-like DSSC.

6.2 Experimental materials and equipment

6.2.1 Experimental materials

All the materials used in the experiments are listed in Table 6.1.

Table 6.1 Experimental materials

Name	Remark	Manufactory

Ti mesh	commercially pure titanium	Hebei anping netting screen production ltd.
Ammonium fluoride	AR. 98+%	Tianjin fuchen chemical reagent factory
Silicon dioxide hydrosol	AR. 98+%	Fluka
Ethylene glycol		Guangzhou chemical reagent factory
Chloroplatinic acid	AR.	Shenyang research institute of nonferrous metals
Titanium tetrachloride	AR. 99%	Guangzhou chemical reagent factor
Ru complex dye	N719	Solaronix
Ethanol	AR.	Guangzhou chemical reagent factory
Anhydrous LiI	AR. 98+%	Fluka
I_2	AR. ≥99.55(RT)	Fluka
Acetonitrile	AR.	Tianjin damao chemical instrument supply station
4-tertbutylpyridine	AR. 99%	Aldrich
Surlyn 1702 film and resin	30μm-100 μm	Du pont
AB epoxy transparent glue		Singapore miradur specialty chemicals ltd.

6.2.2 Equipment

All the equipment is listed in Table 6.2.

Table 6.2 Equipment list

Name	Model	Manufactory
DC Power Supply	GPC-6030D	Guangzhou xinhong trading co., ltd
Keithley 2400		Keithley instruments inc.
Low-temperature resistance furnace	SX-2.5-10	Shanghai wuyangshan international trading co., ltd

Solar simulator	Newport-Oriel 91192	Newport co., ltd
Electrochemical analyzer	PARSTAT 2273	Princeton applied research
UV–Vis–NIR spectrometer	U-4100	Hitachi

6.3 Preparation of photoanode

Three types of Ti meshes (60-mesh, 90-mesh and 120-mesh) were used as the substrates of the photoanodes. As introduced in Chapter 3, the 60-mesh means that there are 60 openings in one square inch of mesh. With the increase of mesh number, the diameter of the openings will be decreased. The meshes were first cut into square pieces, and then folded along a metal nail to form the Ti mesh cylinders. The two edges were connected by employing a Ti wire to wound them together and the diameter of the cylinder is about 4mm, which can be seen from **Figure 6.1 (a)**. Before anodization, the Ti mesh cylinder was cleaned in ultrasonic baths with ethanol first and then deionized water for 3 minutes to remove surface contaminants. The anodization was performed in a two-electrode configuration with the Ti mesh cylinder as the working electrode to grow the titania nanotube films and the platinum foil as the counter electrode under constant potential (30 V) at room temperature (23 ℃). A direct current power supply (GPC-6030D) was to drive the anodization process. The electrode was anodized in the electrolyte containing a mixture of ethylene glycol (50.86 wt.%), polyethylene glycol 600 (47.38 wt.%), H_2O (1.31 wt.%) and NH_4F (0.43 wt.%). In order to achieve different thicknesses of the titania nanotube films, anodization time was arranged from 10 h to 80 h. After anodization, the anodized samples were rinsed with deionized water and treated in oxygen ambient at 480 ℃ for 3 h, with heating and cooling rates of 2 ℃ min^{-1}. After

that the samples were immersed in a 0.05 M $TiCl_4$ aqueous solution at 70 ℃ for 30 minutes, and subsequently rinsed in ethanol and annealed in air at 450 ℃ for 30 minutes. Finally, the anodized Ti mesh cylinders were immersed in a mixture solution of tert-butyl alcohol and acetonitrile (1:1 in volume) of 5×10^{-4} M cis-bis (isothiocyanato) bis(2,2'-bipyrridyl-4-4'-dicarboxylato)-ruthenium(II) bis-tetrabutylammonium dye (N-719 , Solaronix) to get sensitized, as shown in **Figure 6.1 (b)**. After 24 hours, the sensitized samples were rinsed with ethanol to remove nonchemisorbed dyes.

6.4 Preparation of counter electrode

The preparation method of the counter electrodes was almost the same as the photoanodes. In short, three types of Ti meshes (60-mesh, 90-mesh and 120-mesh) were folded into Ti mesh cylinders, while the only difference is the smaller diameter of the cylinder, 2.5mm, as shown in **Figure 6.1 (c)**. They were then washed with acetone and ethanol in an ultrasonic bath for 3 minutes. The Pt thin film was deposited onto the Ti surface by an electrodeposition process which was carried out using an aqueous solution of 5×10^{-3} M $H_2PtCl_6 \cdot 6H_2O$ at room temperature. A digital sourcemeter (Keithley, 2400) was applied as a power supply. Here, the Pt counter electrode (**Figure 6.1 (d)**) was prepared with 15 mA cm^{-2} current density for 30 s.

6.5 Fabrication process

For the solar cell fabrication, the counter electrode (platinized Ti mesh cylinder) was first sprayed with a porous SiO_2 layer as an electrical insulator **[1]**, and then inserted into the internal hole of the photoanode (anodized Ti mesh cylinder sensitized with dye

molecules), as shown in **Figure 6.1 (e)**. Both of them were then put into a small glass tube (inner diameter of 5 mm and total length of 20 mm) with the electrolyte consisting of 0.5 M LiI, 0.05 M I_2, and 0.5 M 4-tert-butylpyridine in acetonitrile. Finally the tube was sealed with stuffing and epoxy, as depicted in **Figure 6.1 (f). Figure 6.1 (g)** shows a fabricated 3-D DSSC with lead wires.

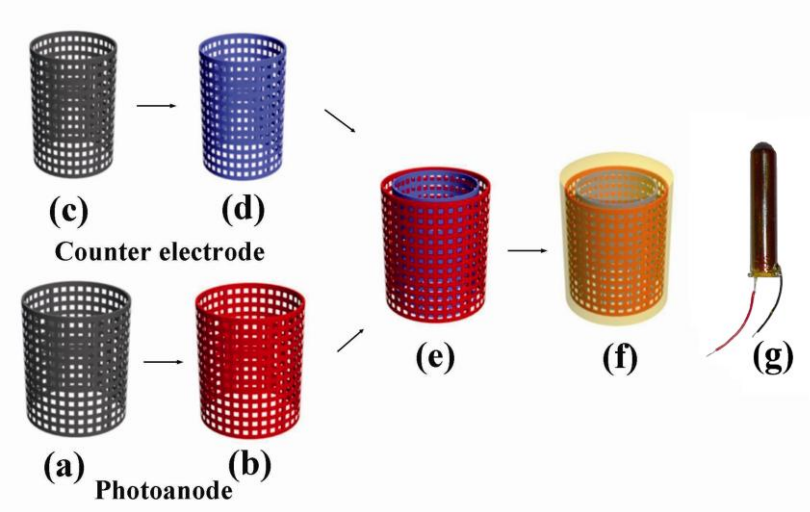

Figure 6.1 Schematic flow diagram for the fabrication of the 3-D DSSC: (a) The Ti mesh cylinder as the substrate of photoanode; (b) The sensitized photoanode; (c) The Ti mesh cylinder as the substrate of counter electrode; (d) The counter electrode based on platinized Ti mesh cylinder; (e) Double deck mesh-like electrodes; (f) A sealed 3-D DSSC; (g) A fabricated 3-D DSSC with lead wires

The operation principles of this 3D double deck mesh-like DSSC are similar to the mesh-like DSSC and DNA-like DSSC, which is briefly summarized as follows (**Figure 6.2**): When the sunlight irradiates through the small glass tube to the dye molecules anchored on the highly ordered titania nanotube arrays, the dye molecules in the original state are stimulated to the excited state (Excitation). The unstable excited dye molecules inject their electrons into the conduction band of highly ordered titana nanotubes

(Injection). The injected electrons subsequently transport through the vertically titania nanotube arrays to the Ti mesh substrate (percolation). Then they were collected to the external circuit. Finally through the external circuit, the electrons are gathered on the platinized Ti mesh (counter electrode). Concurrently the oxidized dye cations are reduced by triiodide ions and triodide ions are oxidized into the iodide ions (Dye regeneration). The iodide ions diffuse through the mesh holes as channels to the platinized Ti mesh in which iodide ions are reduced into triiodide ions again by the Pt catalysis (Electrolyte regeneration). The only difference with the mesh-like DSSC is that the counter electrode here is based on Ti mesh, not Ti sheet.

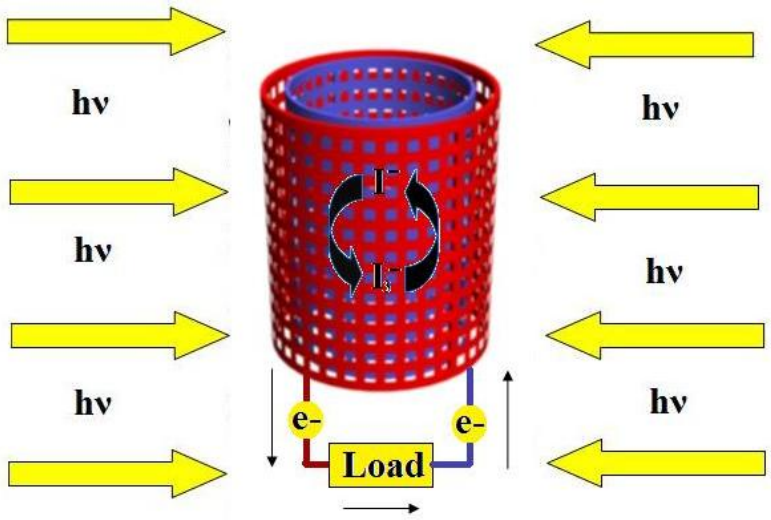

Figure 6.2 The operation principles of 3D double deck mesh-like DSSC

6.6 Morphology

Figure 6.3 (a) is the SEM image of the Ti mesh substrate (60-mesh). The diameter of one Ti wire was about 100 μm which was one third of the side length of the opening. The electrolyte could diffuse through the openings to exchange electrons with electrodes.

Figure 6.3 (b) shows the cross sectional SEM image of one anodized Ti wire in the Ti mesh. It is apparent that after anodization a self-organized titania nanotube layer was in situ synthesized in perpendicular to the wire's surface with average length of 8.6 μm. As shown in **Figure 6.3 (c)**, the nanotubes were packed in approximately cylindrical symmetry with an average inner diameter and wall thickness of 63 nm and 20 nm, respectively. **Figure 6.3 (d)** is the top-view SEM image of the platinized Ti mesh. The Pt particles were distributed onto the Ti surface with the diameter range of 20-25 nm which implied that the Pt particles could provide sufficient surface area to exchange electrons with the electrolyte.

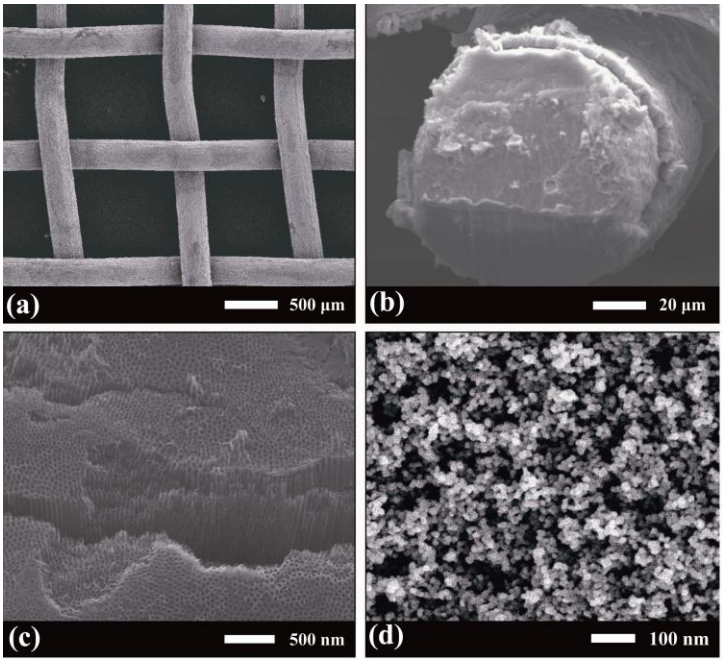

Figure 6.3 The morphology information of the electrodes: (a) The SEM image of the Ti mesh substrate (60-mesh); (b) Cross-sectional view SEM image of one anodized Ti wire from the Ti mesh; (c) Top view SEM image of the anodized Ti wire; (D) The top-view SEM image of the platinized Ti mesh

6.7 Dye loading

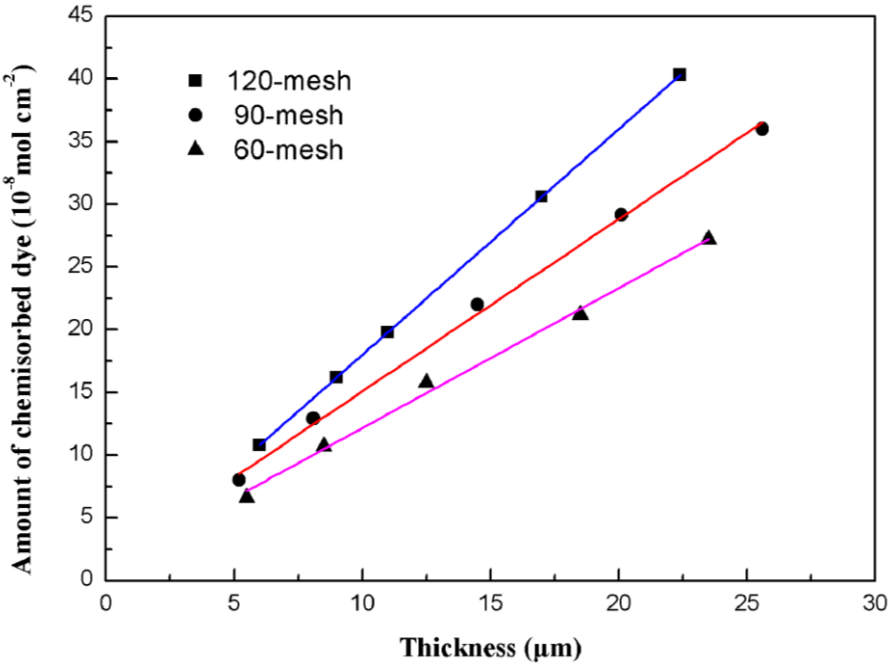

Figure 6.4 Dependence of the amount of chemisorbed dye on the thickness of TiO_2 nanotube film based on three types of photoanodes (60-mesh, 90-mesh, 120-mesh)

For the photoanodes of the DSSCs, the amount of dye adsorption is a key factor to enhance the light harvesting efficiency **[2]**. In order to determine the quantity of chemisorbed dye in the titania nanotube film, dye molecules were desorbed from a nominally identical batch of photoanodes in a mixed solution of 0.1 M NaOH and ethanol (volume ratio: 1/1). **Figure 6.4** shows dependence of the amount of chemisorbed dye on the thickness of titania nanotube film based on three types of photoanodes. The amount of dye adsorption was proportional to the thickness of the titania nanotube film. Besides, for the same thickness titania nanotube film, the dye loading of the photoanode based on 120-mesh was the highest, followed by the one based on 90-mesh and then the one based on 60-mesh. This is probably due to the fact that, with the increase of the mesh number, the surface area of the Ti mesh substrate also increases, which means there will be larger surface area exposed for producing the titania nanotubes. As the

amount of adsorbed dye strongly depends on the surface area of the titania nanotube film, the dye loading is enhanced.

6.8 Active surface area of platinum

The counter electrode of the DSSCs serves to transfer electrons from the external circuit to the electrolyte **[3]**. The role of Pt on the counter electrode is to catalyze the electrochemical reduction of the redox couple. An important parameter of the platinum-based counter electrode is the active surface area (A_s) of Pt because only the Pt atoms on the outside surface can contribute to the catalytic activity. As described in most electrochemical studies **[4-5]** we measured the A_s of the three types of counter electrodes by using the hydrogen-desorption peaks on the cyclic voltammetry (CV) curves in 0.5 M H_2SO_4 aqueous solution. For comparison, all the counter electrodes were cut into 0.5 cm × 2 cm pieces with a Ti mesh (60-mesh) in the same size as the reference sample. **Figure 6.5 (a)** shows the CV curves of the as-prepared counter electrodes and the reference sample. It is obvious that the Ti mesh showed no H adsorption–desorption features, which was in good agreement with the property of Ti substrates **[6]**. Consequently, the electrooxidation peak in the CV curves of the platinized Ti mesh should be resulted from the existence of Pt. The A_s of the counter electrodes can be obtained according to the following equation **[7]**:

$$A_s = (Q_H / Q_e) * A_{Pt} \tag{6.1}$$

where Q_H represents the charges related to oxidization of monolayer hydrogen on the Pt surface, equaling to the calibrated area of the hydrogen desorption peak on the CV

curve; Q_e is the elementary charge (Q_e = 1.602 × 10^{-19} C); A_{pt} is the averaged atomic area of surface Pt atoms and it is 7.69×10^{-20} m^2 according to the atomic density of Pt surface of about 1.3×10^{19} m^{-2}. This equation employs the well-established hydrogen-adsorption stoichiometry for the Pt surface (H:Pt=1:1) **[8]**. **Table 6.3** summarizes the electrochemical data obtained from the CV curves. Obviously, the A_s of the counter electrodes rise with the increment of the mesh number, which was in accordance with the trend of the dye loading on photoanodes discussed above. This result is also attributed to the increased surface area of the Ti mesh substrate. In addition, for a flat smooth Pt sheet plate, Q_H was around 0.21 mC cm^{-2} **[9-10]** which meant A_s was about 1.01 cm^2, only one-tenth of that of the 120-mesh counter electrode. It implies that the mesh structure based counter electrode could provide larger surface area for Pt atoms to disperse in than the one based on flat smooth sheet.

The increased A_s of the counter electrode with larger mesh number is further verified by the CV measurement in the electrolyte solution, containing 5 mM LiI, 1 mM I_2 and 0.1 M $LiClO_4$ as the supporting electrolyte in acetonitrile. The CV curves of I^-/I_3^- redox couple on the three types of counter electrodes are shown in **Figure 6.5 (b)**. It is observed that there were two anodic peaks in the anodic sweep and two cathodic peaks in the cathodic sweep, which were described in detail elsewhere **[11-12]**. The shapes of the curves were similar and the anodic and cathodic peak heights and areas increased along with the mesh number. We believe that the Ti mesh with larger mesh number could provide larger surface area for the platinum deposition, and hence the catalytic activity of Pt toward the reduction of I^-/I_3^- redox couple was enhanced.

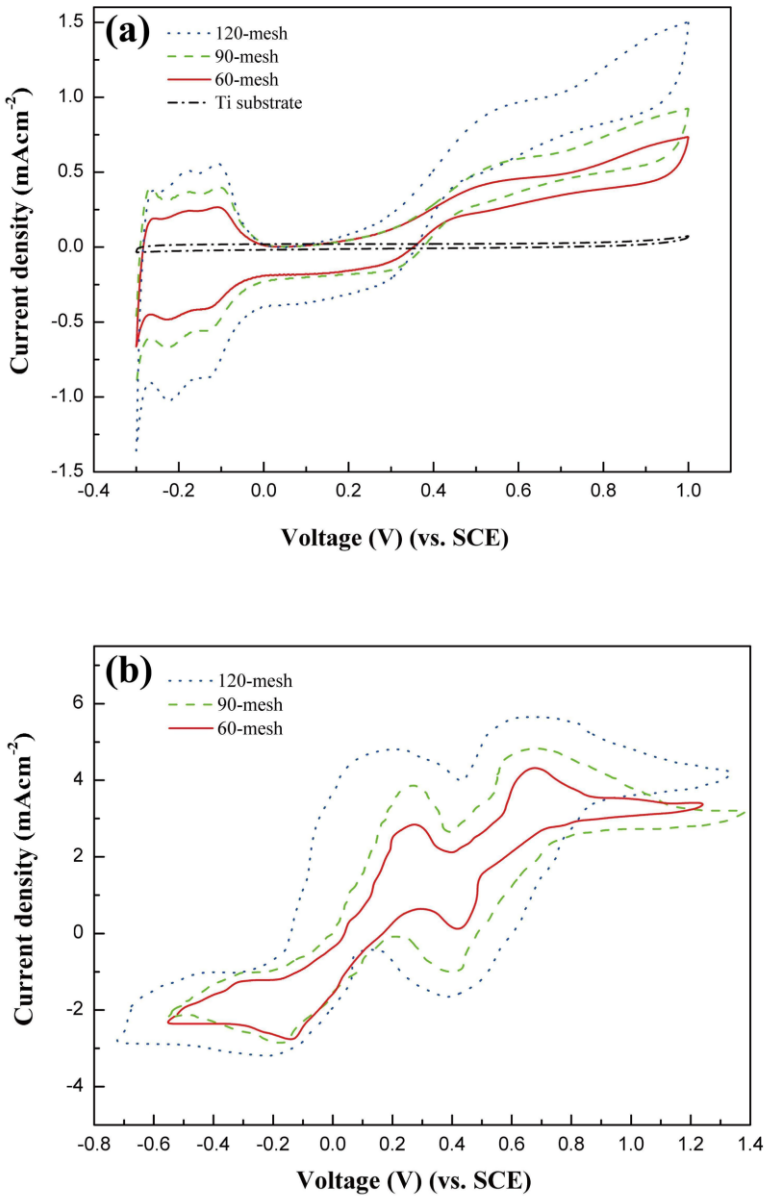

Figure 6.5 Cyclic voltammograms of three types of counter electrodes (60-mesh, 90-mesh, 120-mesh) in (a) 0.5 M H_2SO_4 aqueous solution; (b) the electrolyte solution, containing 5 mM LiI, 1 mM I_2 and 0.1 M $LiClO_4$ as the supporting electrolyte in acetonitrile

Table 6.3 The electrochemical parameters of the counter electrodes obtained from the CV measurements

Counter Electrodes	Q_H (mC cm^{-2})	A_s (cm^2)
120-mesh	2.07	9.96
90-mesh	1.67	8.03
60-mesh	1.02	4.92
Ti mesh	0	0
Pt sheet	0.21	1.01

6.9 Impedance analysis

Electrochemical impedance spectroscopy (EIS) **[13-14]** has been widely used as a useful approach to investigate the influence of different resistance elements on the photoelectrochemical characteristics of the DSSCs. Generally, the impedance spectra of the DSSCs contains three semicircles **[15]**, which are attributed in terms of decreasing frequency to electrochemical reactions at the counter electrode/electrolyte interface (Z_1) in the high-frequency region, the electron transfer at the titania/dye/electrolyte interface (Z_2) in the middle-frequency region, and the Nernst diffusion impedance of the redox species in the electrolyte (Z_3) in the low frequency region. The real parts of Z_1, Z_2 and Z_3 represent the resistance elements as R_1, R_2 and R_3, respectively. The resistive element R_h in the high-frequency region (around 100 kHz) corresponds to the sheet resistance of the substrate. To further explore the influence of the mesh number on the performance of the DSSCs, the electrodes based on different mesh number were assembled to fabricate the devices for EIS measurement. **Figure 6.6** shows the variation in the EIS parameters of the DSSCs (under illumination of 100 mW cm^{-2} at open circuit condition) by changing the mesh number of the electrodes. It could be seen when the mesh number of

the photoanode was fixed to 60-mesh (**Figure 6.6 (a)**), with the increase of the mesh number on the counter electrode, the R_1 decreased from 57.6 Ω to 15.5 Ω. Meanwhile, the R_2 and R_h remained nearly constant and R_3 increased from 40.1 Ω to 60.5 Ω. Correspondingly, when the mesh number of the counter electrode was fixed to 60-mesh (**Figure 6.6 (b)**), with the increase of the mesh number on the photoanode, the R_2 decreased from 74.7 Ω to 29.5 Ω; the R_1 and R_h kept constant and R_3 increased from 40.2 Ω to 80.6 Ω.

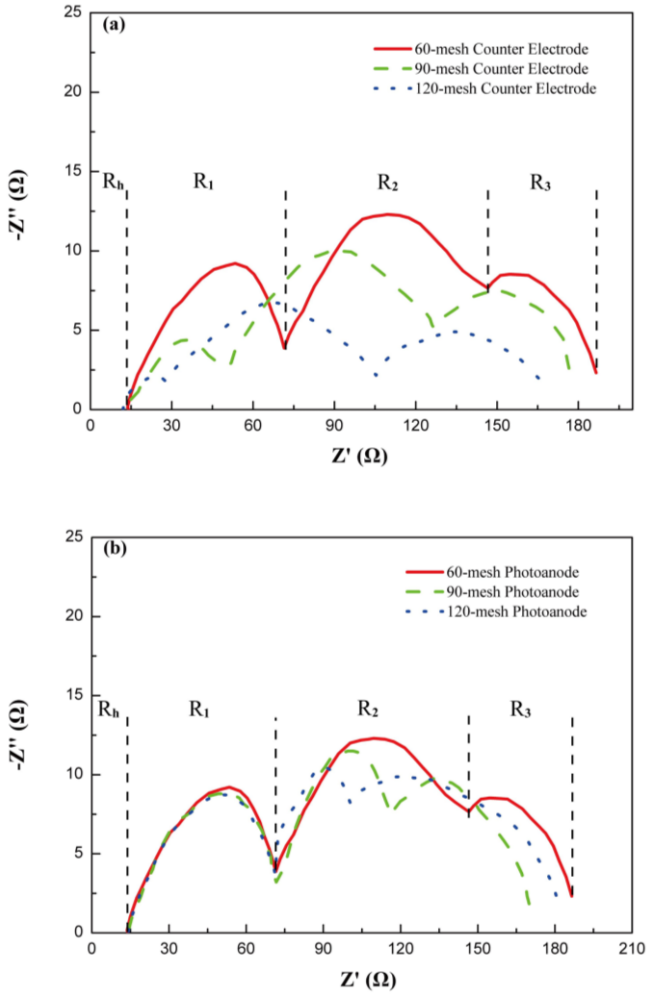

Figure 6.6 Electrochemical impedance spectra of the 3D DSSC (under 1 sun bias illumination at open circuit condition) with different mesh number: (a) Photoanode: 60-

mesh; Counter electrode: 60-mesh, 90-mesh and 120-mesh; (b) Photoanode: 60-mesh, 90-mesh and 120-mesh; Counter electrode: 60-mesh.

The decrease of R_1 in **Figure 6.6 (a)** is mainly caused by the increased active surface area (A_s) of Pt on the counter electrode. The decrease of R_2 in **Figure 6.6 (a)** attributes to the enhancement of the dye loading of the photoanode. For R_3, in both cases, with the increase of the mesh number, the diameter of the opening in the mesh is reduced, which causes the ions in the electrolyte more and more difficult to diffuse. Hence, the R_3 will rise. Besides, as the substrates of this 3D DSSC are based on Ti metal, there is little change in the sheet resistance of the Ti mesh when the mesh number is varied. Consequently, the R_h has scarcely changed for both cases. In general, the increase of the mesh number will lower R_1 and R_2, but enhance R_3 and have little impact on R_h.

6.10 Sunlight utilization

In comparison with the conventional planar DSSCs, one of the merits of this new 3D DSSC is its superior light utilization efficiency. To confirm this point, the angle of the incident sunlight was changed from 0 ° to 180 ° and we measured the corresponding photovoltaic parameters of the device. As shown in **Figure 6.7**, the short circuit current (I_{sc}) and open circuit voltage (V_{oc}) nearly remain unchanged with the variety of the incident angle, which demonstrates that the performance of this 3D DSSC is independent of the incident angle. This is because no matter which direction the constant light source irradiates from, the axial symmetrical structure of the 3D DSSC could capture the same quantity of the sunlight, as indicated in the inset of **Figure 6.7**. Moreover, in the natural environment, cloudy skies may produce more scattered sunlight

than the sunny skies [16]. Considering such sunlight may come from nearly all skyward directions, this 3D DSSCs may work more efficiently than the flat types during cloudy days.

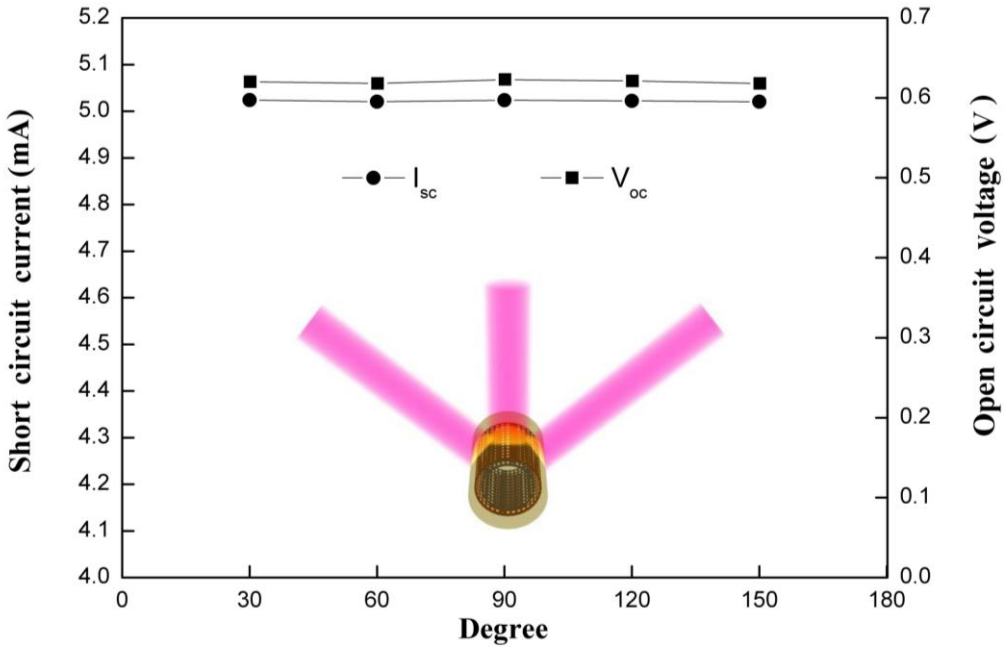

Figure 6.7 The photovoltaic parameters of the 3D DSSC illuminated in different angles of the incident sunlight. The inset shows the schematic diagram of the 3D DSSC under illumination in different angles.

6.11 *I-V* measurement

For the photovoltaic analysis, a series of the 3D DSSCs were fabricated by different combinations of photoanodes (60-mesh, 90-mesh and 120-mesh) and counter electrodes (60-mesh, 90-mesh and 120-mesh). We assume that the irradiated area of this 3D DSSC is the cross section of the cylinder which is a 5 mm × 20 mm rectangle as shown in the inset of **Figure 6.8.** Before the measurement, we firstly tried to optimize the thickness of the titania nanotube film on the photoanode because it is a key factor to influence the

efficiency (η) of the DSSC. From **Figure 6.8** we could see the DSSC (60-mesh photoanode and 60-mesh counter electrode) with 14.5 μm showed the highest conversion efficiency (η) of about 3.2% with the short circuit current density (J_{sc}), open circuit voltage (V_{oc}) and fill factor (*ff*) of 6.30 mA cm^{-2}, 0.73 V and 70.5%, respectively. As a result, we adopted 14.5 μm as the uniform film thickness by controlling the anodization time. Through several parallel experiments, we found the best combination was the 90-mesh photoanode with the 120-mesh counter electrode (η=5.5%), rather than the 120-mesh photoanode with the 120-mesh counter electrode (η=5.1%), as shown in **Figure 6.9**. As discussed in the above, larger mesh number is beneficial to the dye loading and active surface area (A_s) of Pt, but it has a negative impact on the diffusion of the ions in the electrolyte. We believe this is the balanced result of these three factors.

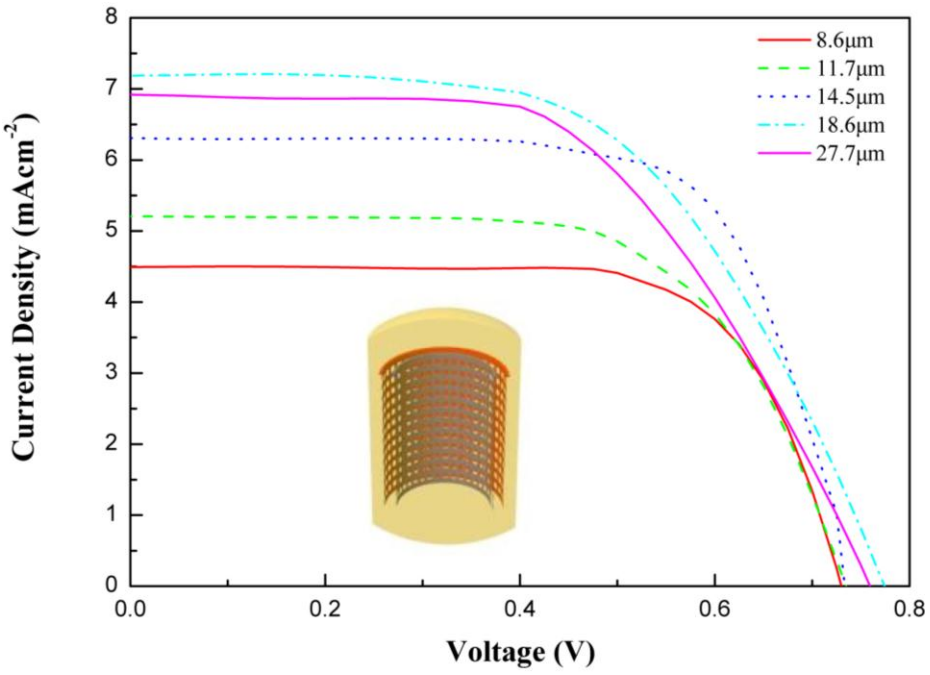

Figure 6.8 *I–V* performances of the 3D DSSCs with different lengths of nanotube layers. *AM 1.5*, 100mW cm^{-2}. The inset shows the irradiated area of the 3D DSSC.

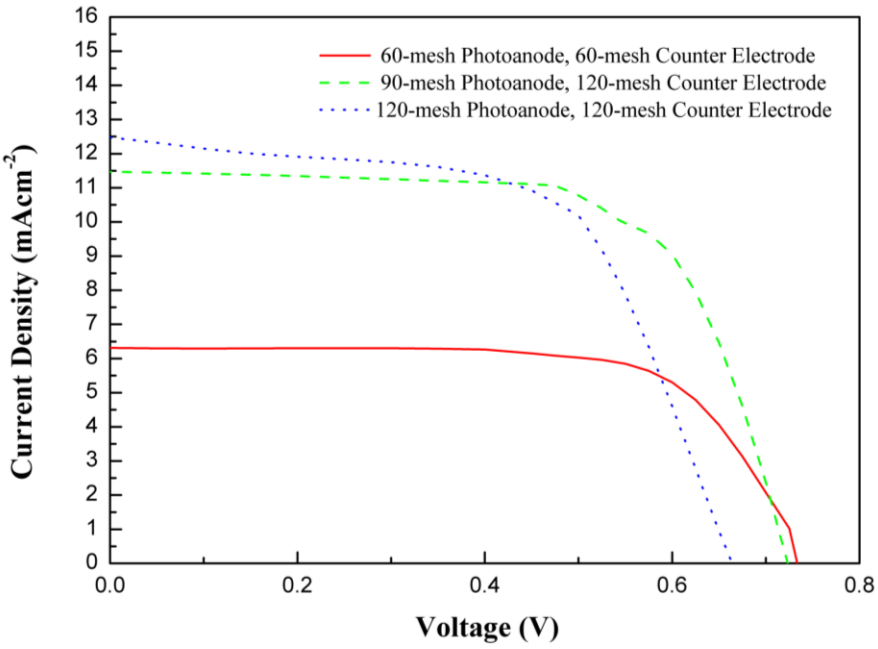

Figure 6.9 *I–V* performances of the 3-D DSSCs based on 60-mesh photoanode with 60-mesh counter electrode, 90-mesh photoanode with 120-mesh counter electrode and 120-mesh photoanode with 120-mesh counter electrode

6.12 Further development

Although this new 3D DSSC showed some superiority over traditional types, there are still some problems to be solved. For example, the sprayed SiO_2 layer on the counter electrode as the electrical insulator is sometimes easy to be broken, which causes the direct contact between the electrodes and lowers the efficiency of the cell. As a result, how to stabilize the electrical insulator layer is a key issue. Besides, the film thickness of the electrical insulator needs to be optimized since it determines the diffusion length of electrolyte. In addition to this, we are now investigating whether there are better ways of insulating the electrodes without blocking the transport of electrolyte, for example, to use a thin plastic mesh as the insulator. This work is currently in progress. We hope by

overcoming these defects, the photovoltaic performance of this 3D DSSC could be further optimized.

6.13 Conclusion

In summary, a new type of the 3D DSSC was firstly proposed by utilizing the cylindrical Ti meshes as substrates of electrodes. With the anodization method, a self-organized titania nanotube layer was in situ synthesized from the Ti mesh as the photoanode material. The morphologies of the electrodes were characterized by the SEM. The influence of the mesh number was tested via the dye adsorption, CV curves and EIS measurement. It is found that the dye loading on the photoanode as well as the active surface area of Pt on the counter electrode increased along with the mesh number, but it was more difficult for the electrolyte to diffuse through the reduced-size holes in the mesh. In the photovoltaic analysis, the 3D DSSC based on 90-mesh photoanode and 120-mesh counter electrode exhibited the highest conversion efficiency of 5.5%. It was also demonstrated that the performance of this 3D DSSC was independent of the incident angle of the solar radiation due to its axial symmetrical structure. Further work is to focus on optimizing the electrical insulator layer, and higher conversion efficiency is expected.

References:

1. S. Ito, S. M. Zakeeruddin, P. Comte, P. Liska, D. Kuang, M. Grätzel. Bifacial dye-sensitized solar cells based on an ionic liquid electrolyte, Nature Photonics, 2008. **2**: 693-98.

2. L. Yang, Y. Lin, J. Jia, X. Xiao, X. Li, X. Zhou. Cauliflower-like TiO_2 rough spheres: Synthesis and applications in dye sensitized solar cells, Microporous and Mesoporous Materials, 2008. **112**: 45-48
3. F. Cai, J. Liang, Z. Tao, J. Chen, R. Xu, Low-Pt-loading acetylene-black cathode for high-efficient dye-sensitized solar cells, J. Power Sources, 2008. **177** : 631-36.
4. T. R. Ralph, G. A. Hards, J. E. Keating, S. A. Campbell, D. P. Wilkinson, M. Davis, J. S. Pierre, M. C. Johnson, Low Cost Electrodes for Proton Exchange Membrane Fuel Cells, J. Electrochem. Soc, 1997. **144**: 3845-57.
5. A. Pozio, M. De Francesco, A. Cemmi, F. Cardellini, L. Giorgi, Comparison of high surface Pt/C catalysts by cyclic voltammetry, J. Power Sources, 2002. **105**: 13-19.
6. E. H. Yu, K. Scott, R. W. Reeve, L. Yang, R. G. Allen, Characterisation of platinised Ti mesh electrodes using electrochemical methods: methanol oxidation in sodium hydroxide solutions, Electrochim. Acta, 2004. **49:** 2443-52.
7. D. Zhao, B. Xu, Enhancement of Pt utilization in electrocatalysts by using gold nanoparticles, Angew. Chem. Int. Ed, 2006. **45**: 4955-59.
8. J. Bett, K. Kinoshita, K. Routsis, P. Stonehart, A comparison of gas-phase and electrochemical measurements for chemisorbed carbon monoxide and hydrogen on platinum crystallites, J. Catal, 1973. **29:** 160-68.
9. M. Grden, A. Paruszewska, A. Czerwinski, Electrosorption of carbon dioxide on Pd---Pt alloys, J. Electroanal. Chem, 2001. **502:** 91-99.

10. L. dos Santos, F. Colmati, E. R. Gonzalez, Preparation and characterization of supported Pt–Ru catalysts with a high Ru content, J. Power Sources, 2006. **159**: 869-77.
11. K. Imoto, K. Takahashi, T. Yamaguchi, T. Komura, J. Nakamura, K. Murata, High-performance carbon counter electrode for dye-sensitized solar cells, Sol. Energy Mater. Sol. Cells, 2003. **79**: 459-69.
12. Z. Huang, X. Liu, K. Li, D. Li, Y. Luo, H. Li,W. Song, L. Chen, Q. Meng, Application of carbon materials as counter electrodes of dye-sensitized solar cells, Electrochem. Commun, 2007. **9**: 596-98.
13. L. Han, N. Koide, Y. Chiba, A. Islam, R. Komiya, N. Fuke, A. Fukui, R. Yamanaka, Improvement of efficiency of dye-sensitized solar cells by reduction of internal resistance, Appl. Phys. Lett, 2005. **86**, 213501-03.
14. N. Koide, A. Islam, Y. chiba, L. Han, Improvement of efficiency of dye-sensitized solar cells based on analysis of equivalent circuit, J. Photochem. Photobiol. A, 2006. **182**: 296-305.
15. K. Lee, C. Hu, H. Chen, K. Ho, Incorporating carbon nanotube in a low-temperature fabrication process for dye-sensitized TiO_2 solar cells, Sol. Energy Mater. Sol. Cells, 2008. **92**: 1628-33.
16. I. Al-Turki, M. Schiler, Predicting natural light in atria and adjacent spaces using physical models, Sol. Energ, 1997. **59**: 241-45.

CHAPTER 7 CONCLUSIONS AND RECOMMENDATIONS FOR FUTURE WORK

7.1 Summary of the research results

As illustrated in Chapter 1, under the premise of no decay of conversion efficiency, the size of a conventional DSSC is hard to be over 1cm^2 due to the high resistance of FTO glass. Although metal substrates such as Ti sheets have the superiority of low resistivity, low production cost and high temperature sinterability compared with the FTO glass, it is hard to realize the DSSCs based on all metal substrates due to their opacity. Besides, although the application of highly ordered titania nanotube arrays on the DSSCs could increase the charge collection efficiency, it is also confined at the backside illuminated configuration due to the same reason of metal substrates. To solve these problems, a series of new structures of the DSSCs have been developed in this project based on metal substrates. Besides, combined with the in situ anodization technique, the titania nanoparticles film is replaced by highly ordered titania nanotube arrays to increase the charge collection efficiency.

First, to master and optimize the basic fabrication techniques of the DSSCs, Grätzel's work on conventional DSSCs was further developed based on TCO glass. The fabrication process of screen printing paste made by P25 type titania was optimized to simplify its procedures. By optimizing various parameters of the device such as film thickness, the highest conversion efficiency based on P25 type titania was 7.79%. However, the conversion efficiency decreased with the increase of device size due to the

high resistance of FTO glass. For comparison, DSSCs based on FTO glass with open-ended titania nanotubes layer was developed. By changing the anodization voltage, a bilayer titania nanotubes film was synthesized and finally split in the middle. The champion cell based on open-ended titania nanotubes achieved conversion efficiency of 8.7% with the device size of 0.3 cm^2. However, the conversion efficiency dropped dramatically when the device size increased to 4 cm^2. Consequently the size effect is unavoidable for the DSSC based on FTO glass.

By using the principle of capillary network in a lung, the mesh-like DSSCs were developed, which contained no TCO glass. The photoanode was prepared by using Ti mesh as the substrate and then through the anodization method to directly synthesize highly ordered titania nanotube arrays as the active layer. The Ti metal mesh served as both the substrate and the source material. As a result, the affinity of titania layer with Ti mesh was better than it was with TCO glass. The counter electrode was prepared by using a Ti sheet as the substrate and electrodeposited with Pt thin film as the catalyst layer. In the mesh-like configuration, the electrolyte could diffuse through the holes on the mesh freely to transfer the redox couple. The structure of this DSSC showed some advantages such as low resistance, cheap fabrication cost over the traditional ones. Different length of nanotube array layers was investigated to find their influence on the photovoltaic performances. The experiment indicated that a proper length of the layer is a key factor to achieve high conversion efficiency. The influences of mesh numbers were also considered and the cell with 90-mesh photoanode exhibited the highest conversion efficiency of 5.3%, which showed superiority compared with the backside illuminated DSSC and other metal-substrate-based DSSC. It is interesting to see that the

device size had only a little impact on the photovoltaic parameters, e.g. the conversion efficiency of the DSSC in 4 cm^2 area was 5.0%, only a little lower than 5.3% in 2 cm^2 area. The flexible mesh-like DSSC were also fabricated by using transparent thermoplastic film as the sealing materials. The bendability were investigated and showed good mechanical and photovoltaic stability.

A brand new 3D DNA-like DSSC was developed by using anodized Ti wire as photoanode and platinized Ti wire as counter electrode. These two wire-like electrodes are twisted together to make a double-helix structure just like a DNA molecule. The optimal thickness of the titania nanotube film was investigated to achieve the best photovoltaic performance and the length in the range of 14-16 μm was favourable with the peak output power of 0.49 mW. It was demonstrated that the symmetrical double-helix structure had the characteristics of a passive tracking light source. Although the output of one DNA-like DSSC was tiny, the characteristics of a series-parallel connection were investigated, which suggested that the DNA-like DSSCs could be connected by integrated circuit technique to make large modules. To further increase the photovoltaic performance, a two-step formation of the titania nanowire-covered nanotube bilayer film technique was developed and applied in the DNA-like DSSCs. The bilayer film was prepared by the electrochemical anodization first to grow the lower nanotube layer and then through the hydrothermal method to grow the upper nanowire layer. From the reflectivity spectrum and scanning electron microscopy it was observed that the nanowire layer on the top could not only decrease the reflectivity of the film, but also played a role to modify the film cracks. Compared with the DSSC based on a single layer electrode, the cell with bilayer film showed higher photovoltaic parameters and

lower dark current, which was due to its higher light harvesting efficiency and lower charge recombination process between the electrolyte and the substrates.

Finally by combining the merits of mesh-like DSSCs and DNA-like DSSCs, a new type of 3D double deck mesh-like DSSCs was developed by utilizing cylindrical Ti meshes as the substrates of electrodes. One of the Ti mesh is anodized to in situ synthesize highly ordered titania nanotue arrays. Another Ti mesh was platinized through electrodeposition as the counter electrode. The morphologies of the electrodes were characterized by SEM. The influence of mesh number was tested via the dye adsorption, CV curves and EIS measurement. It was found that the dye loading on the photoanode as well as the active surface area of Pt on the counter electrode increased along with the mesh number, but it was more difficult for the electrolyte to diffuse through the holes with reduced-size in the mesh. It was demonstrated that the performance of this 3D DSSC was capable of tracking sunlight just like the DNA-like DSSC due to its axial symmetrical structure. In the photovoltaic analysis, the 3D DSSC based on 90-mesh photoanode and 120-mesh counter electrode exhibited the highest conversion efficiency of 5.5%.

The above novel developments provide new ways and guidance for our future work and other researchers for producing advanced DSSCs and finally commercializing this new type of solar cells for solar power production in the future.

7.2 Recommendations for Future Work

For the further work of the developed novel structure DSSCs, it is essential to optimize the sealing materials to avoid leakage of electrolyte. For the flexible mesh-like DSSCs, higher transparent thermoplastic film is needed to increase the light harvesting efficiency. The thickness of Ti mesh should be further decreased as it determines the diffusion length of redox couple. Recently, Dr. Liu **[1]** created a new approach to fabricate the thinner Ti mesh by laser drilling holes on an attenuated Ti sheet. The inclined micro-channels formed by laser drilling acted as multifunctional roles for enhancing the conversion efficiency, light trapping, and pathway for transporting electrolyte and extra surface area for dye loading.

To further increase the flexibility of the substrates and decrease the fabrication cost of the DSSCs, graphite wires or mesh will be used as the new substrates, mainly due to the following points:

(i) The graphite substrate is very cheap as carbon is one of the abundant elements in earth. The fabrication cost of the DSSCs could be reduced by replacing Ti sheet with graphite substrate.

(ii) The graphite substrate could withstand high temperature as high as 1000 ℃.

(iii) The graphite could be made into flexible substrate such as graphite mesh or graphite wire.

(iv) The conductivity of graphite substrate is comparable with TCO substrate.

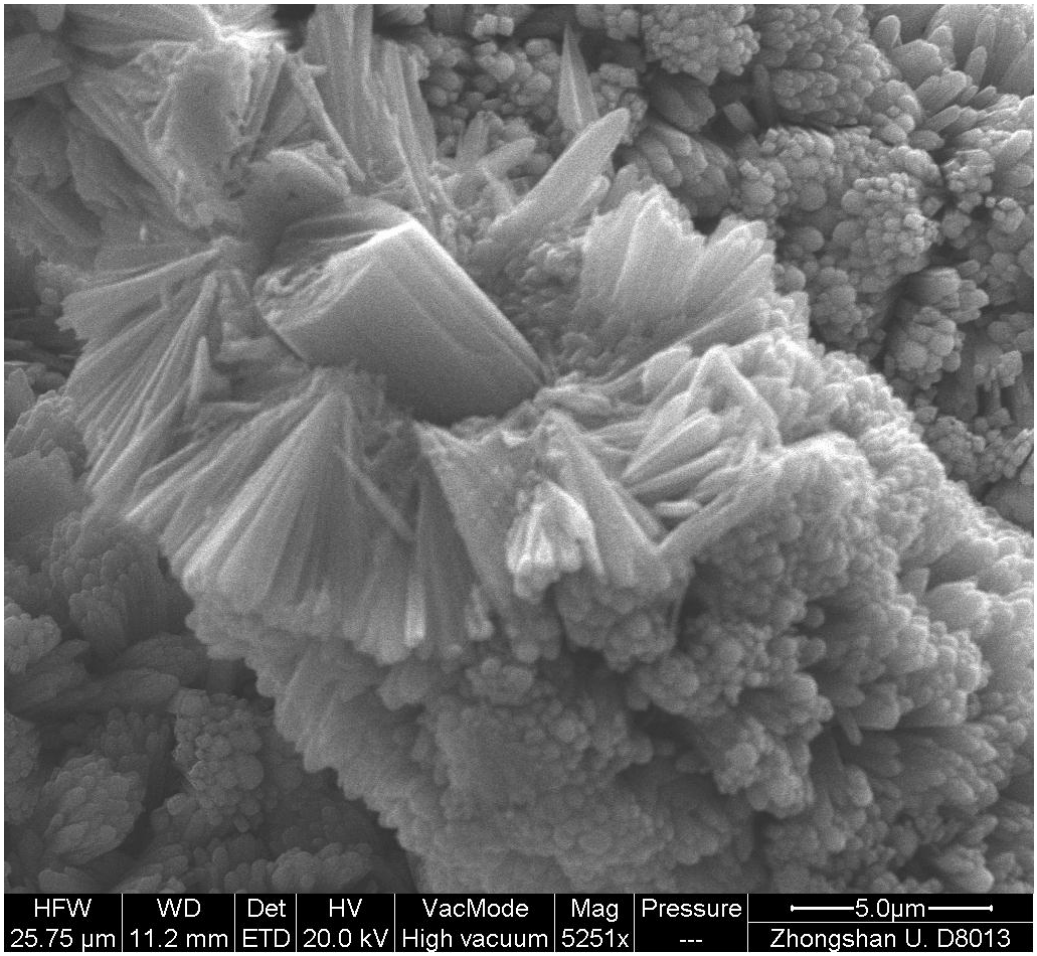

Figure 7.1 SEM image of the graphite fiber covered with titania nanorods

Figure 7.1 is the SEM image of preliminary result of titania nanorods covered on the surface of graphite fibers. It is apparent that one dimensional titania nanorods were in situ synthesized from the surface of graphite fibers, which ensures the affinity between the titania layer with the graphite substrate. The graphite fiber could gather all the electrons generated in the titania nanorods. This work is currently under investigation and will be reported in the near future.

References:

1. Y. Liu, H. Wang, M. Li, R. J. Hong, Q. H. Ye, J. M. Zheng, and H. Shen, Frontside illuminated TiO_2 nanotube dye-sensitized solar cells using multifunctional microchannel array electrodes. Appl Phys Lett, 2009. **95**: 233505.